ENHANCED ADHESION BETWEEN ELECTROLESS COPPER AND ADVANCED SUBSTRATES

A Dissertation
Presented to
The Academic Faculty

By

Harley T. Hayden

In Partial Fulfillment
Of the Requirements for the Degree
Doctor of Philosophy in the
School of Chemical & Biomolecular Engineering

Georgia Institute of Technology
April 2008

ENHANCED ADHESION BETWEEN ELECTROLESS COPPER AND ADVANCED SUBSTRATES

Approved by:

Dr. Paul A. Kohl, Co-Advisor
School of Chemical & Biomolecular Engineering
Georgia Institute of Technology

Dr. Sue Ann Bidstrup Allen, Co-Advisor
School of Chemical & Biomolecular Engineering
Georgia Institute of Technology

Dr. Dennis Hess
School of Chemical & Biomolecular Engineering
Georgia Institute of Technology

Dr. Sankar Nair
School of Chemical & Biomolecular Engineering
Georgia Institute of Technology

Dr. Jianmin Qu
School of Mechanical Engineering
Georgia Institute of Technology

Date Approved: March 27, 2008

ACKNOWLEDGEMENTS

There are many people who have made contributions to this work through their direction and support. I would like to thank my advisors, Dr. Paul Kohl and Dr. Sue Ann Bidstrup-Allen, who helped to provide the structure for this project and were available throughout for discussions and guidance. Dr. Dhananjay Bhusari was heavily involved in the plasma treatments and XPS analysis used in this project, and he deserves my sincere gratitude for teaching me the techniques and fundamentals associated with these processes. I would like to extend my appreciation to the Intel Corporation for funding this work, specifically to Dr. Ravindra Tanikella, Dr. Thomas Dory, and Dr. Christine Tsau for their advice. I also wish to recognize the members of the Kohl-Bidstrup research group—especially Seongho Park and Tyler Osborn—for graciously lending their expertise on a number of subjects and for keeping the mood around the labs light and enjoyable.

In addition, I would like to thank my parents, Tom and Polly Hayden, and my brother, Elliott Hayden, for their constant love and support. Finally, I would like to thank my wife, Emily, for the deep love and friendship we have shared over the last five years. It has only been with her help that I have made it through graduate school, and it is because of her that I continue to improve as a person, student, and husband every day.

TABLE OF CONTENTS

LIST OF TABLES

LIST OF FIGURES

LIST OF SYMBOLS

A – Cross-sectional area

AP – Avatrel/Probelec Blend

Ar – Argon

BE – Electron binding energy

C – Carbon

c – The speed of light

Cu – Copper

E – Energy of photon

h – Height

h – Plank’s constant

KE – Kinetic energy of a photon

L – Length

$Loss_{DIELECTRIC}$ – Signal loss due to the dielectric layer

$Loss_{SKIN}$ – Signal loss due to the skin effect

N – Nitrogen

NH_3 – Ammonia

O – Oxygen

Pd – Palladium

R_{RMS} – Root-mean-square roughness

R_{SKIN} – Effective conductor resistance due to skin effect

Sn – Tin

$\tan \delta$ – Loss Tangent

T_D – Trace Delay

Z_0 – Impedance

δ_x – Skin depth

ε_r – Relative dielectric constant

f – Frequency

μ_0 – Permeability of free space

μ_r – Relative permeability

ρ – Resistivity

v – Signal propagation velocity

ω – angular frequency

SUMMARY

In this work, adhesion between electrolessly deposited copper and dielectric materials for use in microelectronic devices is investigated. The microelectronics industry requires continuous advances due to ever-evolving technology and the corresponding need for higher density substrates with smaller features. Specifically, new dielectric materials with smoother surfaces (to avoid signal scattering and mechanical disconnects) and enhanced electrical properties (to minimize RC delay and loss) are needed. At the same time, adhesion must be maintained in order to preserve package reliability and mechanical performance. In order to meet these requirements two approaches were taken: smoothing the surface of traditional epoxy dielectric materials while maintaining adhesion, and increasing adhesion on advanced dielectric materials through chemical bonding and mechanical anchoring. This work resulted in a number of important conclusion about the roles of chemical bonding and mechanical anchoring in both adhesion and catalyst adsorption.

It was found that NH_3 plasma treatments can be effective for increasing both catalyst adsorption and adhesion across a range of materials. This adhesion is achieved through increased nitrogen content on the polymer surface, specifically N=C. This nitrogen interacts with the palladium catalyst particles to form chemical anchors between the polymer surface and the electroless copper layer without the need for roughness. Chemical bonding alone, however, did not enable sufficient adhesion but needed to be supplemented with mechanical anchoring. Traditional epoxy materials were treated with a swell and etch process to roughen the surface and create mechanical anchoring. This

same process was found to be ineffective when used on advanced dielectric materials. In order to create controlled roughness on these surfaces a novel method was developed that utilized blends of traditional epoxy with the advanced materials. Finally, combined treatments of surface roughening followed by plasma treatments were utilized to create optimum interfaces between traditional or advanced dielectric materials and electroless copper. In these systems adhesion was measured over 0.5 N/mm with root-mean-square surface roughness as low as 15 nm. In addition, the individual contributions of chemical bonding and mechanical anchoring were identified.

The plasma treatment conditions used in these experiments contributed up to 0.25 N/mm to adhesion through purely chemical bonding with minimal roughness generation. Mechanical anchoring accounted for the remainder of adhesion, 0.2-0.8 N/mm depending on the level of roughness created on the surface. Thus, optimized surfaces with very low surface roughness and adequate adhesion were achieved by sequential combination of roughness formation and chemical modifications. These improvements will enable the use of both current and advanced materials in future microelectronic devices without fear of severe performance degradation from surface roughness, low adhesion, or poor electrical properties.

CHAPTER 1

INTRODUCTION

1.1 Motivation

New technologies and processes are being developed to meet the demand for high density interconnects for integrated circuits (ICs). At the board and package level, sequential build-up structures (SBUs) and microvias have been integrated into the manufacture of printed circuit boards (PCBs) as one means of achieving high density interconnections. These features are typically formed on a PCB with alternating dielectric and copper layers. A key to the performance and reliability of these SBUs is the adhesion between the deposited copper and the dielectric materials. Also, new dielectric materials with smoother surfaces (to avoid signal scattering and mechanical disconnects) and enhanced electrical properties (to minimize RC delay and loss) are needed as feature sizes shrink and off-chip frequencies increase. This work investigates traditional epoxy materials and advanced materials in order to find short-term and long-term solutions to these issues by combining mechanical anchoring and chemical bonding to create optimum interfaces in terms of adhesion and roughness.

1.2 Background

The industry requirements of ever-decreasing feature size and increasing off-chip frequency combine to change the needs of metal/polymer interfaces. Polymer surface roughness, for instance, has historically been used to improve adhesion through mechanical anchoring with negligible effects on performance; however in systems with small features and high frequencies this will no longer be the case.[1] High levels of roughness make feature and line fabrication difficult as feature sizes shrink to the same scale as the roughness, while high frequency signals have greater scatter and loss along rough surfaces. Thus, as the feature size shrinks and off-chip frequency increases, the interface between the metal and dielectric material must become smoother. At the same time, adhesion must be maintained to avoid metal delamination and loss of package reliability. In addition, as signal frequency and performance demands increase the need for dielectric materials with improved electrical properties, in particular permittivity and loss, becomes more acute.

These electrical properties have quantifiable effects on the performance of a system. For instance, the dielectric constant, or relative permittivity, which is a measure of the electric flux density of a material when an electric field is applied, affects the RC-delay of a metal line. [2] The velocity of signal propagation depends only on the dielectric constant of the insulator and can be calculated using the following equation.

$$v = \frac{c}{\sqrt{\varepsilon_r}} \tag{1.1}$$

In this equation c is the speed of light, ε_r is the relative dielectric constant of the insulator, and v is the signal propagation velocity. Traditional epoxy materials and epoxy/glass FR4 substrate boards have dielectric constants in the range of 3.7-4.5. As chip and package performance continue to increase, however, this range of dielectric constants and the associated RC-delay becomes unacceptable; thus, lower dielectric constant packaging materials are required. The International Technology Roadmap for Semiconductors (ITRS) projects materials with dielectric constants of 2.5 will be required for build-up structures in the package as soon as 2009.[3] The materials studied in this work have dielectric constants ranging from 2.5 to 3.7.

The loss tangent (or dissipation factor) of a material, which is a measure of the electrical energy dissipated per cycle, also plays a significant role in system performance. The loss tangent can be expressed as the ratio of the real and imaginary portions of the dielectric constant or in terms of conductivity, frequency, and the dielectric constant (Equation 1.2).

$$\tan\delta = \frac{-\varepsilon_{\mathrm{Im}}}{\varepsilon_{\mathrm{Re}}} = \frac{\sigma}{\omega\varepsilon} \qquad (1.2)$$

In this equation $\tan\delta$ is the loss tangent of the dielectric material, $\varepsilon_{\mathrm{Im}}$ is the imaginary part of the dielectric constant, $\varepsilon_{\mathrm{Re}}$ is the real part of the dielectric constant, σ is the conductivity, ω is the angular frequency, and ε is the dielectric constant $= \varepsilon_{\mathrm{Re}} + j\varepsilon_{\mathrm{Im}}$. The importance of the loss tangent to performance is evidenced by the signal loss in the dielectric at high frequencies shown by Equation 1.3.[2]

$$Loss_{DIELECTRIC} = \pi f T_D \tan\theta \tag{1.3}$$

In this equation f is the frequency, T_D is the trace delay, and $Loss_{DIELECTRIC}$ is the signal loss per length of conductor line due to the dielectric material. Dielectric losses increase proportionately to frequencies; thus, at high frequencies an improved loss tangent is required to mitigate dielectric losses.[4]

A second source of signal loss at high frequencies is the skin-effect loss. The skin-effect is a phenomena that occurs at high frequencies when signal propagation occurs mainly on the surface of a conductor and not through the bulk. The skin depth is a measure of the depth below the surface at which the current density drops to 1/e (~37%) of the current density at the surface. It can be calculated for any material at a given frequency using Equation 1.4.[2]

$$\delta_x = 10^9 \sqrt{\frac{\rho}{\pi * f * \mu_0 * \mu_r}} \tag{1.4}$$

where δ_x is the skin depth in nanometers, ρ is the resistivity of the metal in ohm-m, f is the frequency in Hertz, μ_0 is the permeability of free space (1.26×10^{-6} H/m), and μ_r is the relative permeability of the conductor. According to ITRS predictions, off-chip frequencies of 72 GHz will be required by 2020 compared to 2007 industry standards of 3.5-3.8 GHz.[3] This dramatic increase in frequency will correspond to a decrease in the skin depth of copper (Figure 1.1).

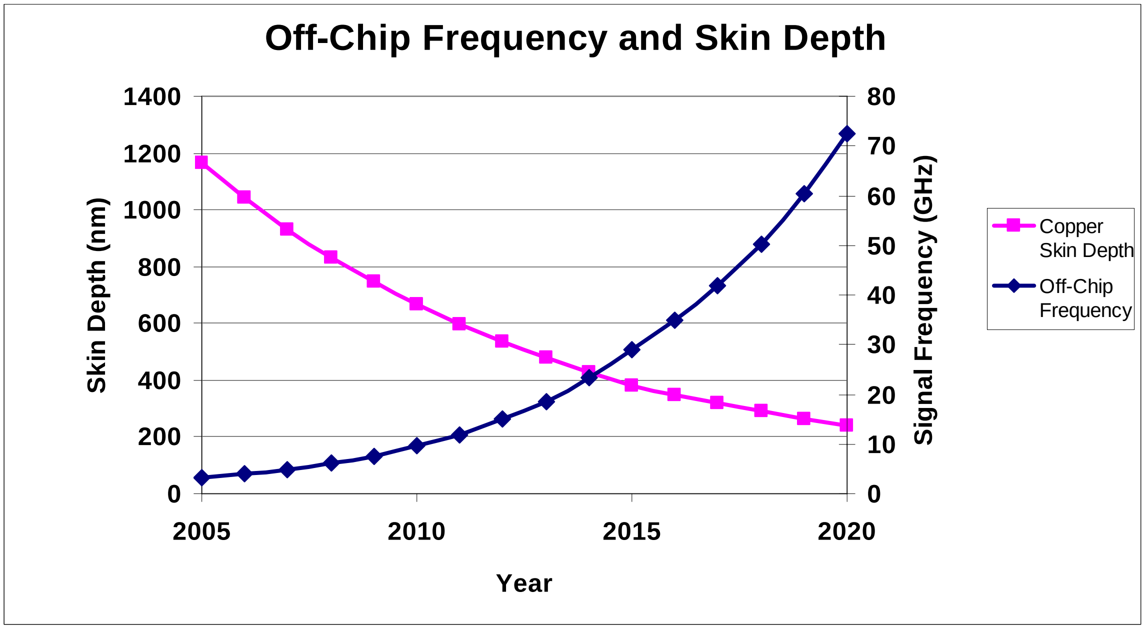

Figure 1.1: Projected Signal Frequency and Skin Depth

Decreasing skin-depth associated with increased signal frequencies leads to a majority of the signal propagating along the surface of the metal conductor lines. The effective cross-sectional area of the conductor is reduced when the signal propagates in this manner, increasing conductor resistance and signal loss as shown in Equations 1.5 and 1.6.

$$R_{SKIN} = \frac{\rho L}{A} \tag{1.5}$$

$$Loss_{SKIN} = \frac{1}{2}\frac{R_{SKIN}}{Z_0}\sqrt{f} \tag{1.6}$$

In these equations R_{SKIN} is the resistance of the conductor accounting for the skin depth, ρ is the conductor resistivity, L is the line length, A is the cross sectional area of signal propagation, Z_0 is the impedance , f is the signal frequency, and $Loss_{SKIN}$ is the signal loss per length of conductor line due to the skin effect.[4] Signal losses caused by signal scatter on rough surfaces also increase when the signal is propagating along the skin of the conductor in this manner. Thus, smoother interfaces between metal lines and the polymer dielectric surfaces are required. Achieving a smooth metal-dielectric interface is especially challenging, however, because adhesion between traditional phenolic epoxy materials and electroless copper is due mainly to the mechanical anchoring provided by a rough interface.[5, 6]

Strong adhesion between an electroless copper layer and a dielectric material is not something that can be eliminated for performance enhancements. Poor adhesion leads to delamination of copper from the dielectric layer and ultimately to the failure of the feature, thereby reducing package reliability. Increasing adhesion, though, is not a simple undertaking as adhesion is a complex issue with many contributing factors. There are six main theories which deal with possible mechanisms for adhesion between any two materials. [7]

1. Mechanical interlocking

   This theory involves simple anchoring of one material by filling of cavities, holes, or tunnels in the surface of the second material.

2. Electronic theory

    Electron transfer occurs between two materials resulting in electrostatic forces which contribute to adhesion

3. Theory of boundary layers and interphases

    Mixing and modifications which inevitably occur at the interface lead to a weak boundary layer with properties which differ from either bulk material.

4. Adsorption theory

    Contribution to adhesion is based on interatomic and intermolecular forces such as van der Waals and Lewis acid-base interactions.

5. Diffusion theory

    Generally applied to polymers, this theory involves diffusion of the polymers into each other creating a separate phase between the two bulk materials

6. Chemical bonding theory

    Ionic or covalent bonding between the two materials provides adhesion.

In many cases a combination of mechanisms is responsible for the overall adhesion observed between two materials. In the system of interest here, metal-polymer adhesion, mechanical interlocking, chemical bonding, and van der Waals interactions can all play a role in adhesion.[1, 8-10] In the specific case of electroless copper adhesion to a dielectric material, contributions from both chemical bonding and mechanical anchoring to adhesion have been observed.[5, 11, 12] Traditional epoxy materials, however, utilize mainly mechanical interlocking, achieved through surface roughening, to enhance adhesion. The required surface roughness in these systems is on the order of

100-500 nm root-mean-square (RMS) roughness, with surface features (such as pores and hillocks) larger than 1 micron.[1, 13] This surface morphology is produced by the multi-step, swell and etch process shown in Figure 1.2.[13]

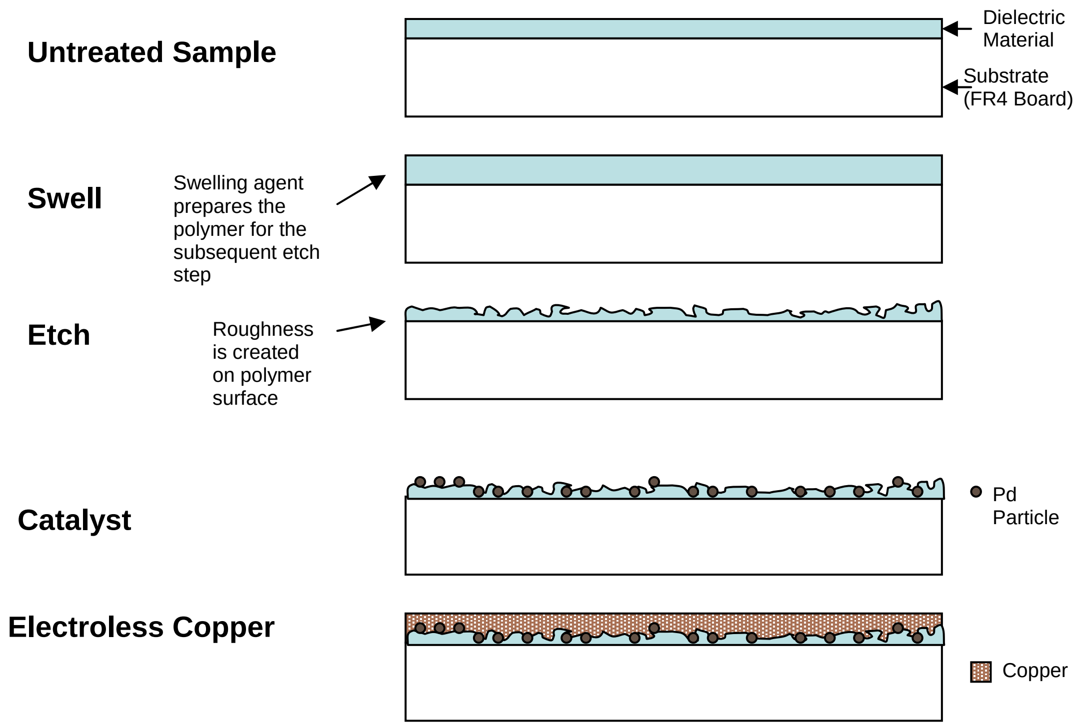

Figure 1.2: Electroless Copper Deposition Process Flow

The first process step, swelling, involves a solution diffusing into the free volume of the polymer. This causes the polymer to swell, reorienting polar groups into packets on the polymer surface.[14] A typical swelling solution consists of aqueous 2-(2-butoxyethoxy)ethanol or a similar substance. The second step, etching, involves an alkaline oxidizing solution containing $KMnO_4$, or an acid oxidizing solution containing

$K_2Cr_2O_7$. During this step the polymer surface is roughened as the etchant is thought to preferentially attack the polar groups of the epoxy surface creating pores, crevices, and tunnels.[5, 14] The etch mechanism, as proposed by Siau et al. is presented in Figure 1.3.[15] This mechanism shows that the etch treatment attacks the ether linkages formed by the opening of epoxide rings during polymer curing. In traditional epoxy materials, these linkages are located in the polymer backbone, allowing each etch reaction to remove significant portions of the polymer chain. As each ether linkage is broken, it exposes the subsequent linkage for attack, allowing the etch process to move down the polymer chain and remove large chunks of polymer, creating the pore-type roughness needed for mechanical anchoring. Following the etch process the sample is immersed in a neutralizing bath that removes any remaining oxidation products from the polymer surface.

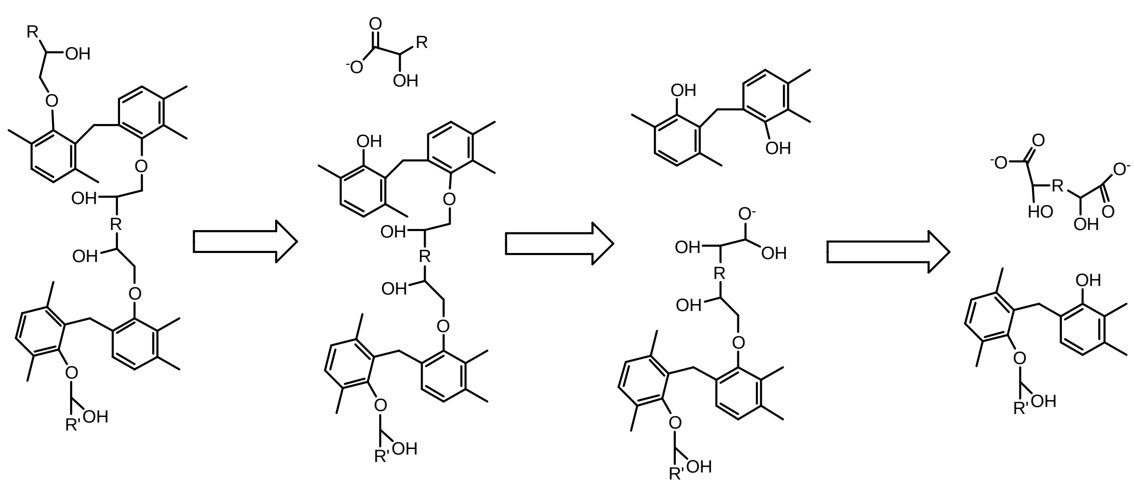

Figure 1.3: Probelec 81/7081 Proposed Etch Mechanism[15]

Advanced epoxies, polyimides and other high performance materials have been shown to have poor adhesion to electroless copper with only these pretreatment steps, mainly because much less surface roughness is created.[16] In order to increase adhesion between these materials and electroless copper, techniques such as plasma surface treatments for chemical and physical modifications of the polymer surface, graft polymerization to insert adhesion improving groups in the polymer structure, coupling agents, and adhesive metal layers have been investigated. These have been applied with varying levels of success, and each approach has advantages and limitations.

Plasma treatments have been used across a variety of materials and with a number of different purposes. Polyimides, poly(tetraflouroethylene), polynorbornene, liquid-crystal polymers, and traditional phenol-novolac epoxies are a few examples of materials of interest as dielectric layers that have been studied with plasma treatments.[5, 17-21] These treatments have been used to increase surface roughness, change surface chemical compositions, and increase adhesion between various metal layers and the polymer surface. With polyimides, Ar and O_2 plasma treatments have been utilized to create roughness on the surface while O_2, N_2, and NH_3 treatments have all been shown to chemically modify the surface and provide catalyst adsorption and adhesion improvements.[17, 22-27] The effect on adhesion has been mixed in these studies, with many treatments increasing adhesion between sputtered metal layers and the polyimide surface while not enhancing catalyst adsorption or adhesion for electroless copper.

Work with other polymer materials shows similar trends. Investigations of Ar, O_2, CHF_3, N_2, NH_3, He, and H_2 plasma treatments with polymer materials have produced a wealth of information on the mechanical and chemical effects of plasma treatments on polymer surfaces.[18, 28-38] These treatments have been shown to increase roughness and modify chemical compositions of the surface, changing bonding configurations of elements already on the surface while also adding nitrogen or oxygen functionalities. Connecting these changes to adhesion, and more specifically to adhesion with electroless copper has not been studied as deeply. Adhesion gains of up to 0.5 N/mm have been achieved with sputtered metals following plasma treatments, typically by adding oxygen containing groups to the surface.[39, 40] Nitrogen containing plasma treatments have been shown to increase catalyst adsorption for electroless copper deposition but there are no detailed studies quantifying the effect on adhesion with electroless copper.[41, 42] Overall, plasma treatments show promise in their ability to chemically modify a variety of polymer materials without significant surface roughening. It is clear from the body of work in the literature that careful consideration of factors such as plasma gas, RF power, and exposure time is required when choosing to use plasma treatments for polymer surface modifications.

Another approach is the addition of functional groups onto the surface of polymers through wet-chemical synthesis as well as ultraviolet, thermal, and plasma grafting processes. Wet-chemical synthesis processes have been used to add organosilanes such as 2-(trimethoxysilyl)ethyl-2-pyridine and 2-(diphenylphosphino)ethyltriethoxysilane, which contain nitrogen groups, to silicon and glass surfaces in order to enable electroless nickel deposition.[43-46] Other work has shown the effect of adding nitrogen containing groups such as iminodiacetic acid, imidazole, and 2-mercaptopyrimidine to a traditional phenol-novolac epoxy surface.[47, 48] These treatments have the advantage of being more cost effective than plasma treatments, but have not been demonstrated to have the same efficacy. Grafting processes have similarly been used to add nitrogen containing groups to a variety of surfaces, including silicon, glass, polytetrafluoroethylene, polyimide, polyethylene, and SiLK.[9, 18, 39, 46, 49-55] Plasma grafting has also been used to add oxygen-containing groups to polymer surfaces for adhesion enhancement with evaporated metal layers.[56-59]

A common link in many of the plasma and wet-chemical investigations is the addition of nitrogen-containing functional groups on the surface. These groups have been shown to enhance catalyst adsorption and adhesion with electroless copper. In many cases these nitrogen groups are thought to interact with the palladium catalyst used for electroless copper deposition and also with the copper layer itself.[17, 39, 55] Details of the interaction between the modified surface and either palladium catalyst particles or electolessly deposited copper have not been determined. With sputtered or evaporated metals, however, it is oxygen containing groups that have been found to be more effective in enhancing adhesion.[58]

A final method for improving adhesion is the application of a thin metal layer between the polymer and Cu to promote adhesion. Chromium, zinc oxide, indium tin oxide, and titanium have all been used to improve adhesion in this manner.[60-63] These metals interact more strongly with the polymer surface than copper, resulting in greater adhesion. The exact mechanisms are still unclear with many researchers believing metals such as chromium form a covalent bond with the polymer.[61, 64, 65] A problem with this approach is the possibility of increased water adsorption in the thin metal layer, which can decrease the reliability of the package. Another issue is the effect of the metal layer on the electrical performance of the features since the metals used for adhesive layers typically have worse electrical properties than copper.[23, 61, 66] Chromium, for instance, has a resistivity of 12.7 mΩ cm, which is nearly eight times higher than copper (1.7 mΩ cm). Recalling the equation for conductor resistance:

$$R_{SKIN} = \frac{\rho L}{A} \tag{1.7}$$

The increased resistivity of any adhesive metal layer will increase the effective resistance of the signal line. As signal frequency rises and skin depth decreases a larger percentage of the signal will propagate in this thin layer, causing ever-increasing line resistance and signal loss.[2, 3] This effect makes the use of adhesive layers more problematic as off-chip frequencies increase dramatically over the coming years; thus, their use will not be explored in this work.

There are a number of possible approaches that can be taken to prepare a polymer surface for plating with electroless copper. Adhesion can be increased through traditional means (surface roughening) or more advanced techniques that take advantage of chemical bonding. The body of work in the literature points to the efficacy of nitrogen-containing functional groups for chemical bonding improvements in terms of both catalyst adsorption and adhesion with electroless copper. The focus of this investigation will also be to increase nitrogen concentrations on the surface in order to take advantage of these findings. This work will be carried out in conjunction with an investigation to increase mechanical anchoring on advanced materials.

The purpose of each of these treatments is to prepare the polymer surface for electroless copper deposition by creating a surface that is more suitable for catalyst adsorption and adhesion. Electroless deposition of copper is a method of metallizing a polymer surface that does not require external applied voltages, vacuum equipment, or seed layers. Instead, deposition of copper occurs through a series of chemical reactions that are facilitated by a catalyst on the polymer surface. Deposition takes place in simple liquid baths, offering the possibility of batch processing for high throughput. These baths are less expensive than the equipment required for other deposition techniques such as the vacuum chambers required for sputter deposition. Electrolessly deposited copper, therefore, offers the advantage of being a simple process with low costs.[67] The general process for preparing a polymer surface for plating is outlined in Figure 1.4. A polymer surface is first prepared to enhance catalyst adsorption and adhesion through any of the techniques discussed previously.

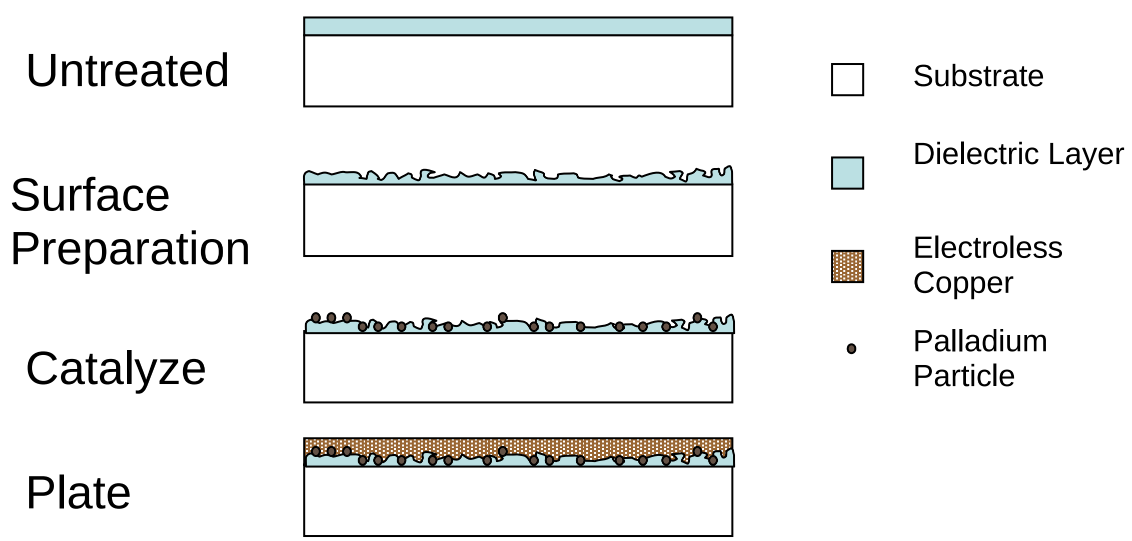

Figure 1.4: Electroless Copper General Process Flow

Once the polymer surface has been prepared for enhanced adhesion, it must be activated with a catalyst, palladium in most cases, in order to enable electroless copper plating. Pd catalyst particles are adsorbed on the polymer surface using a solution containing $PdCl_2$ and $SnCl_2$. The Sn in this solution interacts with surface oxygen, adsorbing onto the surface, and enabling the reduction of Pd from Pd^{2+} to Pd^0 (Equation 1.8).[68] The Pd^0 adsorbs on the polymer surface in small clusters of particles and is an active catalyst for the electroless copper deposition reaction.

$$Pd^{2+} + Sn^{2+} \rightarrow Pd^0 + Sn^{4+} \tag{1.8}$$

Once the surface is activated, copper is deposited only where catalyst is present, making it possible to develop a fully additive build-up process. This type of process creates less waste than global deposition processes, where copper is deposited over an entire surface and etched away where not desired, reducing the environmental hazard and cost of disposing of large quantities of copper etchant. The copper deposition reaction is complex, however, with a number of steps required in order to reduce Cu^{2+} to the metallic Cu^0 on the surface. The typical electroless copper bath contains $CuSO_4$ (copper source), NaOH (pH control), H_2CO (reducing agent), EDTA (stabilizer), and H_2O. The anodic partial reactions, cathodic partial reactions, and the overall reaction for the electroless copper deposition process are presented in Equations 1.9-1.18.[69]

Anodic Partial Reaction:

Hydrolysis of formaldehyde:

$$H_2CO + H_2O = H_2C(OH)_2 \tag{1.9}$$

Dissociation of methylene glycol:

$$H_2C(OH)_2 + OH^- = H_2C(OH)O^- + H_2O \tag{1.10}$$

Dissociative adsorption

$$H_2C(OH)O^- = [HC(OH)O^-]_{ads} + H_{ads} \tag{1.11}$$

Charge transfer

$$[HC(OH)O^-]_{ads} + OH^- = HCOO^- + H_2O + e \tag{1.12}$$

Hydrogen desorption (on Pd or Pt)

$$H_{ads} = H^+ + e^- \tag{1.13}$$

Hydrogen desorption (on Cu)

$$H_{ads} = \tfrac{1}{2}H_2 \tag{1.14}$$

Cathodic Partial Reaction:

Formation of electroactive species

$$Cu[EDTA]^{2-} = Cu^{2+} + EDTA^{4-} \tag{1.15}$$

First electron transfer (rate-determining step)

$$Cu^{2+} = Cu^{+} + e^{-} \tag{1.16}$$

Second electron transfer

$$Cu^{+} = Cu + e^{-} \tag{1.17}$$

Overall Reaction:

$$Cu^{2+} + 2HCHO + 4OH^{-} \rightarrow Cu + 2HCOO^{-} + H_2 + 2H_2O \tag{1.18}$$

The deposition of copper begins on the adsorbed catalytic palladium clusters and continues until the surface is uniformly coated. The initial reactions include desorption of hydrogen as shown in Equation 1.13 due to the presence of palladium at the reaction site. Once this palladium has been completely covered the reaction continues on the copper surface, which is also a catalyst for the reaction, with the hydrogen desorption step transitioning to that shown in Equation 1.14. The rate of the copper deposition reaction can be controlled by temperature, additives, and pH. Temperature affects the kinetics of each partial reaction thereby creating significant changes in reaction and deposition rates. Additives, meanwhile, can have accelerating or decelerating effects on the copper deposition, guanine and adenine have been shown to accelerate plating while other additives such as dipyridyl and NaCN have been shown to have an inhibiting effect on plating rate.[70-73] These additives also play a role in the microstructure of the copper deposits by affecting copper grain size, ductility, and resistivity. The pH of the solution has the most direct effect on the rate of deposition, mainly due to the role of the OH^- group as a reactant in both the methylene glycol dissociation reaction (Equation 1.10) and in the charge transfer reaction (Equation 1.12). The plating rate of a typical formaldehyde-based electroless copper bath has been shown to increase nearly ten-fold by increasing pH from 11.5 to 12.5.[69] In this study, the electroless copper bath conditions were maintained to ensure consistent plating rates and copper quality through all samples tested. The details of these conditions are discussed in the experimental section of this report.

1.3 Research Objectives

Based on the background information discussed above, there are a number of key objectives in this research project. Each is a step towards the ultimate goal of advanced dielectric materials with smooth surfaces and strong adhesion to electroless copper, as required for future microelectronic devices. The first objective is the development of an understanding of the mechanisms responsible for adhesion at the interface between electroless copper and the dielectric material. Understanding these mechanisms, and quantifying the contribution of each to adhesion, is a key to designing materials and processes with optimal interfaces in terms of roughness and adhesion. A second objective is to minimize surface roughness requirements for traditional epoxy materials. This is a short-term solution to the problems discussed in this chapter. Traditional epoxy materials, with their high dielectric constants and loss tangent values, can continue to be used in the near future if roughness can be reduced while maintaining adhesion. These materials are not a long-term solution because of their poor electrical properties, which will cause unacceptable performance problems as feature sizes continue to shrink and signal frequencies increase. A long-term solution is to utilize advanced dielectric materials with enhanced electrical properties. In order to enable these materials two main advances must be made: increased catalyst adsorption and increased adhesion with electroless copper. This report focuses on understanding and addressing these four objectives in order to create optimum systems with enhanced dielectric materials, smooth surfaces, and strong adhesion.

This thesis will present the results of the research done towards achieving these objectives in a systematic manner. Chapter 1 has presented an overview of the motivation for the project as well as the relevant background information needed to understand the challenges that must be overcome and the approaches that will be taken. Chapter 2 discusses the materials, processes, and analytical techniques used to investigate adhesion enhancement. Chapter 3 focuses on plasma treatments with a polyimide material, PI2555. These treatments were used to independently create chemical and morphological changes on the polymer surfaces for increased catalyst adsorption. Chapter 4 presents results from work done on traditional and advanced epoxy materials. This work encompasses wet-chemical treatments, plasma treatments, and combined treatment protocols to enhance adhesion. An attempt to quantify individual contributions of chemical bonding and mechanical anchoring to adhesion is made in this chapter as well. Finally, Chapter 5 offers a summary of the progress made in this research project and offers directions for future work. Thus, a comprehensive understanding of the challenges faced in the electroless copper/dielectric system, as well as a number of approaches for solving these problems is presented.

CHAPTER 2

EXPERIMENTAL

In this chapter a detailed review of experimental procedures and analysis techniques used to investigate adhesion between electrolessly deposited copper and dielectric materials is presented. The conditions used to fabricate polymer surfaces and treat those surfaces to enable electroless copper plating and adhesion are discussed. Processes and solution recipes for electroless and electroplating of copper are presented. Finally the analysis techniques utilized to monitor the conditions of interest on the surfaces are detailed.

2.1 Materials

Four polymer systems have been studied in this investigation: PI 2555 (HD Microsystems); Probelec 81/7081 (Huntsman); Avatrel 2190P (Promerus LLC.); and a blend of Avatrel 2190P and Probelec 81/7081 (henceforth identified as AP blend). The PI 2555 is a BTDA-ODA-MPD polyimide with the structure shown in Figure 2.1. Probelec 81/7081 is a traditional phenol-novolac epoxy (Figure 2.2) and Avatrel 2190P is a norbornene-based epoxy (Figure 2.3). A list of material properties for each of these polymers can be found in Table 2.1. Other materials used in this study are summarized in Table 2.2 with manufacturer name and application specified for each material.

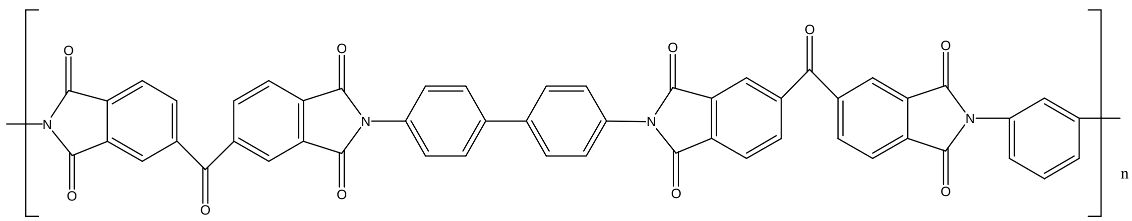

Figure 2.1: Polyimide PI 2555 chemical structure

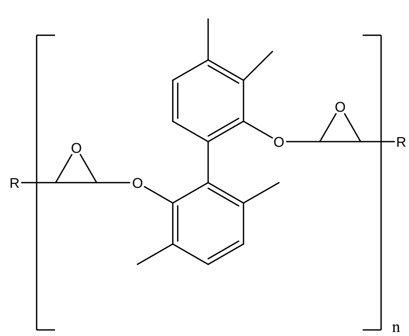

Figure 2.2: Probelec 81/7081 chemical structure

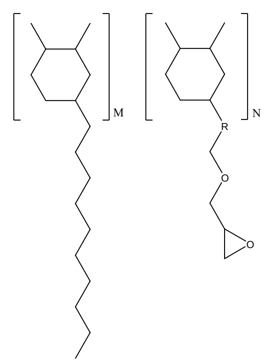

Figure 2.3: Avatrel 2190 P chemical structure

Table 2.1: Polymer properties[74-76]

Material	Dielectric Constant	Loss Tangent
Probelec 81/7081	3.6	0.025
PI 2555	3.3	0.002
Avatrel 2190 P	2.55	0.01

Table 2.2: List of Materials and Suppliers

Product	Supplier	Process Step/Application
G200	Isola	BT board
Silicon Wafer		Wafer Substrate
PI-2555	HD Microsystems	Polyimide Dielectric Material
Probelec 81/7081	Huntsman	Epoxy Dielectric Material
Avatrel 2190P	Promerus LLC.	lorbornene-based Dielectric Materia
VM-652	HD Microsystems	Adhesion Promoter
Circuposit MLB 211	Shipley	Swell
Cuposit Z	Shipley	Swell
Circuposit 3308A	Shipley	Etch
Circuposit 3308B	Shipley	Etch
Circuposit 3314	Shipley	Neutralize
Cataprep 404 Salts	Shipley	Pre-Dip and Catalyst
Cataposit 44	Shipley	Catalyst
Circuposit 3350 A	Shipley	Electroless Copper
Circuposit 3350 B	Shipley	Electroless Copper
Circuposit 3350 M	Shipley	Electroless Copper
PC-2000 Carrier	Shipley	Electroplating
PC-2000 Brightener	Shipley	Electroplating
Copper Sulfate	Sigma-Aldrich	Electroplating
Sulfuric Acid	Sigma-Aldrich	Electroplating
Copper Foil (349151-11g)	Sigma-Aldrich	Copper Plating Anode

2.2 Polymer Processing

The four polymer materials were processed in a similar method. The work began with a substrate material, either a glass fiber and epoxy board (FR-4) or a silicon wafer, onto which was spin-coated a thin layer of the polymer material. The spin speed, acceleration, and duration were varied in order to create films with approximate thicknesses of 8 μm for the polyimide and 15 μm for the epoxy materials. Spin speed curves for all three materials are presented in Figures 2.4-2.6. Following spin coating the polymers were cured with the processing steps detailed in Table 2.3. Blends of Avatrel and Probelec (AP blends) were prepared by mechanical mixing of the two materials for 24 hours. This was followed by ultrasonic agitation for 0-8 hours and one final hour of mechanical mixing. After all mixing steps were completed the AP blend was spin-coated and cured using the same conditions as the pure Avatrel 2190P material.

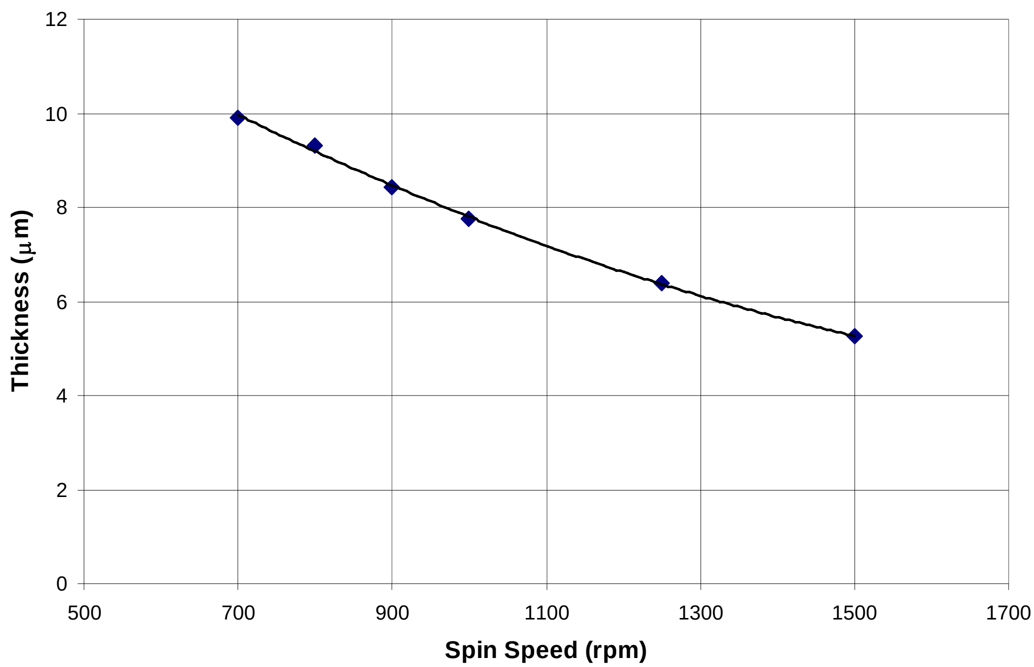

Figure 2.4: Polyimide 2555 spin speed versus film thickness curve.

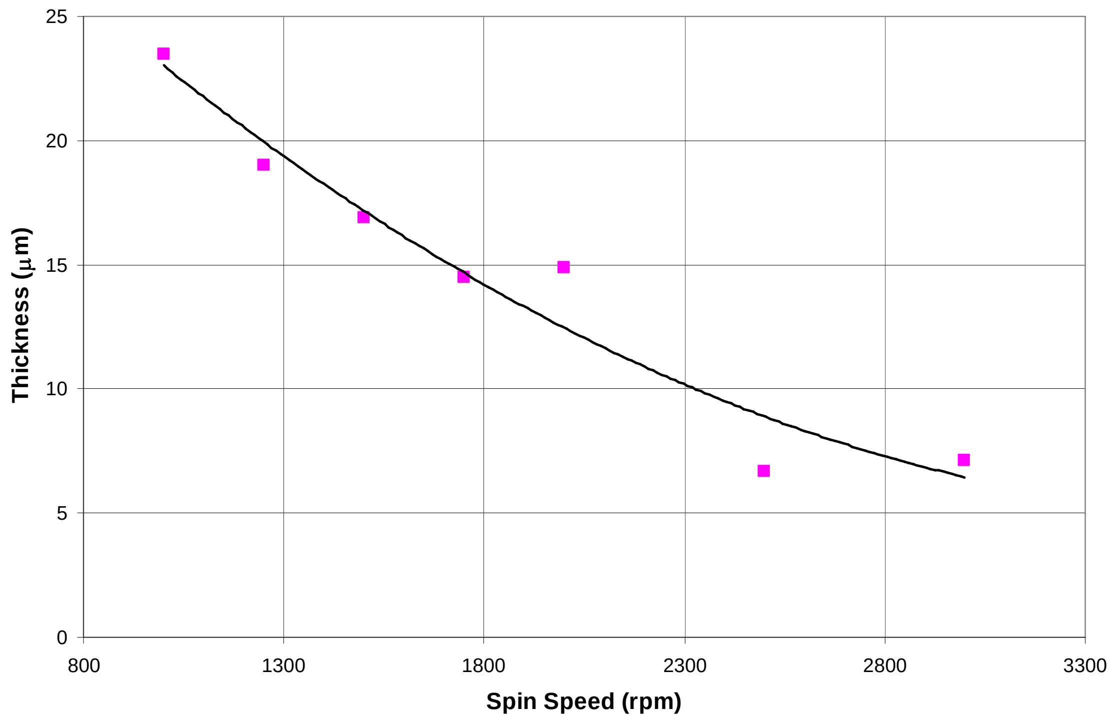

Figure 2.5: Probelec 81/7081 spin speed versus film thickness curve.

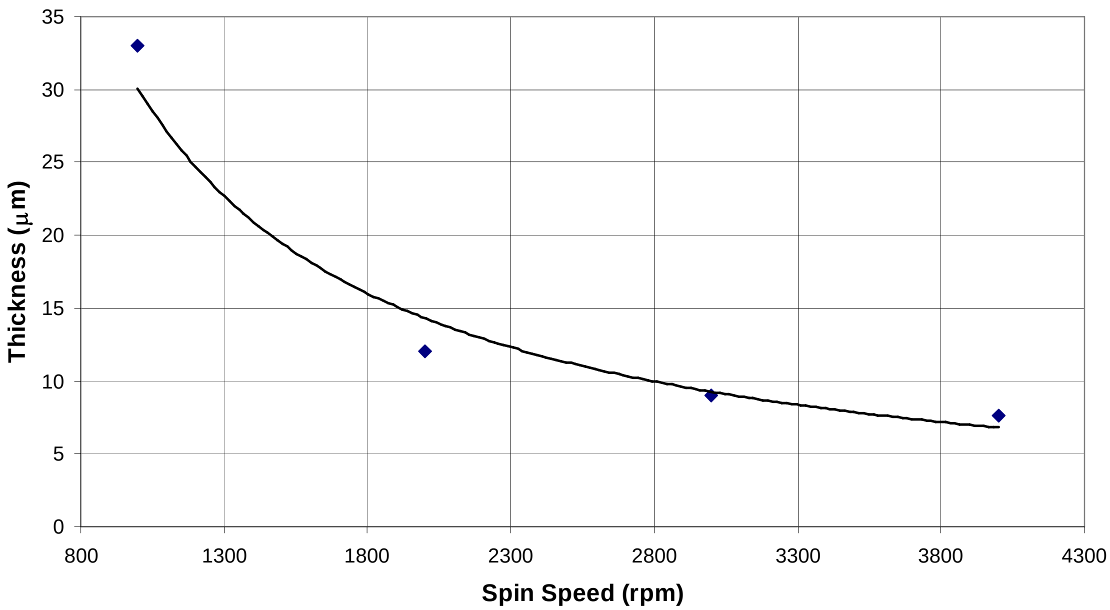

Figure 2.6: Avatrel 2190P spin speed versus film thickness curve.

Table 2.3: Polymer cure process conditions

Material	Soft Bake	Exposure Dose	Hard Bake	Cure
PI2555	3 min @ 100 C	None	None	3C/min ramp to 350 C hold for 1 hour (N_2 ambient)
Probelec 81/7081	30 min @ 100 C	1400 mJ/cm^2	60 min @ 100 C	55 min @ 145C (air ambient)
Avatrel 2190P	10 min @ 100 C	200 mJ/cm^2	20 min @ 100 C	3C/min to 160 C hold for 1 hour (N_2 ambient)

Wet-chemical treatment processes have been utilized in this work in order to roughen polymer surfaces. Specifically this process consists of three steps; swelling, etching, and neutralizing. The sweller treatment consists of Shipley Circuposit MLB 211 (20% vol.), Shipley Cupozit Z (10% vol.) and the remainder DI water. This process is performed at 80 ^{0}C with constant stirring for a variable amount of time (0-10000 seconds). The next step is an etch bath consisting of Shipley Circuposit 3308A (10% vol.), 3308B (15% vol.), and the remainder DI water. This process step is also performed at 80 ^{0}C with constant stirring for a variable amount of time (0-10000s). The third step is a neutralizing bath consisting of Circuposit 3314 (15% vol.), hydrogen peroxide (5% vol.), and the remainder DI water.

Plasma treatments were also utilized for polymer surface modifications. Plasma enhanced chemical vapor deposition (PECVD) with NH_3 was conducted in a Unaxis PECVD chamber, while reactive-ion etching (RIE) with Ar was conducted in a Plasma-Therm chamber. The typical NH_3 plasma treatment parameters were: 20 sccm NH_3 flow rate, 200 mTorr chamber pressure, 150^{o}C substrate temperature, 30-200 W RF power, and 0.5 to 5 min treatment times. The Ar RIE parameters were: 200 sccm Ar flow rate, 250 mTorr chamber pressure, 25^{o}C substrate temperature, 50-400 W RF power, and a 5 min treatment time. Combined wet-chemical and plasma treatments were performed sequentially, with the wet-chemical treatments followed by plasma treatments for greatest efficacy of each.

Following wet-chemical or plasma surface treatments samples were activated in a catalyst bath and electrolessly plated with copper. Both of these processes were performed with standard industry solutions purchased from Shipley. The specific products used and their concentrations can be found in Table 2.4. Samples were rinsed in a predip bath for 2 minutes at room temperature then immediately immersed in the catalyst bath, which was maintained at 46 ^{o}C, for 5-30 minutes. Samples were thoroughly rinsed with DI water for 2 minutes following catalyst activation. They were then placed in the electroless copper bath, maintained at 46 ^{o}C, for 5-300 seconds in order to plate a continuous layer of electroless copper on the surface. Following electroless copper deposition the samples were annealed for 1 hour at 150 ^{o}C under ambient air. Electroplating was performed to increase copper thickness to 40 μm, using the solution recipe given in Table 2.3 with a current density of 0.026 A/cm2 at room temperature with mechanical stirring and nitrogen bubbling. Following electroplating samples were annealed for 1 hour at 150 ^{o}C under ambient air conditions.

Table 2.4: Solution components and recipes

Solution	**Components**			
Swell	Circuposit MLB 211 (20%)	Cupozit Z (10%)	DI Water (70%)	
Etch	Circuposit 3308 A (10%)	Circuposit 3308 B (15%)	DI Water (75%)	
Neutralize	Circuposit 3314 (15%)	35% Hydrogen Peroxide (5%)	DI Water (80%)	
Pre-Dip	Cataprep 404 Salts (XXX gms)	350 ml DI Water		
Catalyst	Pre-Dip Solution (97%)	Cataposit 44 (3%)		
Electroless Copper	Circuposit 3350 A (4.2%)	Circuposit 3350 B (10%)	Circuposit 3350 M (12%)	DI Water (73.8%)
Electroplating Copper	Copper Sulfate (80 g/L)	Sulfuric Acid (225 g/L)	Sodium Chloride (75 mg/L)	DI Water (remainder)

2.3 Analysis Techniques

In order to analyze the polymer surfaces and quantify adhesion a number of analysis techniques have been utilized. The first of these techniques is atomic force microscopy (AFM), which has been used to quantify surface roughness and qualitatively observe the surface morphology. AFM analysis produces a 3-dimensional image of the sample surface that can be used to quantify surface roughness through root mean square (RMS) roughness calculations. A sample image is shown in Figure 2.7. RMS roughness is calculated using the following formula[77]:

$$R_{rms} = \sqrt{\frac{1}{n}\sum_{i=1}^{n}\left(h(x_i) - \bar{h}\right)^2} \tag{2.1}$$

Where n is the number of lattice points, $h(x_i)$ is the height function across the surface and $\bar{h}$ is the average height defined as:

$$\bar{h} = \frac{1}{n}\sum_{i=1}^{n} h(x_i) \tag{2.2}$$

AFM images were gathered using two different pieces of equipment, a Veeco AFM (Model Nanoscope IIIa) system and a Molecular Imaging Picoplus system. The AFM tip diameter was 40 nm for the Veeco machine and less than 10 nm for the Picoplus. In all cases, AFM measurements were taken in tapping mode.

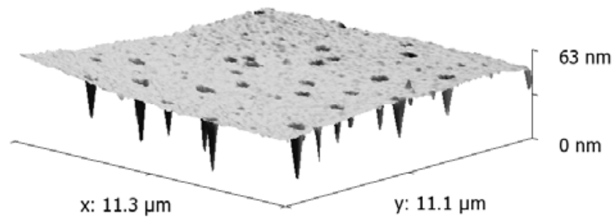

Figure 2.7: Sample AFM image of a polymer surface

SEM images of the polymer surfaces were used to aid in qualitative analysis of surface modifications caused by wet-chemical treatments. A Zeiss SEM (Model Ultra 60) was utilized for these imaging experiments. The advantage of the SEM comes from the large range of magnifications possible with one experimental setup. The AFM has a limited scan window of 100 μm^2, while the SEM can be used at magnifications as low as 10X and as high as 250,000X with resolution of 1 nm. This allows the user to identify large features (>50 µm) located sporadically across the surface as well as small features (<1 µm), giving a more complete picture of surface topography. Figures 2.8-2.10 illustrate the ability of the SEM to identify large features at low magnification and image those same features in high resolution and at high magnification.

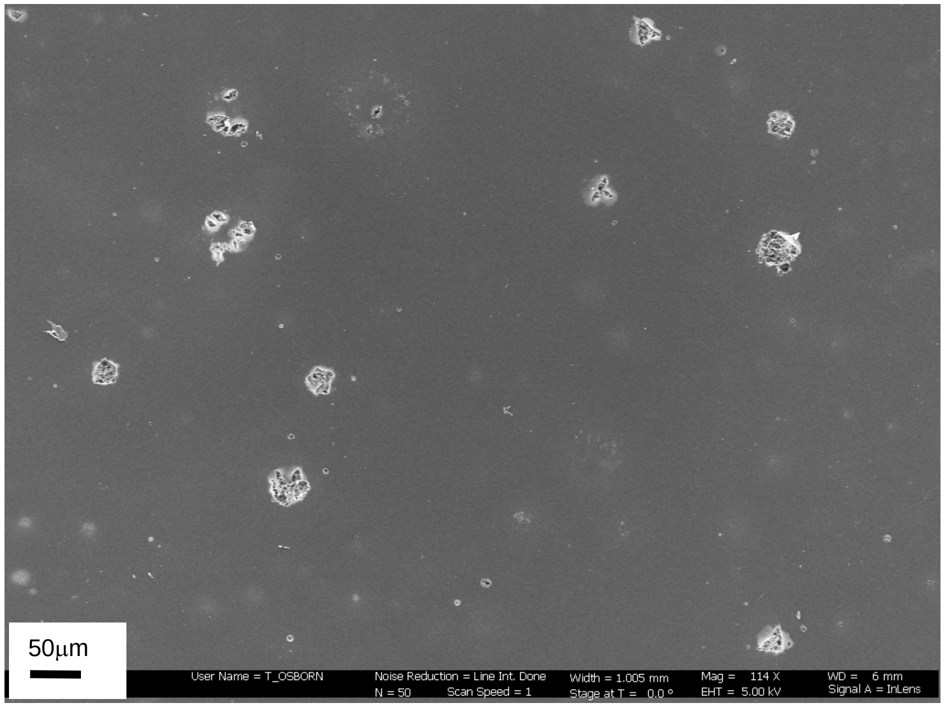

Figure 2.8: Sample SEM image taken at a magnification of 114X

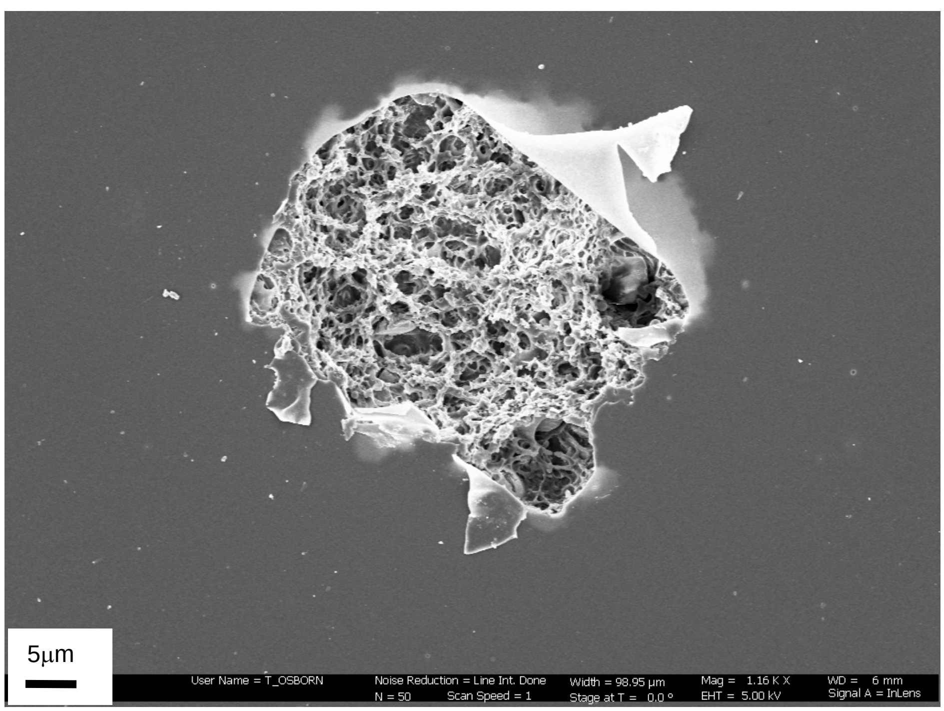

Figure 2.9: Sample SEM image of large feature on a polymer surface (1160X magnification)

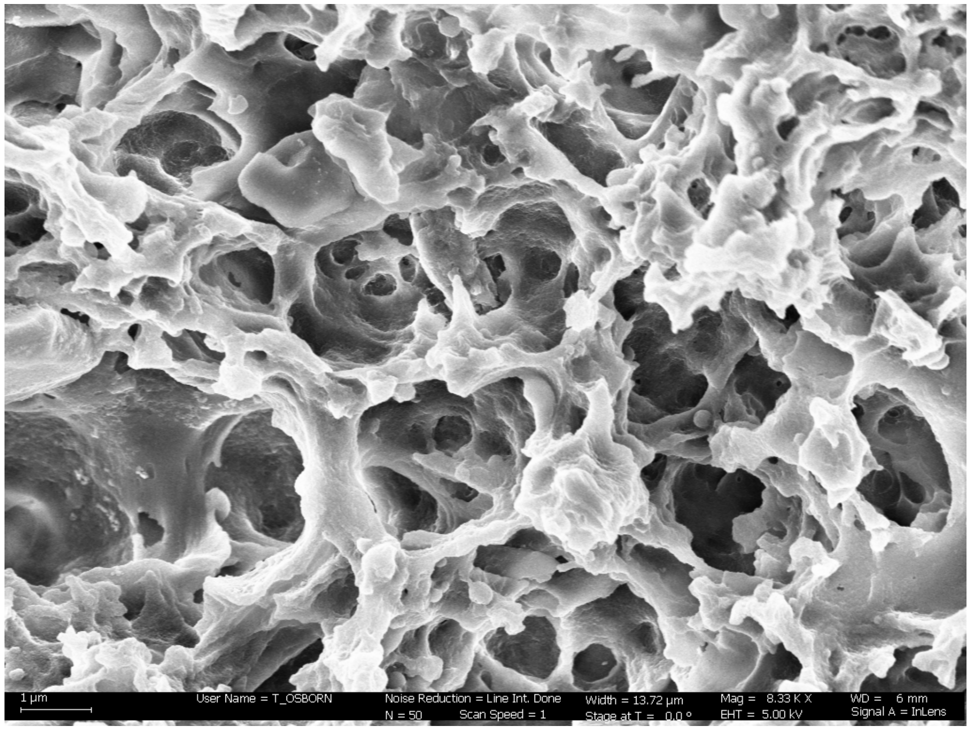

Figure 2.10: Close-up SEM image of large feature on polymer surface (8330X Magnification)

In order to analyze chemical modifications of the polymer surfaces x-ray photoelectron spectroscopy (XPS) was employed. A Perkin Elmer XPS system (Model PHI 1600) was used for these experiments. XPS analysis is a surface sensitive technique that can be used to measure chemical compositions and bonding states in the top 5-10 nm of a sample. XPS proceeds by exposing a sample surface to photons that have the energy given in Equation 2.3. In this equation E is the energy of the photon, h is Plank's constant, and v is the frequency of the radiation in Hz

$$E = hv \tag{2.3}$$

These photons are absorbed by an atom, which leads to the emission of a core electron. The kinetic energy of this emitted electron is then measured with an electron energy analyzer and compared to the energy of the photoelectron employed. This difference is the binding energy of the electron (Equation 2.4).

$$BE = h\nu - KE \tag{2.4}$$

Where BE is the electron binding energy, and KE is the measured kinetic energy of the photoelectron. There is a unique binding energy associated with every core orbital for each element, thus specific elements and bonding configurations can be determined from this binding energy data. Figure 2.11 presents a sample of a XPS survey scan charting photoelectron binding energy (in electron volts) on the X-axis and signal intensity (in arbitrary units) on the Y-axis. In this sample, there are intensity peaks present at binding energies of 285 eV (corresponding to carbon), 398 eV (nitrogen), and 531 eV (oxygen) indicating that these three elements are present on the surface.

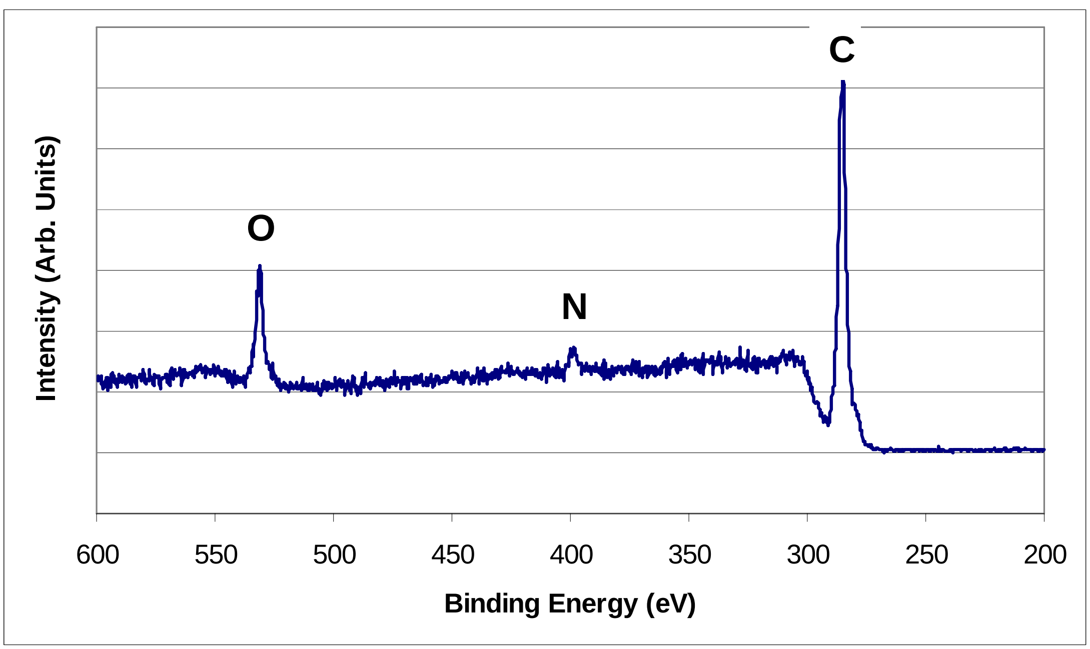

Figure 2.11: XPS survey scan

Looking at each binding energy peak in more detail can allow users to determine specific bonding states of elements on a sample surface. Figure 2.12 shows a sample of a N1S spectrum that shows the presence of two peaks representing different bonding configurations. In this case these bonding configurations correspond to N-C (398.4 eV) and N=C (399.5 eV) indicating that these two bonding configurations of nitrogen are present in this sample.

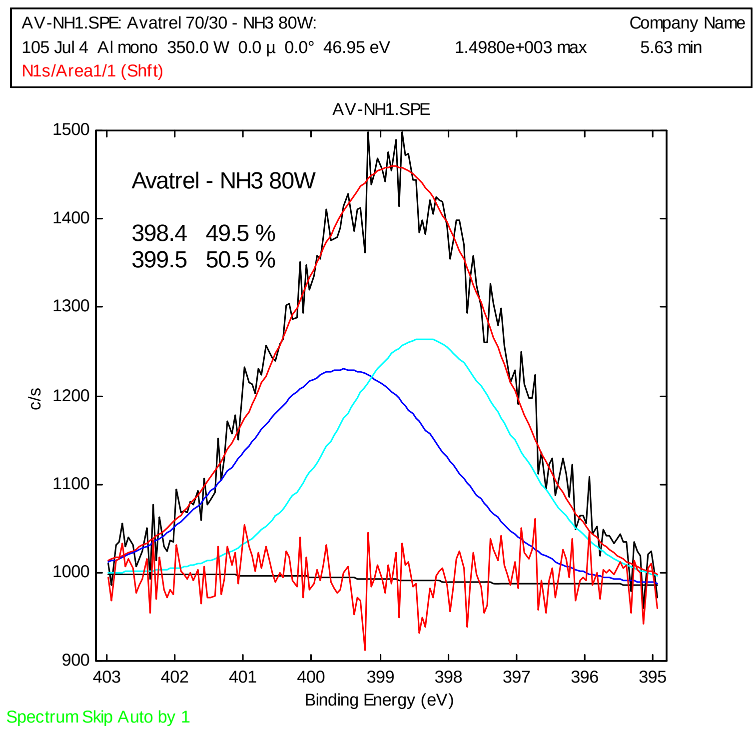

Figure 2.12: Sample XPS N1S spectrum.

Ninety degree peel tests were performed in order to quantify adhesion between the deposited copper layer and the dielectric materials. A uniform 40 µm layer of copper was plated on each sample before peel testing in order to maintain consistency from sample to sample and provide mechanical stability of the copper layer. Following ASTM B 533-85 copper is peeled at a rate of 25 mm/min and a force versus extension chart is produced.[78] Figure 2.13 shows a sample peel force versus extension chart with data in blue, the average value of this data is represented by the red line. This average force is calculated and divided by the width of the peel strip to give a peel strength in units of N/mm. The sample preparation and equipment setup is presented in Figure 2.14. This test method is widely used for quantifying adhesion both in industry and literature, making it suitable for comparison across many studies.

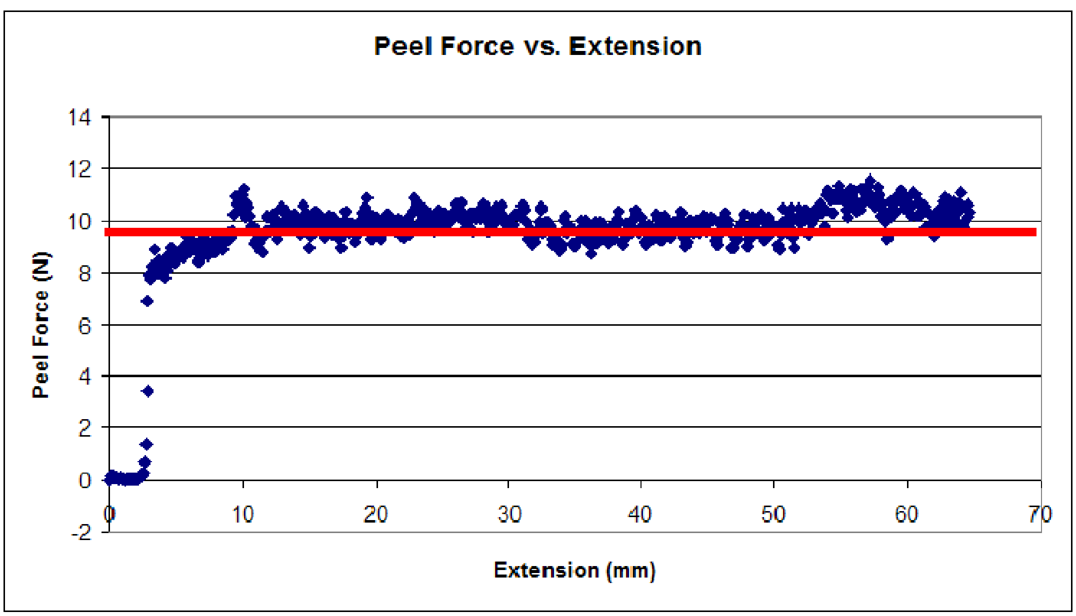

Figure 2.13: Sample Peel Force vs. Extension Chart

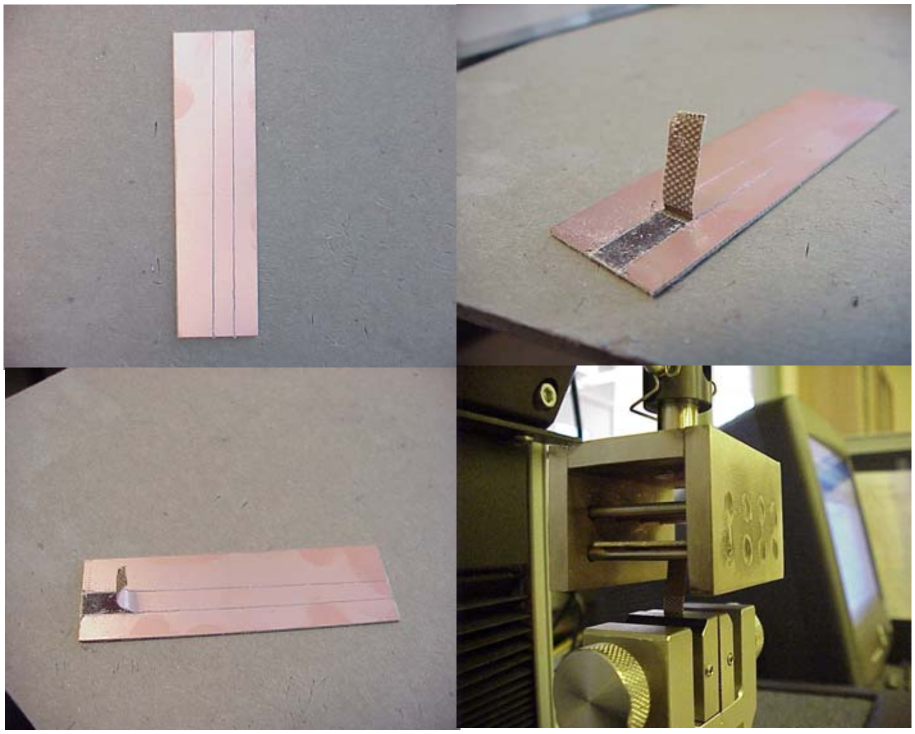

Figure 2.14: Peel test sample preparation and equipment set up: A) Sample with scored lines for peel strip; B) Sample with peel tab started; C) Sample ready for peel test apparatus; D) Peel test apparatus with sample during testing.

CHAPTER 3

PLASMA SURFACE TREATMENTS WITH A POLYIMIDE

3.1 Objective

The effect of surface treatments on catalyst adsorption and the adhesion between electrolessly deposited copper and polyimide (PI) films is explored in this chapter. PI films are subjected to one of three plasma treatments: NH_3 plasma, Ar-ion reactive ion etching (RIE), or Ar RIE followed by NH_3 plasma. The NH_3 treatment is conducted in a plasma-enhanced chemical vapor deposition (PECVD) chamber on a grounded electrode under low power conditions. The NH_3 plasma conditions are designed to chemically modify the surface of the polymer without significant surface roughening by maintaining low powers (30-80W) that produce minimal ion bombardment.[23] The Ar RIE treatment occurs on a powered electrode, allowing for higher energies of ion bombardment and increased physical etching. Thus, the Ar RIE provides mechanical roughness increases with minimal chemical modifications.[17] Any chemical modifications occurring during the RIE treatment are caused by differential sputtering and ion-bombardment induced reordering. The combined Ar and NH_3 treatment endeavors to combine the beneficial effects of each individual treatment producing a roughened surface with enhanced chemical bonding. In order to optimize the plasma treatments plasma power, chamber pressure, and treatment time were varied. Atomic force microscopy, X-ray photoelectron spectroscopy, and 900 peel tests were utilized to quantify the effectiveness of plasma treatments.

3.2 Background

Polyimides are an important class of polymers for microelectronics applications, specifically as inter-level dielectric materials, because of their excellent properties. The conventional swell and etch treatment, however, has been found to be ineffective when attempting to activate the PI surface for electroless Cu deposition. The PI backbone is not susceptible to chemical attack with the standard etch solutions; thus, several alternative surface treatments have been attempted in order to activate the PI surfaces.[16] In work performed by Okamura et al.[79], a KOH treatment has been used to cleave the imide ring of the PI creating carboxyl and amide groups on the PI surface, which presumably, enhances adhesion with electroless copper. A combined KOH and standard swell and etch treatment improves the adhesion by a factor of five to a value of ~150 N/m. However, this treatment not only affects the surface of the polymer, but also cleaves the imide rings deep in the bulk of the material if the treatment time is not closely controlled. Modification of the PI by graft copolymerization with amines has been attempted in order to add the adhesion promoting groups to the PI backbone.[54, 80-82] This approach has improved the adhesion strength between copper and PI to 40-60 N/m. Adhesive layers of other metals such as chromium, zinc, tin, and indium have been used at the PI - electroless metal interface, and the strength of adhesion improved to several hundreds of N/m.[64, 65, 83]

The use of plasma treatment to produce chemical and physical surface modifications of polymers has been widely reported. PIs have been subjected to Ar, O, N, and NH_3 plasma treatments in order to make the polymer surface more reactive towards electroless copper deposition and improve adhesion.[22-27] Ion-beam treatment of PIs with oxygen, nitrogen, and argon ions have been reported to increase the surface concentration of the respective species at low ion energies, while high ion energies result in differential sputtering leaving the surface carbon-rich.[23] The argon-ion reactive ion etching (RIE) treatment has been shown to decrease the surface nitrogen and oxygen concentration and results in rearrangement of the surface nitrogen bonding to form >C=N- and pyridine-like species on the PI surface.[24] Oxygen RIE treatment has been shown to increase the surface oxygen concentration by 70-180%, while nitrogen and carbon concentrations decrease by 10-30%. The oxygen plasma treatment is also reported to increase the oxygen surface concentration and the carbonyl bonding on the surface.[25] Further, interactions of the modified and unmodified PI surfaces with various metals such as chromium, aluminum, germanium, and copper have also been studied for electroless copper deposition.[61, 84-86] The increase in surface nitrogen concentration brought about by N_2 or NH_3 plasma treatment has been found to be beneficial, resulting in improved adsorption of the catalysts Sn and Pd.[87] Nevertheless, a detailed study of the modification in surface chemical composition and morphology of PI surface with various plasma treatments has not been reported so far. Further, a detailed understanding of the interactions between surface chemical states of PI and metals such as tin, palladium, and copper is also necessary to determine the mechanism for improving the adhesion strength between PI and copper. In this study, a detailed analysis of the PI surface with different plasma treatments, such as NH_3 plasma and Ar RIE, through each step of the electroless copper deposition process has been carried out and the effect of these treatments on adhesion has been measured.

3.3 Results

Figure 3.1 presents XPS survey scans of the polyimide surface with the following treatments: A) No Treatment; B) 80 W NH_3 plasma; C) 150 W Ar; and D) 150 W Ar followed by 30 W NH_3. Each scan shows the presence of carbon, oxygen, and nitrogen, the three elements present in the untreated polyimide. The presence of a silicon impurity can also be seen in each scan which is the result of residuals in the chamber. The morphology and magnitude of roughness development for each of these samples can be observed in the AFM images presented in Figure 3.2. The untreated polyimide shown in Figure 2A is relatively smooth with a root-mean-square (RMS) roughness of 0.4 nm. Subsequent plasma treatments roughen the surface to varying degrees. The 80 W NH_3 plasma increases roughness to 2.9 nm (Figure 3.2B), the 150 W Ar treatment increases roughness to 17.6 nm (Figure 3.2C), and the combined 150 W Ar and 30 W NH_3 treatment produces roughness of 18.3 nm (Figure 3.2D).

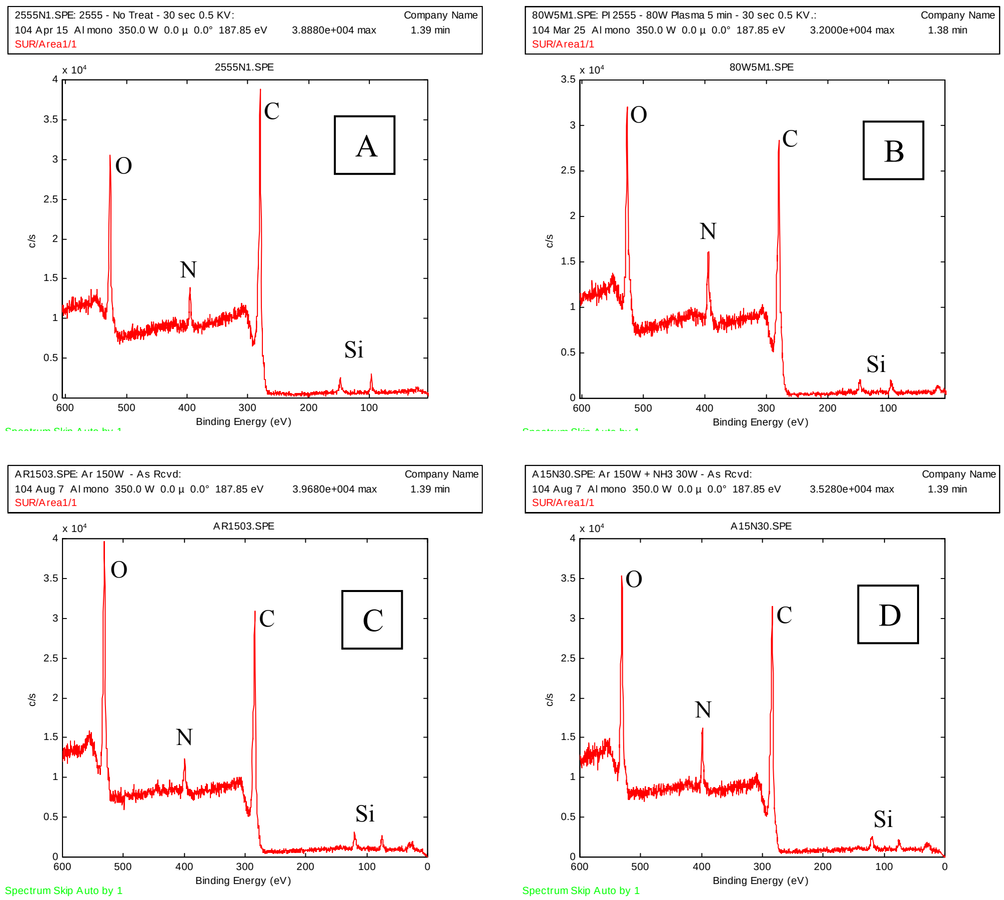

Figure 3.1: XPS spectra of PI samples with plasma treatments: A) No Treatment; B) NH_3 80 W Plasma; C) Ar 150 W RIE; and D) Ar 150 W RIE followed by NH_3 30 W Plasma.

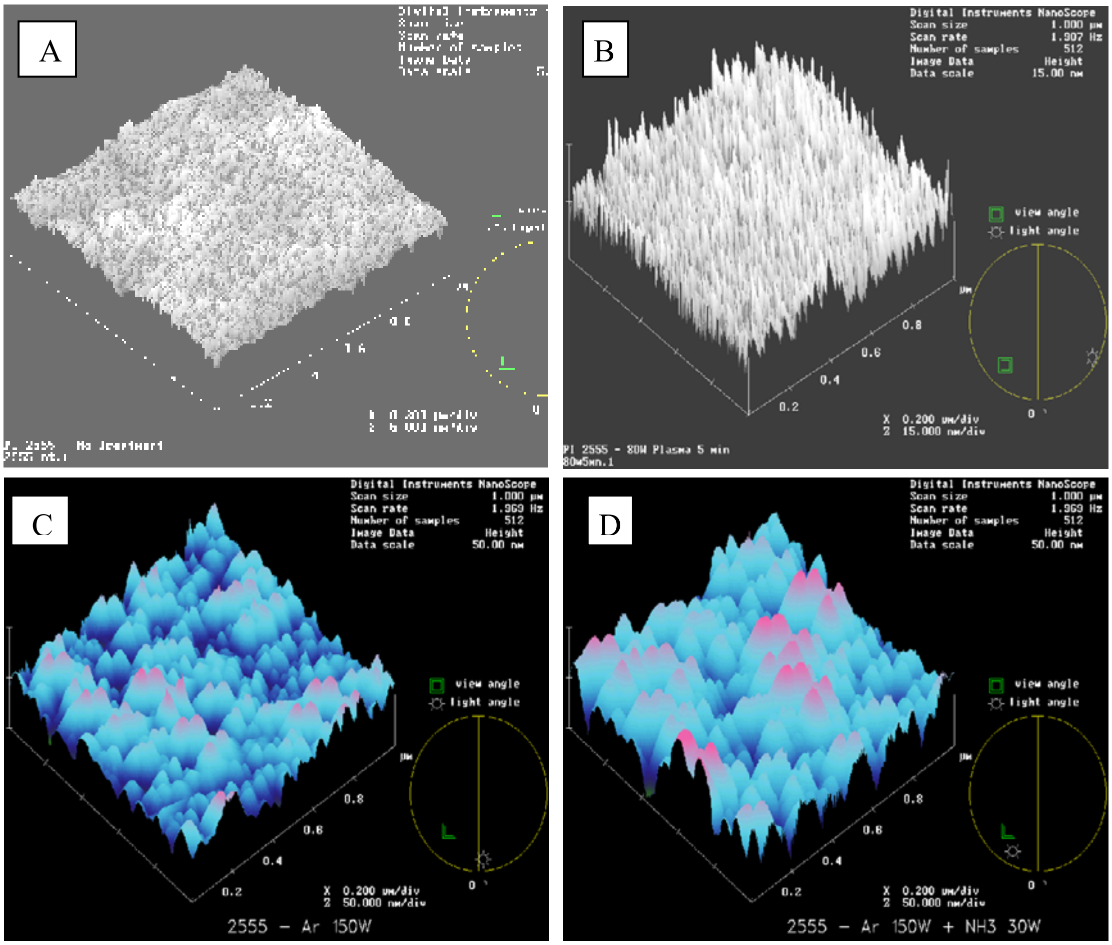

Figure 3.2: AFM images and RMS roughnes values of PI films following plasma treatments: A) No Treatment (Rrms = 0.4 nm); B) NH_3 80W Plasma (Rrms = 2.9 nm); C) Ar 150 W RIE (Rrms = 17.6 nm); and D) Ar 150 W RIE followed by NH_3 30 W Plasma (Rrms = 18.3 nm).

The quantitative results from all XPS spectra and AFM scans with varying plasma treatments are presented graphically in Figures 3.3-3.6. These figures display the atomic concentrations of nitrogen (Figure 3.3), carbon (Figure 3.4), and oxygen (Figure 3.5) as well as the RMS roughness for each treatment (Figure 3.6) as a function of plasma power.

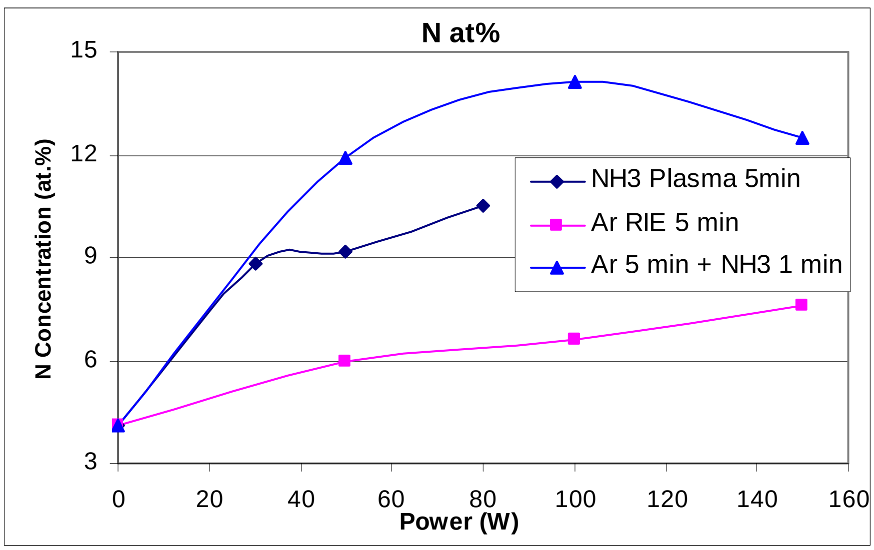

Figure 3.3: Variation in the surface concentration of nitrogen with plasma power.

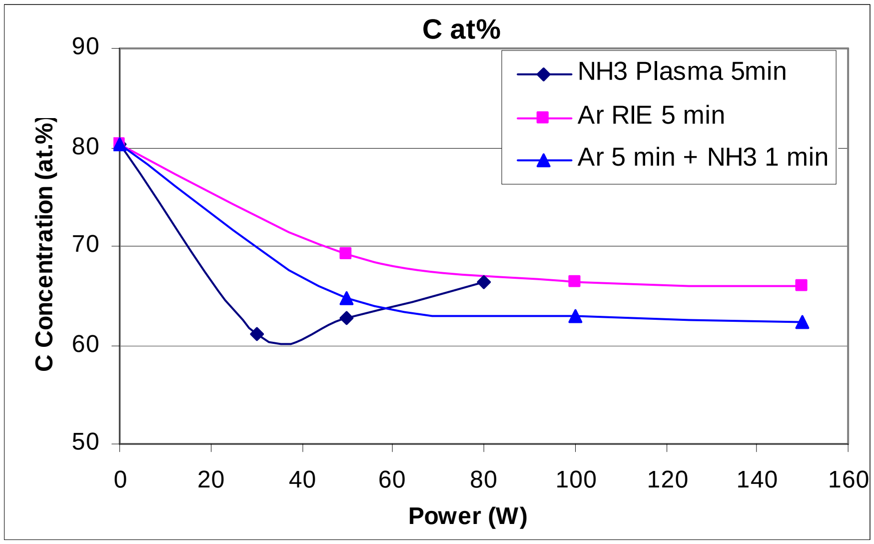

Figure 3.4: Variation in the surface concentration of carbon with plasma power.

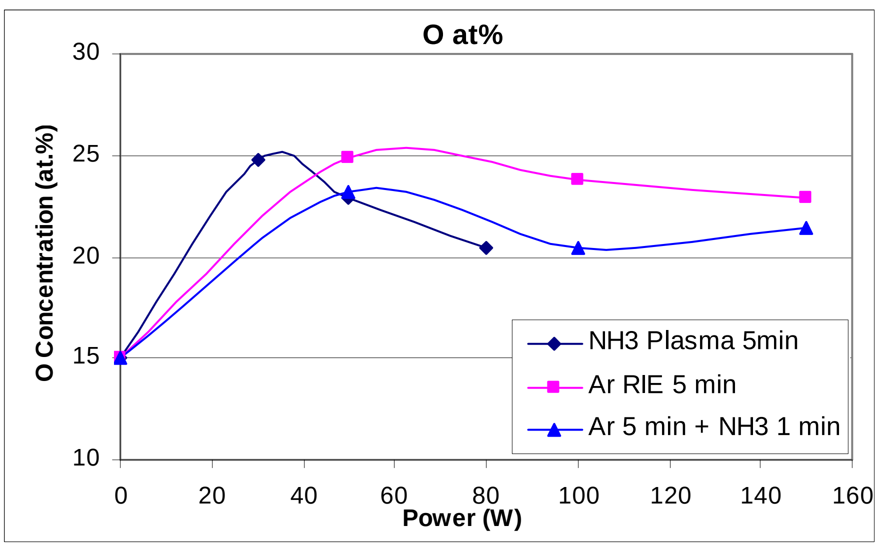

Figure 3.5: Variation in the surface concentration of oxygen with plasma power.

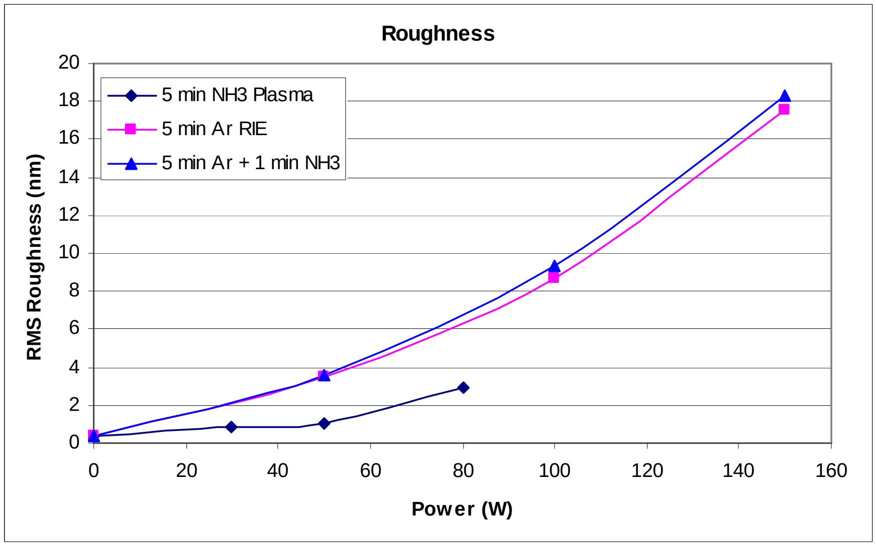

Figure 3.6: Variations in the surface roughness with plasma power.

Following NH_3 plasma treatments, nitrogen content on the polymer surface increased significantly (Figure 3.3). While untreated polyimide contains only 4.1 atomic percent nitrogen, a 30 W NH_3 treatment increased the concentration to 9.0% with higher power plasma enabling even larger concentration increases. This is due to the bombardment of the surface with nitrogen radicals that can react with the surface and form covalent bonds. These radicals are present in ever higher concentrations as the plasma power is increased, leading to the further increase of nitrogen concentration observed. The NH_3 plasma treatment also showed a strong tendency to decrease carbon concentrations on the surface (Figure 3.4) with a 30 W treatment decreasing the carbon concentration from 80% to 61%. Since the magnitude of this concentration drop (~20%) is larger than the magnitude of nitrogen addition to the surface (~6%), the carbon concentration decrease is likely caused by both the nitrogen increase and a carbon etching process. The oxygen concentration increases on the surface of the polyimide from 15%

on the untreated surface to a maximum of 25% following a 30 W NH_3 plasma treatment (Figure 3.5). Increasing the plasma power above 30 W increases oxygen concentrations to a smaller degree (20-23%). This indicates that at low plasma power the oxygen is etched at a significantly slower rate than carbon; while at higher powers, the relative rate of oxygen etching increases. Along with these chemical changes on the surface, there is some moderate roughness generation. Figure 3.6 illustrates the relatively small change in roughness (0.4 nm – 2.9 nm) resulting from NH_3 plasma treatments. The NH_3 treatment, thus, has been shown to chemically modify the surface, without significant roughness generation.

The Ar plasma treatment resulted in more moderate chemical modifications on the surface. The surface concentration of nitrogen increased gradually with increasing plasma power, reaching a maximum of 7.6% (Figure 3.3). The carbon concentration steadily declined with increasing plasma power (Figure 3.4). This steady decline is the result of preferential etching of the carbon atoms with respect to oxygen and nitrogen in this plasma environment. Oxygen concentrations on the surface mimicked the behavior seen with pure NH_3 plasma (Figure 3.5). This indicates the same phenomenon is occurring, with slow oxygen etching at low plasma power and faster etching at higher plasma powers. A maximum oxygen concentration of 24.9% was observed with a 50 W Ar treatment. The roughness generation measured following Ar etching is larger than that observed with the NH_3 treatment (Figure 3.6). Roughness increases rapidly with increasing plasma power and reaches a maximum of 17.6 nm, which is nearly an order of magnitude greater than the roughness achieved with NH_3 plasma. The Ar only treatment, therefore, has served to significantly roughen the polyimide surface with less chemical modification than achieved with the NH_3 plasma treatment.

The sequential plasma treatment of 5 min Ar followed by 1 min NH_3 produced surfaces with larger concentrations of nitrogen on the surface than the NH_3 treatment alone (Figure 3.3). Nitrogen concentration reached a maximum of 14% with a 100 W Ar treatment followed by a 30 W NH_3 treatment, which compares favorably to the maximum of 10.5% observed with NH_3 only treatment. This increased nitridation of the surface is possibly due to the fact that the Ar treatment preferentially etches the carbon and oxygen and may simultaneously create a more reactive surface for the subsequent NH_3 treatment. The carbon and oxygen concentrations (Figures 3.4 and 3.5) mimic the response of the pure Ar treatment, with the offset between data sets due to the further increase in nitrogen on the surface. The roughness of the surface following the combined treatment also correlates well with the roughness from the Ar-only treatment (Figure 3.6). This combined treatment creates a surface with the large nitrogen and oxygen concentrations of the NH_3 only treatment and the large roughness of the Ar-only treatment. Controlling the conditions of each plasma step in the sequential process allows for a specific tailoring of the surface for a desired surface chemical state and roughness.

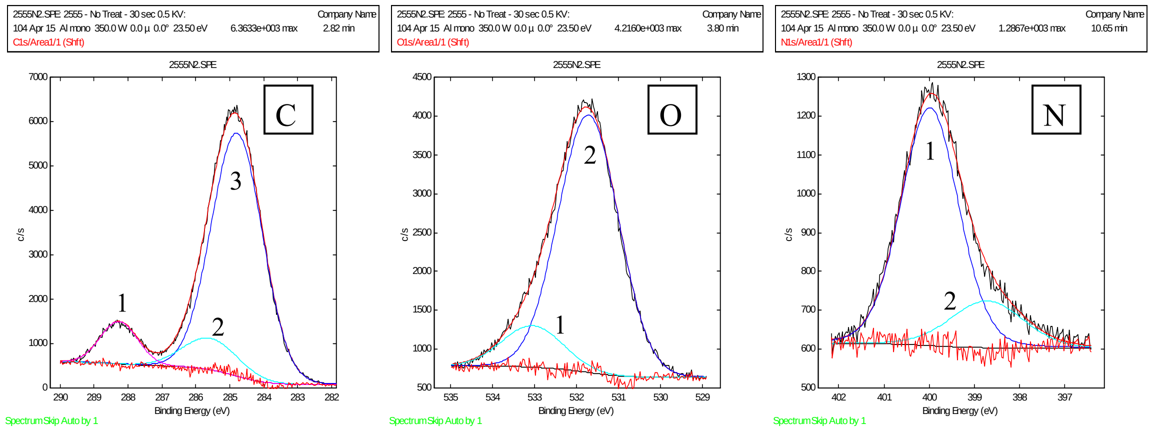

Figure 3.7: Core level XPS spectra of C, O, and N in untreated PI films.

The use of XPS allows the detailed chemical states of the elements on the surface to be analyzed. Figure 3.7 presents the core level spectra for carbon, oxygen, and nitrogen in the untreated polyimide. In PI, carbon can be found in three bonding states: C-C, C-N, and C=O. The XPS carbon spectrum contains three peaks that correspond to these bonding states: C=O at 288.3 eV (peak 1), C-N at 285.5 eV (peak 2), and C-C at 284.7 eV (peak 3).[88] The relative fractions of these bonding states as measured by XPS are C-C: 78.9%, C-N: 11.5%, and C=O: 9.6%, while the theoretical fractions determined from the molecular structure of the polymer are C-C: 71.4%, C-N: 15.6%, and C=O 13%. Oxygen in the untreated polyimide should theoretically be present only in the O=C bonding state, but two bonding states are observed in the XPS: O-C found at 533.2 eV (peak 1) and O=C found at 531.9 eV (peak 2).[88] This difference is likely due to interactions between atmospheric oxygen and the polymer surface.

The nitrogen XPS spectrum also contains two peaks although the theoretical analysis indicates that nitrogen is present in only the N-C configuration. The carbon to which the nitrogen is bonded, however, can be found in two different states: as part of the aromatic ring >C-C< or the carbonyl group >C=O. It has been reported that this change in carbon bonding can cause correlating shifts in the nitrogen spectra.[23, 24, 89] Our belief is that the peak located at 400.2 eV (peak 1) corresponds to N-C=O as reported in the literature; while the peak located at 398.5 eV (peak 2) corresponds to either N-C-C bonding or is the result of incomplete imidization of the polymer.

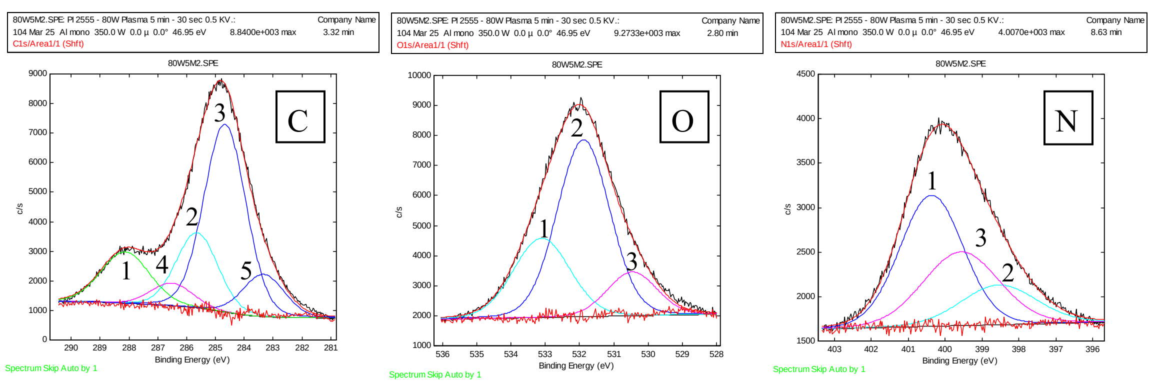

Figure 3.8: C, O, and N core level XPS spectra after 80W NH_3 plasma treatment.

Figure 3.8 presents the XPS core-level spectra for carbon, oxygen, and nitrogen following an 80 W NH_3 plasma treatment. It is apparent through comparison with the untreated sample that significant changes have take place during this treatment. New peaks were added in the carbon spectrum, the first corresponding to C-O bonding at 286.3 eV (peak 4) and the second corresponding to C-Si bonding 283.4 eV (peak 5). The C-Si bond development is likely due to silicon contamination of the plasma chamber while the C-O bonding most likely stems from the breaking of C=O bonds during the plasma treatment. Also of note in the carbon spectrum is the increase in relative concentration of the C-N bonding state (peak 2) to 19.2% from 11.5% in the untreated polyimide. This increase is evidence that the nitrogen added to the surface through this plasma treatment is bonded to carbon. The concentration of the C-C bonding state (peak 3) drops sharply to 48.9% from 78.9% following NH_3 treatment while the concentration of the C=O bonding state increases from 9.6% to 15.4%. This indicates that the C-C bonding state is more susceptible to etching than the C=O bonding state as is expected since C-C has a lower dissociation energy than C=O. The oxygen spectrum also displays the development of a new peak following NH_3 plasma treatment. This peak appears at 530.5 eV (peak 3) and belongs to O-Si bonding caused by the previously mentioned silicon impurity in the plasma chamber. An increase in the O-C bonding (peak 2) from 15.4% to 27.1% as well as a decrease in O=C bonding (peak 1) from 84.6% to 58.6% were observed as well.

The nitrogen spectrum shows the largest contribution from new peaks following the NH_3 plasma treatment. The new peak appears at 399.5 eV (peak 3) which has been identified as the N=C bonding state in the literature.[24] The concentration of N=C bonding increases with increasing plasma power and reaches a maximum of 33.5% following an 80W NH_3 treatment.   The assignment of the 399.5 peak to N=C is difficult; however, since chemical shifts in the N 1s spectrum corresponding to bonding changes are smaller in magnitude than with the O 1s or C1s spectra. Any variations in nitrogen bonding environment are difficult to distinguish based on the N 1s results alone. In this case the C 1s spectra, which could help confirm the findings, is cluttered with five peaks and C=N would appear very close to >C-N. Ultimately, the 399.5 eV peak has been assigned to C=N based on the results of Flitsch et al.,[24] but it may not be unique as C≡N would also appear in the same range of binding energies (399.6-399.7 eV).[88] The NH_3 treatment has been shown to significantly alter the chemical composition of the polyimide surface. Specifically, the NH_3 plasma treatment preferentially etches carbon while adding nitrogen to the surface in the form of C=N.

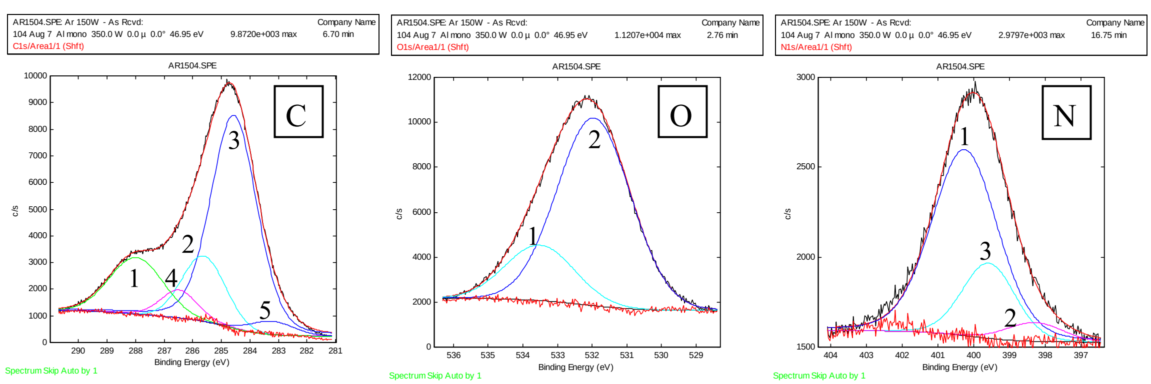

Figure 3.9: C, O, and N core level XPS spectra after 150W Ar plasma treatment.

Core level XPS spectra of the polyimide surface following a 150 W Ar RIE treatment are shown in Figure 3.9. This treatment occurred in RIE mode to permit the use of higher energies of bombardment in order to increase the surface roughness of the polyimide. These high kinetic energy ions can also induce rearrangements of bonding states on the surface. It has been shown in Figure 3.4 that the concentration of carbon decreases continuously with increasing Ar plasma power. The carbon spectrum presented in Figure 3.9 indicates that the majority of this decrease is due to a loss of C-C (peak3) bonds, which are reduced from 78.9% in the untreated polyimide to 59.0% after the 150 W Ar treatment. The C-N (peak 2) and C=O (peak 1) bonding states see slight increases in concentration with Ar plasma treatments. These results indicate that the C-C bonding state is etched most rapidly by the plasma treatment while both the C-N and C=O bonding states are etched more slowly. The oxygen spectrum shows only a small increase in the O-C bonding concentration (15.4%-21.2%) when compared with untreated polyimide, which is consistent with the behavior of the C-O peak in the carbon spectrum.

The nitrogen spectrum does show significant changes from the untreated polyimide. Specifically, a third peak develops at 399.5 eV (peak 3) that belongs to N=C bonding as was observed in the NH_3 plasma treatment. This bonding state is present at lower concentrations following the Ar treatment (21.3%) as compared to the NH_3 treatment (33.5%). Since no nitrogen is added to the surface during the Ar treatment, the development of this new bonding state signifies that a rearrangement of nitrogen bonds occurs on the surface due to the ion bombardment and sputter etching of the RIE treatment. Flitsch et al. [24] have reported a similar rearrangement of nitrogen bonds following an Ar plasma treatment. The nitrogen spectrum also indicates a reduction in the concentration of N-C-C bonding groups (peak 2) caused by the etching of carbon from the aromatic ring. The Ar RIE treatment therefore, has been shown to increase C=O and C=N concentrations on the surface, though to a lesser extent than the NH_3 treatment, while causing significant surface roughening.

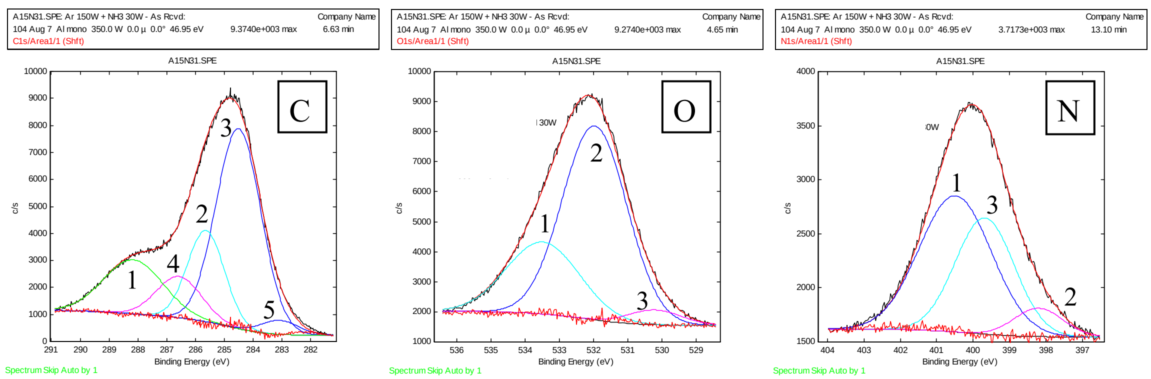

Figure 3.10: C, O, and N core level XPS spectra after combined plasma treatment with 150W Ar followed by 30W NH_3.

The XPS spectra of the polyimide surface after a 150 W Ar RIE treatment followed by a 30 W NH_3 plasma treatment are shown in Figure 3.10. This combined treatment showed similar effects to both individual plasma treatments. The carbon spectrum shows an increase in the concentration of C-N bonding (peak 2) to 18% and an increase in the C=O bonding (peak 1) to18.1%. There was also an increase in the C-O bonding (peak 4) to 9.9%, which is greater than the increase seen in this bonding environment with either individual treatment. The oxygen spectra also shows an increase in this O-C bonding (peak 1) above that seen with either individual plasma treatment (28.2% as compared to 21.2 % for Ar only and 27.1% for NH_3 only treatment). The concentration of nitrogen on the surface, which was shown to be larger than that of the NH_3 only treatment in Figure 3.3, is seen to increase mainly in the form of N=C (peak 3). The concentration of this bonding group reaches a maximum of 37.4% in the combined treatment, a larger increase than was observed in the NH_3 only treatment (33.5%). These results along with the RMS roughness data presented in Figure 3.6 indicate that the sequential plasma treatments provide the benefits of each individual treatment. The roughness generation of the Ar RIE is maintained and the chemical modifications caused by the NH_3 plasma are maintained or enhanced through the combined treatment, creating a rough surface with the desired chemical bonding groups.

In order to compare these results with "traditional" treatments, a wet-chemical swell and etch process was tested with the polyimide material. In this process, samples are exposed to a swelling solution (Shipley Circuposit 3302) at 80°C for 10 minutes and etched in an alkaline sodium permanganate bath (Shipley Circuposit 3308) at 80°C for 5 and 30 minutes. AFM analysis indicated that these treatments increased RMS roughness from 0.4 nm untreated to 0.7 nm after a 5 min etch and to 1.1 nm following a 30 min etch. These increases are smaller than those observed following NH_3, Ar, or combined plasma treatments. XPS analysis showed surface concentrations of 75.2% for carbon, 18.3% for oxygen, and 4.3% for nitrogen following a 30 min treatment, with a 5 min etch treatment providing similar results. These concentrations are similar to the untreated polyimide with the largest change being an increase in oxygen concentration due to the oxidation of the surface in the etch bath. These physical and chemical modifications of the surface did not enable catalyst adsorption or electroless copper plating on the polymer surface. The wet-chemical treatment, therefore, was shown to be less effective for both surface roughening and chemical modifications than the plasma treatments and was not studied further. These results are consistent with the findings in the literature.[16]

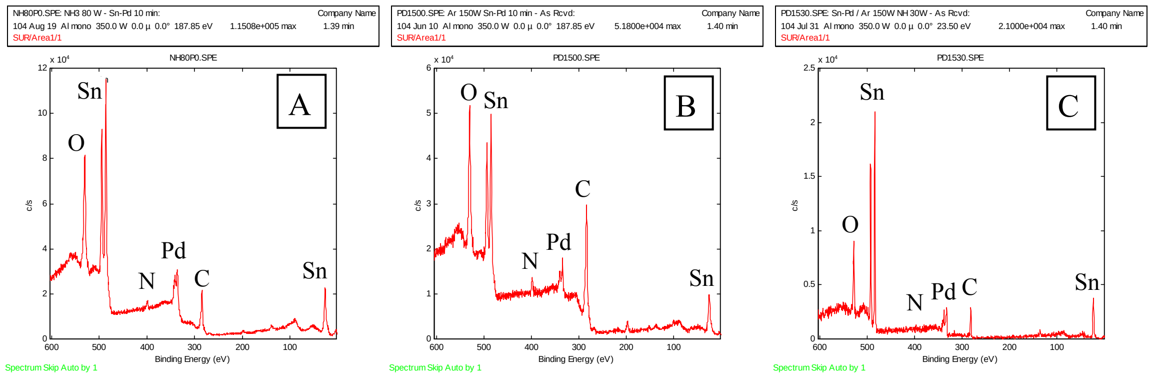

Figure 3.11: XPS survey scans of NH_3 80W, Ar 150W, and Ar 150W + NH_3 30W plasma treated PI samples after the Sn-Pd activation step.

After undergoing the plasma treatments described above, polyimide samples were immersed in a $SnCl_2$-$PdCl_2$ bath in order to activate the surface for electroless copper plating. Electroless copper cannot plate on the polyimide surface until it has been seeded with a catalyst. Previous work[87] indicates that wet-chemically treated or oxygen etched polyimide surfaces react with $SnCl_2$ in the bath to produce C-O-Sn linkages. These Sn groups then aid in the reduction of $PdCl_2$ to Pd(0) on the surface. It has been reported that polymer surfaces treated with nitrogen plasma can enable palladium interactions with the surface nitrogen as well as the C-O-Sn linkage.[87] These surfaces adsorb more Pd than wet-chemically treated and oxygen plasma treated surfaces. This increased surface coverage is beneficial for the electroless copper deposition since the Pd on the surface initiates the copper deposition reaction. In order to measure the effects of the NH_3 and Ar plasma treatment the concentrations and oxidation states of Sn and Pd on the surface were measured with XPS. Figure 3.11 presents the XPS survey scans for samples with 80 W NH_3 plasma, 150 W Ar RIE, and sequential 150 W Ar and 30 W NH_3 plasma treatments.

Table 3.1: Surface chemical compositions of PI samples subjected to different plasma treatments before and after the Sn-Pd activation.

Surface treatment		C	O	N	Sn	Pd
No Treat		80.3	15	4.1		
30W NH3		61.1	24.8	8.8		
	Sn-Pd	44.8	40.9	4.5	7.9	1.7
80W NH3		66.4	20.4	12.3		
	Sn-Pd	34.2	41.8	3.3	16.2	4.3
50W Ar		69.1	24.9	6.5		
	Sn-Pd	55.9	30.1	6	7.3	0.7
150W Ar		66	22.9	7.6		
	Sn-Pd	58.4	28.6	4.3	7.6	1.2
50Ar+30NH		64.8	23.2	11.9		
	Sn-Pd	33.7	39.7	4.3	17.6	3.5
150Ar+30NH		62.4	21.4	12.5		
	Sn-Pd	31.7	40.5	3.2	21.1	4.7

These XPS survey scans show a number of significant changes from scans taken before the Sn-Pd treatment. First, new peaks can be observed at 486 eV and 337 eV corresponding to the presence of tin and palladium respectively, confirming the adsorption of each on the surface of the polyimide. Second, there are large changes in the surface concentrations of carbon, oxygen, and nitrogen following Sn-Pd treatment. The concentrations of carbon and nitrogen generally decrease following Sn-Pd treatment while the concentration of oxygen generally increases. This phenomenon is more pronounced in the samples treated with the NH_3 plasma and the combined plasma treatments. The surface concentrations for each sample, both before and after Sn-Pd treatment, are presented in Table 3.1. The reduction of carbon and nitrogen concentrations observed following Sn-Pd treatment is likely due to coverage of the surface by the tin and palladium. The oxygen increase is caused by bonding of atmospheric oxygen to tin and oxidation of the tin to higher order oxides. This theory is supported by the oxygen core-level spectra, which consistently showed an increase in O-metal bonding. Figure 3.12 shows the oxygen spectra for a 30 W NH_3 treated sample before and after Sn-Pd treatment. The level of O-metal bonding (peak 3) increases from 12.9% to 16.8% due to the increase in Sn-O interactions. A decrease in C=O bonding (peak 2) from 74.4% to 57.9% is also apparent following the Sn-Pd treatment. This indicates that the Sn interacts with the C=O bonding sites on the surface of the polymer.

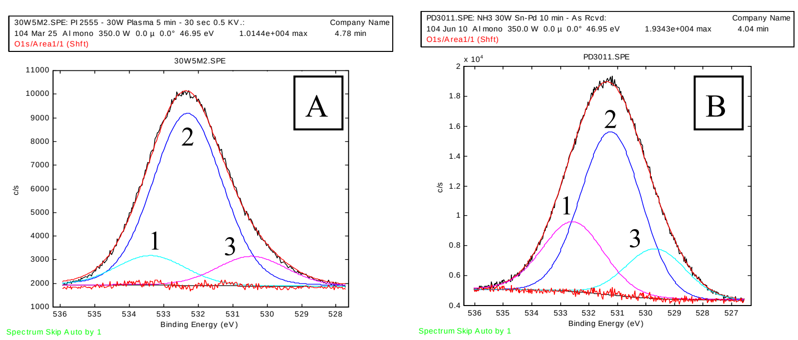

Figure 3.12: Oxygen core level XPS spectra for 30 W NH_3 treated polyimide: A) before Sn-Pd treatment; B) following Sn-Pd treatment.

The core-level spectra for Sn following plasma treatments that are presented in Figure 3.13 support the conclusion that Sn is reacting with surface and atmospheric oxygen as it is present on the surface mainly in the Sn^{2+} oxidation state, which corresponds to Sn-O bonding. The sample treated with an 80 W NH_3 treatment is the only one to show a second bonding state for Sn. In this case, the second bonding state (peak 2) corresponds to metallic Sn. Both the Ar-only and combined plasma treatments exhibit only Sn^{2+} on the surface following the Sn-Pd treatment. This behavior is consistent with results found in the literature.[87] The total concentration of Sn, however, does not correlate with the surface concentration of oxygen following plasma treatments. For example, each of the samples detailed in Table 1 has an oxygen concentration before plasma treatment of 20-25% and yet the Sn concentration on these samples varies widely from 7.3-21.1%. Further investigation of specific oxygen bonding states and Sn concentrations also yielded no clear correlations. Overall, the Sn concentrations on the surface have been raised as high as 21% following Sn-Pd treatment, but no correlation between specific surface functional groups and the Sn was found.

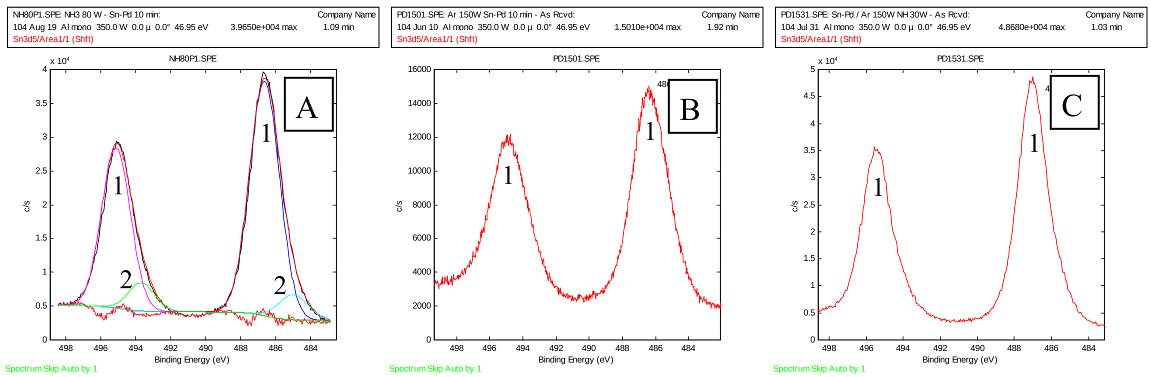

Figure 3.13: Core level XPS spectra of Sn on PI surface with three different plasma treatments (A) NH_3 80W, (B) Ar 150W, and (C) Ar 150W + NH_3 80W.

The concentrations of Pd following the Sn-Pd treatment are much smaller than those of Sn as expected based on other studies in the literature (Table 3.1).[87, 90] The Pd in these systems is found in two bonding environments, Pd^{2+} located at 337.7 eV (peak 1) and Pd^0 located at 335.5 eV (peak 2) as shown in the Pd XPS core level spectra of Figure 3.14. For the Ar-only treatment (Figure 3.14B) the Pd is found in only the Pd^0 oxidation state indicating that purely physical adsorption of the Pd on the surface. The NH_3-only treatment produced both Pd^0 (53%) and Pd^{2+} (47%) as did the combined plasma treatment (59% and 41% respectively). The Pd^{2+} peak, which is located at 337.7 eV, is likely not due to Pd-O since this bonding state occurs at 338.5 eV. It is believed, then, that this Pd^{2+} is caused by Pd-N bonding, since nitrogen has lower electronegativity than oxygen the binding energy shift should be smaller.

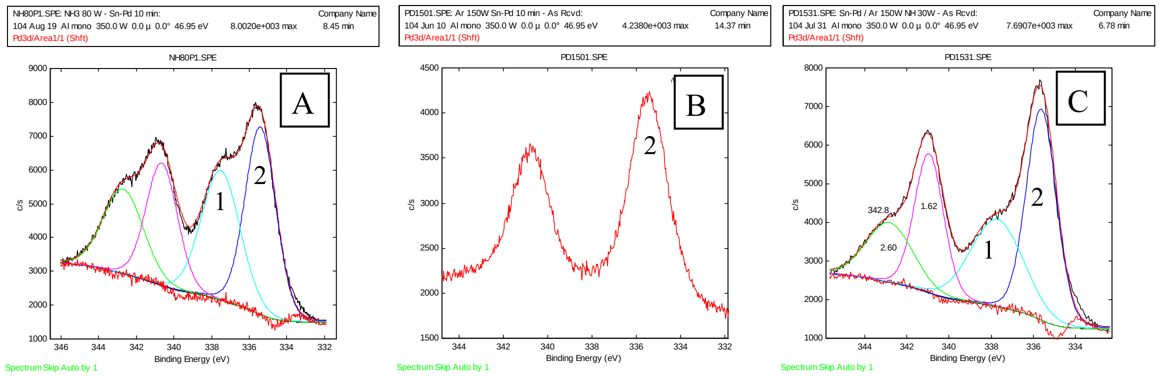

Figure 3.14: Core level XPS spectra of Pd on PI surface with three different plasma treatments (A) NH_3 80W, (B) Ar 150W, and (C) Ar 150W + NH_3 80W.

This theory is also supported by the charts presented in Figure 3.15. The first chart (Figure 3.15A) shows the correlation between nitrogen surface concentration before Sn-Pd treatment and the subsequent Pd surface concentration. The concentrations were determined from the integrated areas under their photoelectron peak and the sensitivity factors. A clear relationship between the nitrogen surface concentration and the amount of Pd adsorbed on the surface can be seen. The second chart (Figure 3.15B) compares the number of nitrogen sites covered during the Sn-Pd treatment (N_{plasma}-$N_{Sn\text{-}Pd}$) and the Pd surface concentration. It is apparent that the surface nitrogen groups are effective nucleation sites for Pd adsorption on the surface. The decrease in nitrogen concentration following Sn-Pd treatment is due to coverage of these groups on the surface by Pd during the activation process. Finally, Figure 3.16 compares the concentration of N=C bonding groups on the surface and Pd adsorption. Once again a correlation can be seen indicating that this specific bonding group, which is added during the plasma treatment, is responsible for the enhanced catalyst adsorption observed. Overall, Figures 3.15 and 3.16 support the premise that Pd is bonded to N on the surface, specifically to N in the

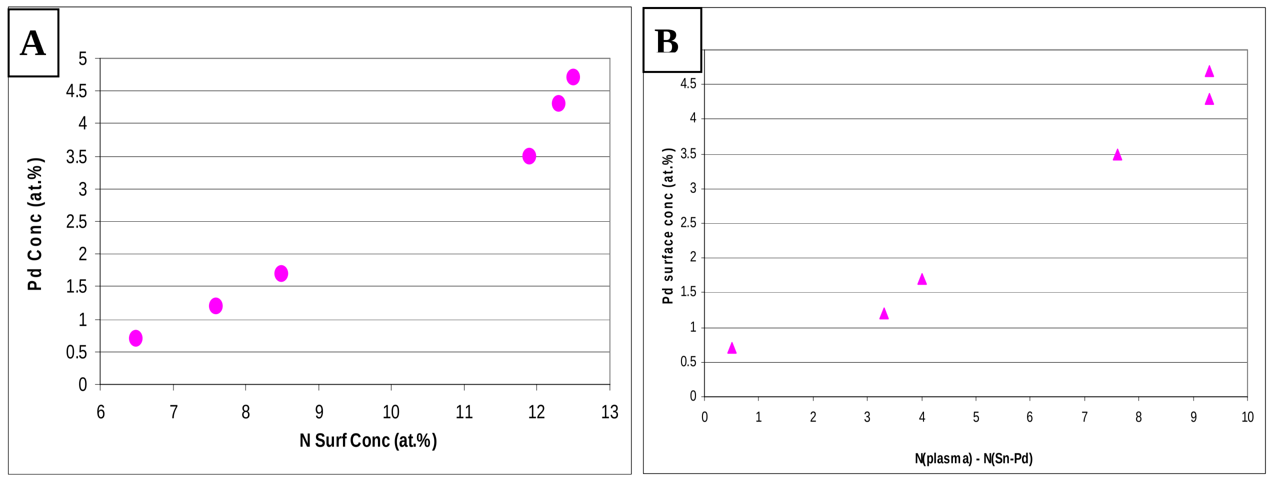

Figure 3.15: Correlation between (A) N surface concentration and amount of Pd adsorbed and (B) reduction in N surface concentration and amount of Pd adsorbed.

N=C bonding state. This interaction is independent of the method for producing N=C bonding as NH_3-only, Ar-only, and combined treatments are all used for the correlation.

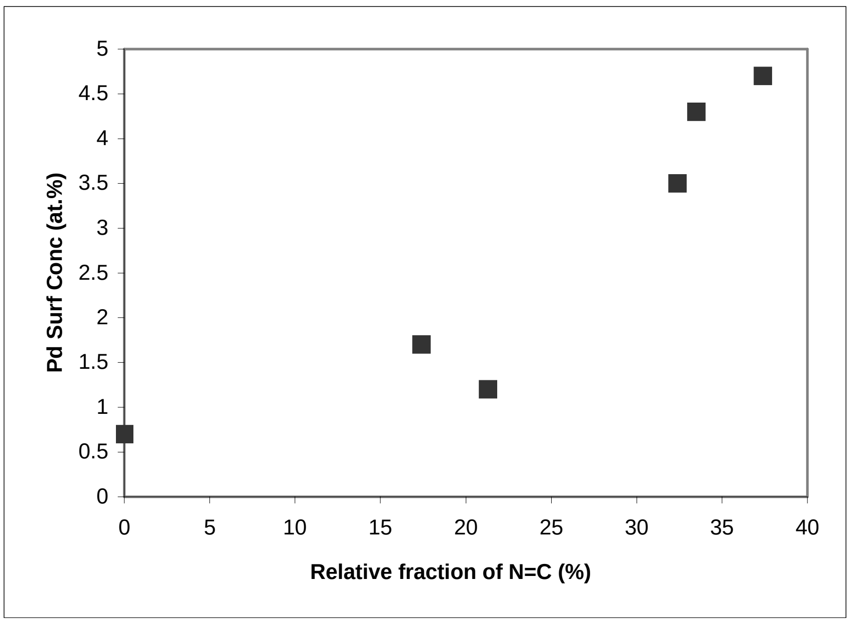

Figure 3.16: Correlation between relative fraction of N=C and Pd surface concentration.

Following Sn-Pd activation samples were immersed in an electroless copper bath for 5 seconds, which was sufficient time to initiate plating resulting in the formation of a few monolayers of copper. These samples were then analyzed using XPS to produce the survey scans shown in Figure 3.17. In these spectra the Cu^0 peak is located at 932.8 eV and is present for each sample. The samples treated with NH_3 plasma produce strong Cu signals, and corresponding high copper concentrations, while the Ar-only treatment displays a weak Cu signal and lower concentration. It can be seen from the data in Table 3.2 that the Ar-only treated surfaces exhibit low concentrations of copper (0.3-0.4%) while the NH_3 and combined plasma treatments enable a higher level of copper plating after 5 seconds (4.9-27.4%). Table 3.2 includes detailed surface composition data on the polyimide following each plasma treatment including data from before and after the Sn-Pd activation and electroless copper deposition steps.

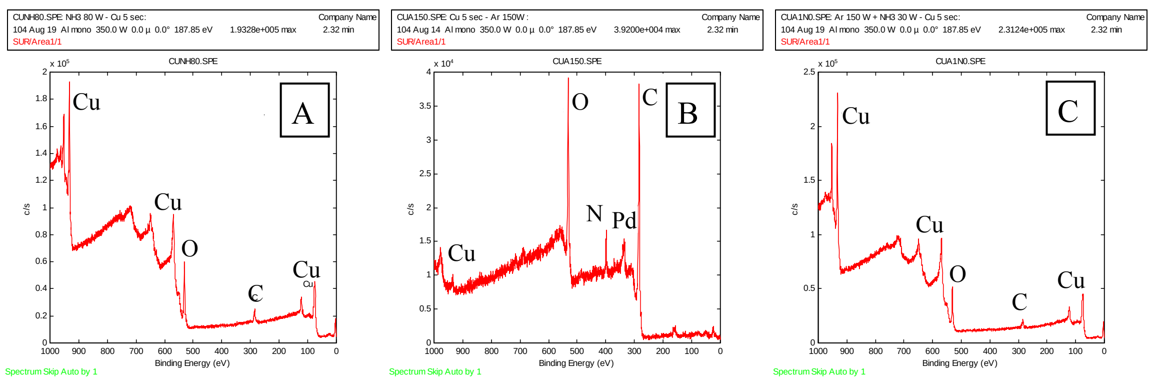

Figure 3.17: XPS survey scans after 5 sec electroless Cu deposition for different plasma treatments (A) NH_3 80W, (B) Ar 150W, and (C) Ar 150W + NH_3 80W.

The core-level XPS spectra for Cu are shown in Figure 3.18. It is clear from the multiple peaks that Cu is present in three bonding states in all three samples. The two most prevalent bonding states in the NH_3-only and Ar-only samples are Cu-O bonding located at 934.8 eV (peak 1) and Cu^0 bonding located at 932.7 eV (peak 2).[90] The Cu-O bonding is likely due to Cu surface oxidation from atmospheric oxygen. The sequential Ar and NH_3 treatment produces a surface with a significant third Cu bonding state located at 931.6 eV (peak 3).[90] This peak corresponds to Cu-Pd bonding and is prominent in all samples that received combined plasma treatments and is present though weak in all plasma treated samples. Overall, it is clear that NH_3-only and combined plasma treatments enable far greater Cu deposition than the Ar-only treatment and that the majority of the Cu on the surface is present in the metallic state, independent of the type of plasma treatment.

Table 3.2: Surface composition of PI after various plasma treatments and different electroless Cu deposition times.

Surface Treatment		**C**	**O**	**N**	**Sn**	**Pd**	**Cu**
Theoretical		78.1	15.6	6.2			
No Treat		80.3	15	4.1			
30W NH_3		61.1	24.8	8.8			
	Sn-Pd	44.8	40.9	4.5	7.9	1.7	
	Cu (5 sec)	61.3	28.1	4.3	-	1.3	4.9
	(10 sec)	66.7	25.6	2.2	-	-	5.5
	(20 sec)	53.1	34.1	3.8	-	-	9.1
	(30 sec)	34.2	45.2	0.7	-	-	19.9
80W NH_3		66.4	20.4	12.3			
	Sn-Pd	34.2	41.8	3.3	16.2	4.3	
	Cu (5 sec)	32.2	45.9	1.3	-	-	20.6
50W Ar		69.1	24.9	6.5			
	Sn-Pd	55.9	30.1	6	7.3	0.7	
	Cu (5 sec)	73.2	21.4	5.1	-	0.6	0.3
	(30 sec)	49.8	35.3	3.6	-	-	9.95
150W Ar		66	22.9	7.6			
	Sn-Pd	58.4	28.6	4.3	7.6	1.2	
	Cu (5 sec)	70.6	22.5	5.5	-	1	0.4
	(30 sec)	28.6	45.2	1.5	-	-	24.7
50W Ar+30W NH_3		64.8	23.2	11.9			
	Sn-Pd	33.7	39.7	4.3	17.6	3.5	
	Cu (5 sec)	34.9	44.3	-	-	-	20.9
150W Ar+30W NH_3		62.4	21.4	12.5			
	Sn-Pd	31.7	40.5	3.2	21.1	4.7	
	Cu (5 sec)	26.9	45.7	-	-	-	27.4
Surface Treatment		**C**	**O**	**N**	**Sn**	**Pd**	**Cu**
Epoxy	No Treat	81.9	18.1				
	Wet Etch	77.6	22.4				
	Sn-Pd	36.4	39.9	1.7	19.1	2.9	
	Cu (5 sec)	55.7	29.9				14.4

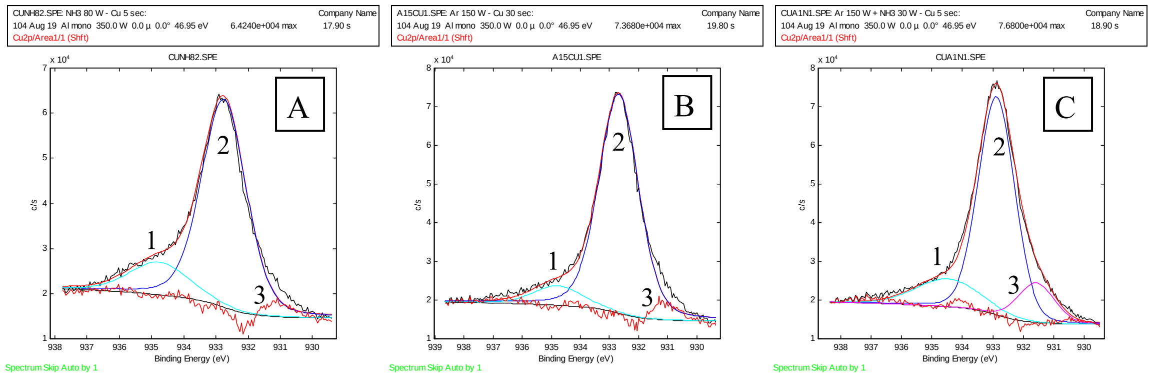

Figure 3.18: Core level XPS spectra of Cu on PI surfaces with different plasma treatments (A) NH_3 80W, (B) Ar 150W, and (C) Ar 150W + NH_3 80W.

The data in Table 3.2 indicates that Cu coverage as a function of deposition time is dependent on the surface pretreatment. Figure 3.19 shows the specific relationship between Pd surface concentration and Cu coverage following 5 seconds of plating. A relationship between Pd concentration and Cu coverage can be observed because of the catalytic nature of the Pd for the electroless Cu deposition reaction. This indicates that the increased Pd adsorbed on the surface maintains catalytic activity even though a large portion is found in the Pd^{2+} oxidation state. Also, as mentioned previously, Pd surface concentration exhibits a linear correlation with nitrogen concentrations and, specifically with N=C bonding, indicating that the Cu concentration should also correlate with these surface groups.

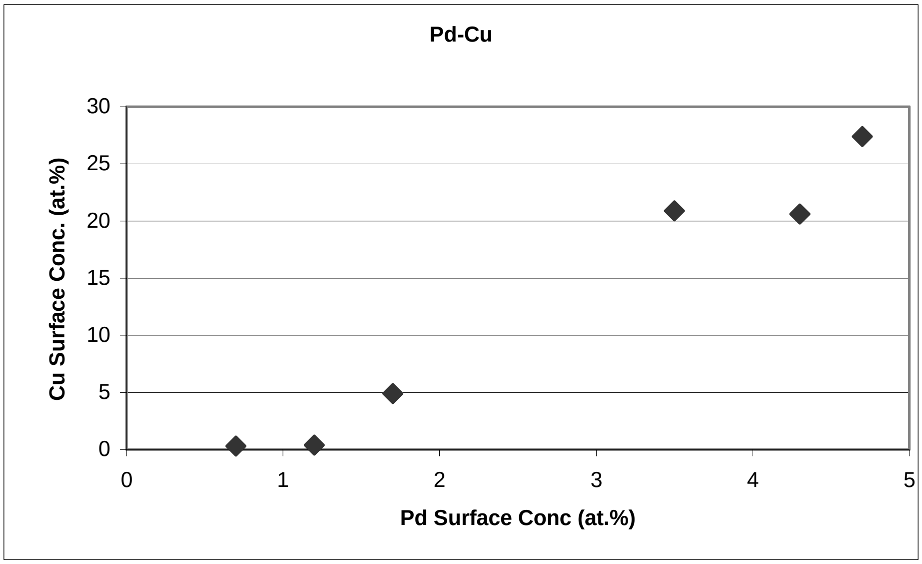

Figure 3.19: Correlation between Pd surface concentration and Cu surface coverage.

Peel tests were conducted in order to quantify the adhesion between these electrolessly deposited copper layers and the polyimide surface. In order to produce a copper layer with adequate mechanical strength for peel testing, an electroplated copper layer (~40 μm) was plated on top of the initial electroless copper (~0.6 μm). Untreated polyimide samples do not enable adequate catalyst adsorption during the Sn-Pd activation step to allow for electroless copper deposition. Since copper could not be plated on these surfaces peel tests could not be performed. Table 3.3 displays the peel test results for samples with various plasma treatments. In all cases, the peel strengths measured on these polyimide samples are an order of magnitude below those typically seen with roughened epoxy polymers (0.5-1.0 N/mm).[91] The difference in the magnitude of adhesion between these materials is likely due to large differences in surface roughness (1.8 nm for PI compared to 100-500nm for epoxy). The increased roughness of the epoxy material allows for strong mechanical anchoring that is thought to be responsible for the majority of adhesion in these systems.[1] The polyimide has an extremely smooth surface and, therefore, much more limited mechanical anchoring.

Table 3.3: Electroless Copper Peel Tests.

Pretreatment	RMS Roughness (nm)	Peel Strength (N/mm)
Ar 150 W	17.6	0.03
NH_3 30 W	1.2	0.04
NH_3 80 W	2.9	0.06
Ar 150 W+ NH_3 30 W	18.0	0.06

There is, however, a noticeable improvement in the polyimide samples studied here, with the Ar-only treatment showing adhesion of 0.03 N/mm while the combined treatment, with nearly identical roughness, showing adhesion of 0.06 N/mm. This change in adhesion with identical roughness values indicates that chemical bonding, and not purely mechanical anchoring, is playing a role in the adhesion of this system. This chemical bonding likely comes from the interactions between surface nitrogen added during plasma treatments and the Pd catalyst as well as the deposited Cu. Figure 3.17, which displays XPS survey scans of both the polymer and copper strip sides of the sample following peel tests, support this conclusion. The polyimide side of the sample shows no trace of metal following peel tests, while the copper strip side shows evidence of Cu, Pd, Sn, C, and O. This indicates that failure occurs at the PI-catalyst interface, thus adhesion from the PI-Pd interactions likely leads to the peel strength increases observed. These results, while encouraging for the improvement of catalyst adsorption and plating on smooth surfaces do not enable the formation of strong mechanical or chemical bonding between the PI surface and electroless copper.

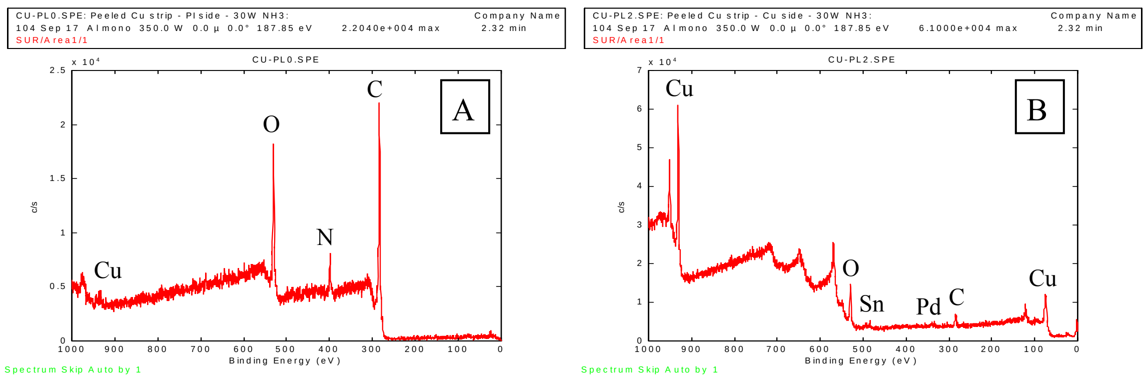

Figure 3.20: XPS analysis of the (A) PI and (B) Cu surfaces after peeling the Cu film.

3.4 Conclusions

The work presented in this chapter has focused on the use of plasma treatments to enhance catalyst adsorption and adhesion between a polyimide surface and electroless copper. It has been found that NH_3 plasma increases nitrogen content on the surface, specifically adding nitrogen to the surface in the -N=C< bonding state while causing only minimal roughening of the surface. The Ar RIE has proven to significantly roughen the polymer surface while causing moderate chemical modifications on the surface due to preferential etching of carbon and the subsequent bond rearrangements this etching causes. The sequential Ar RIE followed by NH_3 plasma treatment has been shown to incorporate the benefits of both individual treatments, increased surface roughening and enhanced chemical modifications. These chemical bonding enhancements enabled increasing catalyst adsorption during the Sn-Pd activation step and improved electroless copper deposition uniformity. Small increases in adhesion were also observed, although the adhesion remained significantly below that of roughened epoxy dielectric materials. This is likely due to the significant roughness difference between these materials. Overall, the plasma treatments on PI have shown to be effective in chemically modifying the surface for catalyst adsorption and electroless copper plating but have not adequately enhanced adhesion for use in microelectronic devices.

CHAPTER 4

EPOXY MATERIALS

4.1 Introduction

New technologies and processes are being developed to meet the demand for high density interconnects for integrated circuits (ICs). At the board and package level, sequential build-up structures (SBUs) and microvias have been integrated into the manufacture of printed circuit boards (PCBs) as one means of achieving high density interconnections. These features are typically formed on a PCB with alternating dielectric and copper layers. A key to the performance and reliability of these SBUs is the adhesion between the deposited copper and the dielectric materials. Surface roughness causes scattering of electrons at high frequency; however, roughness improves the mechanical anchoring of the metal film. As the feature density and off-chip frequency increase, the average feature size shrinks, and the interface between the metal and dielectric materials must become smoother to avoid surface scattering. Future dielectric materials must also have improved electrical properties, in particular permittivity and loss, in order to enable the smaller features and higher frequency performance.

Achieving a smooth metal-dielectric interface is especially challenging because the metal-to-dielectric adhesion is achieved through a combination of chemical bonding and mechanical anchoring.[1, 8, 49] Enhancing adhesion while minimizing roughness requires advances in chemical bonding and reduced dependence on mechanical anchoring. In order to achieve this, it is important to identify the individual contributions of each mechanism to adhesion. In the case of traditional phenolic epoxy materials and electroless copper metallization, it has been shown that physical anchoring accounts for the majority of adhesion.[5, 6] Improving adhesion with these materials is typically achieved through physical modification of the dielectric surface.

This physical modification occurs through a multi-step swell and etch process that generates root mean squared (RMS) roughness up to 500 nm with peel strengths as large as 1.5 N/mm.[91] The development of pore-type roughness on the surface of a traditional epoxy has been well documented in the literature. Siau et al. has postulated a mechanism for pore development in which the swelling agent rearranges polar groups in the polymer into packets and the etch solution then preferentially attacks these packets forming pores.[15, 92] The schematic in Figure 4.1 shows the proposed etch mechanism for the epoxy system. The site of attack for the etch solution is the ether linkage formed by the opening of the epoxide ring during the curing process. In traditional epoxy materials, this ether linkage is located in the polymer backbone, allowing the etch reaction to remove a small segment of the polymer chain and expose the next linkage for subsequent etch attack. In this manner, the etching process works down the polymer chain, eventually removing the entire chain and beginning the process of forming pores on the surface. This swell and etch process on epoxy materials typically creates a surface with pore-type roughness, where the pores can be micrometers in diameter and depth.[1] It is these large pores, with feature sizes in the range of the skin depth of copper at high frequencies, which cause electron scattering and signal distortion. This effect is increasingly important because the off-chip frequency is projected to increase by 25% per year for the next decade reaching 41 GHz by 2017. This corresponds to a decrease in copper skin depth from 1000 nm in 2007 to 315 nm in 2017.[3] Minimizing the need for large pores is a key to achieving high performance substrates using current materials.

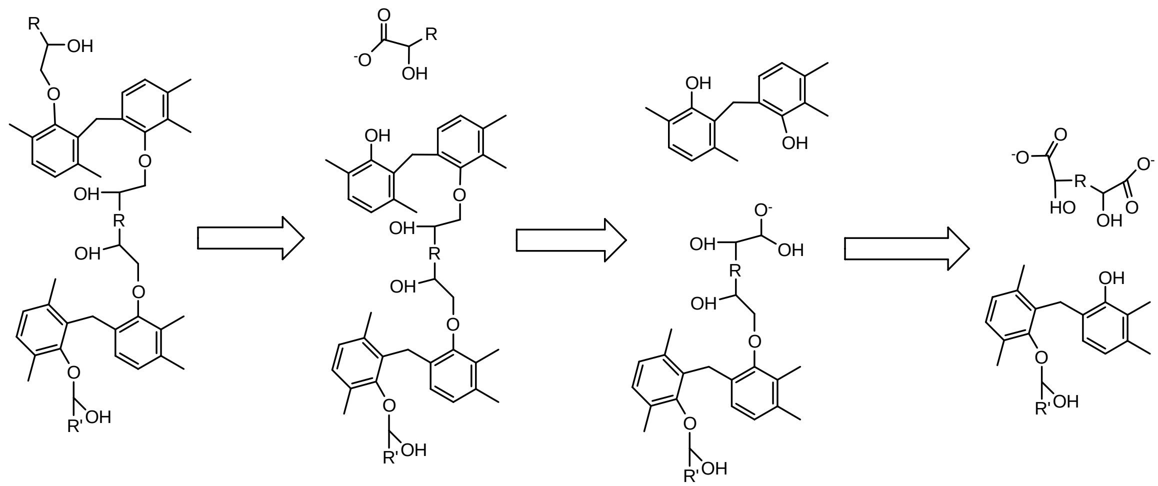

Figure 4.1: Phenol-novolac etch mechanism schematic

One method for reducing the need for large pores and the mechanical anchoring they provide is to increase chemical bonding, which has the ability to enhance adhesion without creating roughness on the surface.[8, 10, 93, 94] In order to enhance chemical bonding between a dielectric material and electroless copper, the concentration of active chemical groups on the surface of the polymer must be increased. Wet-chemical treatments such as graft polymerization, coupling agents, and surface synthesis techniques have been studied by numerous researchers as means of increasing the content of certain active groups on the surface.[9, 44, 46, 49, 54] Plasma treatments have also been utilized with a variety of materials to activate surfaces.[17, 21, 39, 50, 95] A common link in many of these studies is the role of nitrogen containing functionalities on the surface. These have been shown to enhance catalyst adsorption on polymer materials and to enhance adhesion by as much as 0.5 N/mm in some systems.[17, 39] Although the exact interaction mechanism between electroless copper and these nitrogen groups is unclear, it appears that both nitrogen-palladium and nitrogen-copper complexes are formed on the surfaces, aiding adhesion.[44, 48, 52] Previous work with polyimides has shown that 5 min 80 W NH_3 plasma treatments are effective for enabling catalyst adsorption and enhancing adhesion through nitrogen incorporation.[17] In this study, similar NH_3 plasma treatment conditions have been utilized on polymer surfaces in an attempt to increase nitrogen concentrations and enhance chemical bonding.

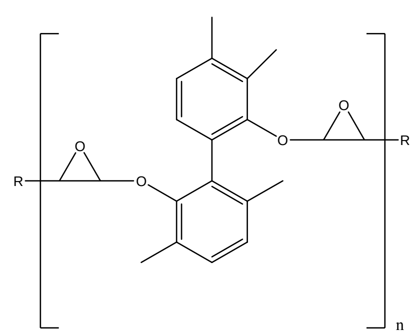

Figure 4.2: Probelec 81/7081 chemical structure

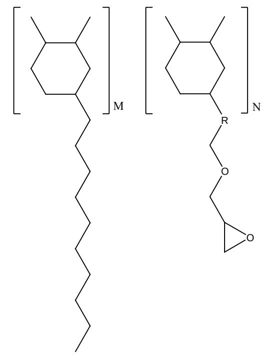

Figure 4.3: Avatrel 2190 P chemical structure

The goal of this work is to utilize both chemical and mechanical bonding in order to enhance adhesion while minimizing the necessary surface roughness of the dielectric material. Two material sets have been studied in this investigation, Probelec 81/7081 (Huntsman), a traditional phenol-novolac epoxy, and Avatrel 2190P (Promerus LLC) an addition polynorbornene-based epoxy. The chemical structure for Probelec is given in Figure 4.2. The Avatrel structure is given in Figure 4.3. Probelec contains epoxy groups in the backbone of the polymer, while Avatrel is an advanced epoxy material that has a polynorbornene backbone with epoxy side-groups used for crosslinking. Although the goal of strong adhesion with smooth surfaces for these two materials is the same, the approach and challenges are quite different. With Probelec, a rough, highly adherent interface is readily available through traditional surface treatments. The challenge is to minimize surface roughness and replace the lost mechanical anchoring with chemical bonding to maintain adhesion. Avatrel is less susceptible to the swell and etch process and does not enable electroless copper plating in the untreated, as-cured state. Hence, the challenge here is to understand why the material behaves differently during the swell and etch process and to identify suitable processing methods for enhancing contributions of mechanical anchoring and chemical bonding to adhesion.

4.2 Results

Roughness formation on Probelec and Avatrel surfaces following a swell and etch treatment is quantified in Figure 4.4. RMS roughness values for Probelec increase with increasing etch treatment times, reaching a maximum of 800 nm with extended etching. Traditional treatment conditions of a 480 s swell and a 600 s etch produce RMS roughness of 400 nm with corresponding adhesion of up to 1.5 N/mm. The surface roughness that forms in Avatrel, however, is more than an order of magnitude less than with Probelec, with a maximum RMS roughness development of 35 nm. These treatment conditions produced no measurable adhesion between Avatrel and electroless copper. The roughness morphology also depends on the kind of material (Figure 4.5). The Probelec surface develops a pore-type roughness forming large, deep pores with extended etching times. The Avatrel surface, however, does not exhibit pore-type roughness formation. Instead, surface roughness increases are realized in the form of peak-valley structures, which are uniform across the surface.

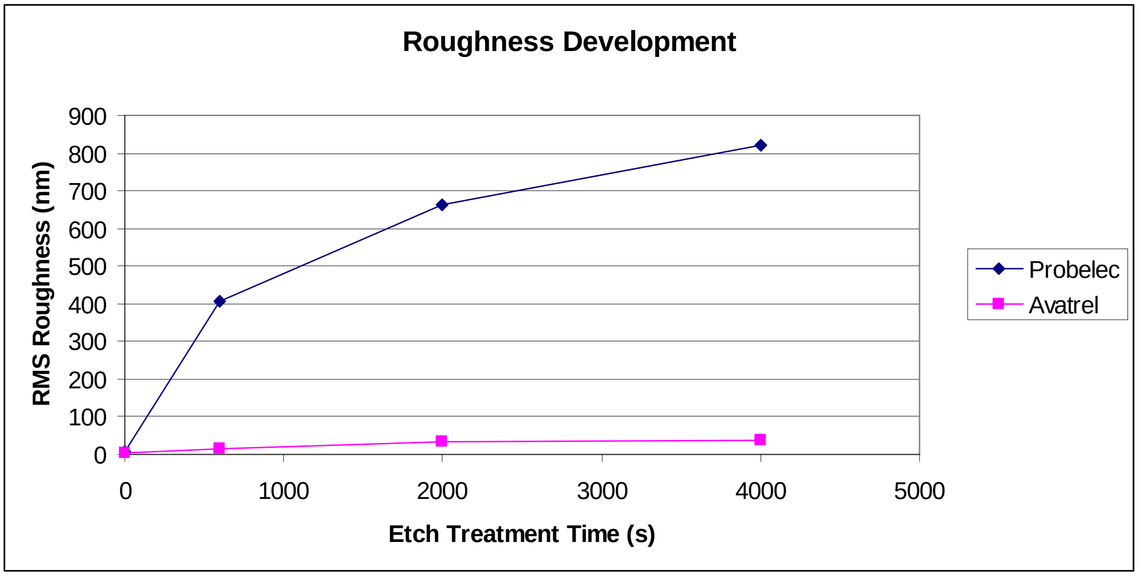

Figure 4.4: Roughness development versus etch treatment time following a 480 s swell treatment for Probelec and Avatrel

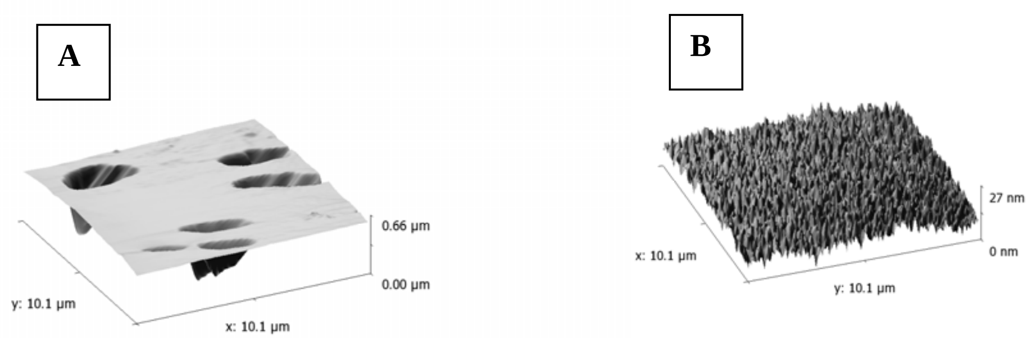

Figure 4.5: AFM images of A) Probelec and B) Avatrel following a swell and etch treatment

In order to form pore-type roughness on the Avatrel surface, AP mixtures were used. Figure 4.6 shows the resulting surfaces when these mixtures are exposed to a 2000 s swell and 2000 s etch treatment. Figure 4.6A shows a sample with 5% Probelec in the mixture. Only one pore can be seen in this 100 μm^2 scan after the swell and etch process. Figure 4.6B is for the 10% Probelec sample, which shows the presence of approximately 30 pores in the 100 μm^2 scan. Figure 4.6C is for a sample with 20% Probelec yielding 40 pores in the 100 μm^2 scan. In each case, the pores are of the same approximate size, 200-500 nm diameter and are evenly dispersed across the polymer surface. Changing the concentration of Probelec in the mixture affects pore concentration and not pore size or depth. Figure 4.6D is a 3-dimensional AFM image of the 20% Probelec sample illustrating that the pores formed on the surface are a maximum of 65 nm deep.

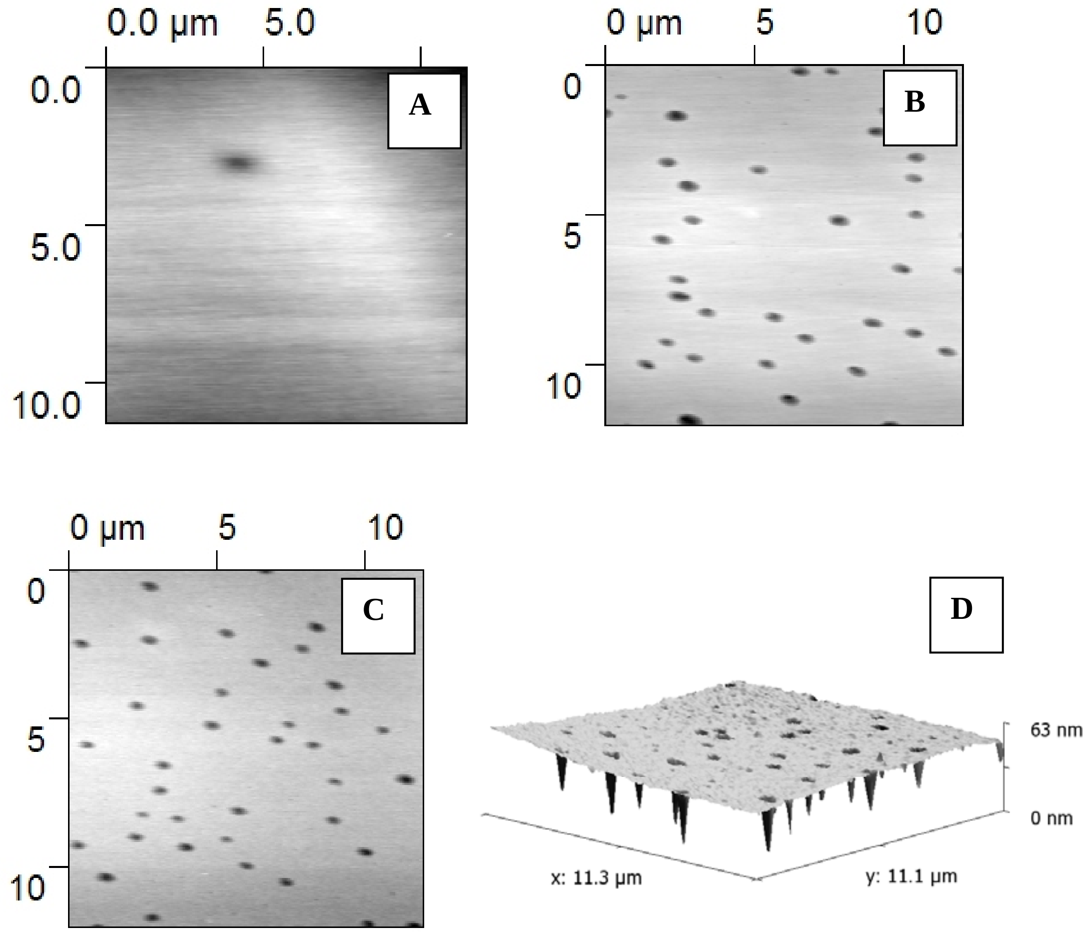

Figure 4.6: AFM scans of Avatrel/Probelec mixture surface following 2000 s swell and 2000 s etch treatment: A) 5 % Probelec, B) 10 % Probelec, C) 20 % Probelec, D) 20 % Probelec 3D image

Mechanical and ultrasonic mixing techniques were studied with the 20% Probelec AP mixture in order to understand the effect on pore size and distribution. Figure 4.7 and Figure 4.8 present two SEM images of the polymer surface following 24 hours of mechanical mixing and a 2000 s swell and 2000 s etch treatment. The smooth, dark field in these images is the Avatrel material, which is largely unaffected by the swell and etch process. The lighter areas are Probelec regions that have been etched to create roughness. It can be seen in Figure 4.7 that there are many large Probelec particles, up to 50 μm in diameter, still present following purely mechanical mixing. Figure 4.8 is a higher magnification image of one of these particles that shows the rough features created when large areas of Probelec are left in the mixture. AFM images indicate that in addition to these large Probelec areas, there are also well dispersed, smaller particles as evidenced by the small pores seen in Figure 4.6. Figure 4.9 and Figure 4.10 shows SEM images of a solution that was mechanically mixed for 24 hrs and then subjected to ultrasonic agitation for a further 8 hrs. Figure 4.9 shows a wide field SEM image with Probelec features as large as 10 μm. The majority of this surface contains very small features, as shown in Figure 4.10, with a diameter of 200-500 nm. AFM scans confirm the presence of well-dispersed 200-500 nm Probelec areas on the surface. Thus ultrasonic mixing breaks up the largest Probelec particles, creating more uniformly sized pores on the surface. Despite these advances in roughness development, the surfaces of the AP mixture did not enable catalyst adsorption or electroless copper deposition without further treatment. Thus, the role of purely mechanical bonding could not be quantified using this approach alone.

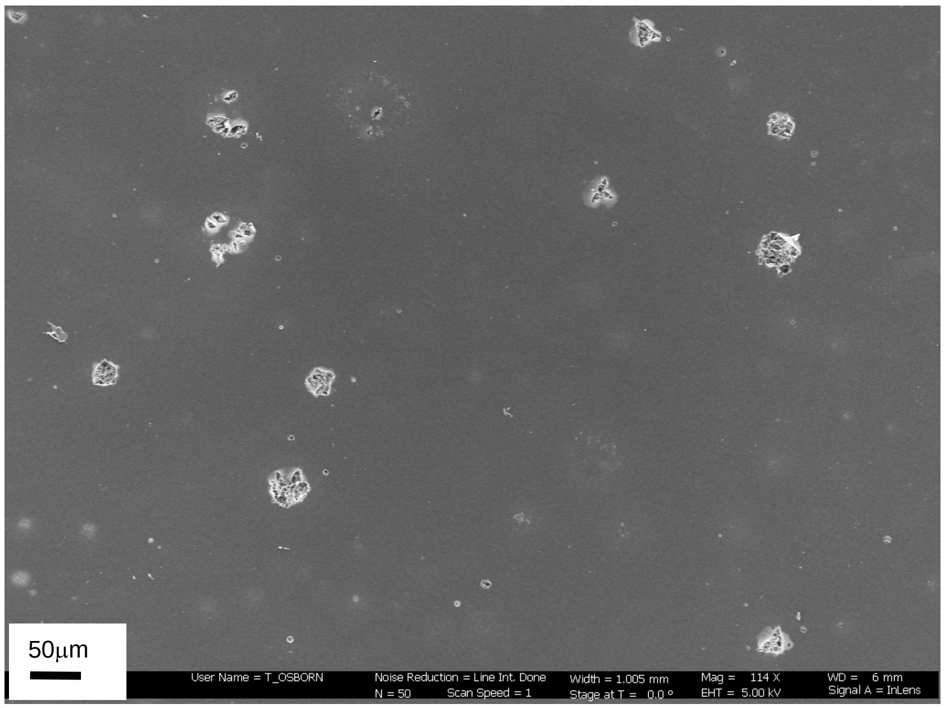

Figure 4.7: SEM image of Avatrel/Probelec (20 % Probelec) mixture with 24 hr mechanical mixing following a 2000s swell and 2000 s etch treatment at 114 X magnification

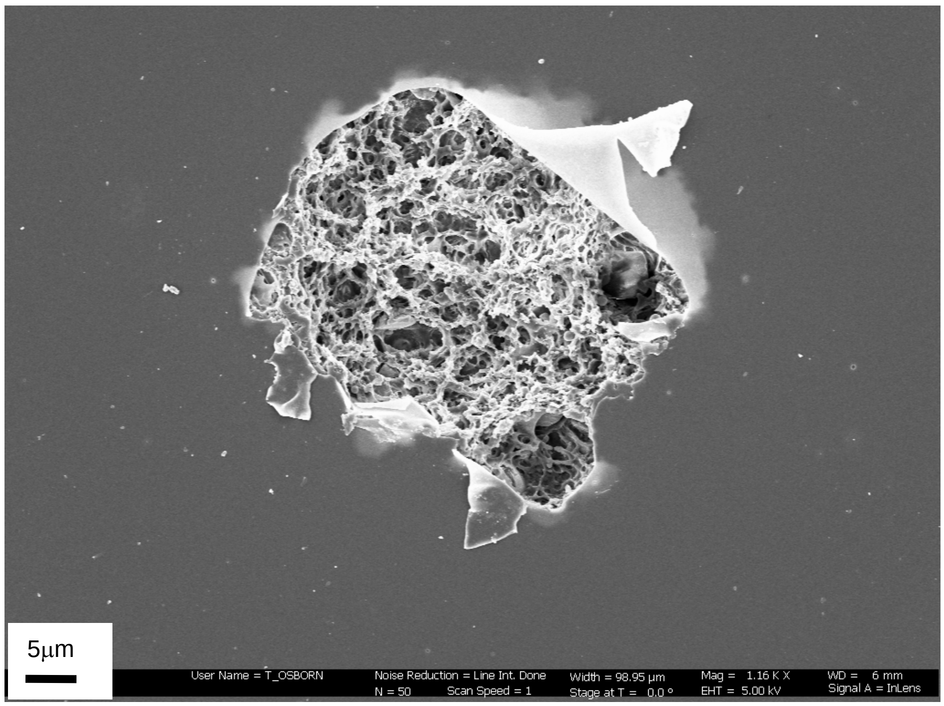

Figure 4.8: SEM image of Avatrel/Probelec (20 % Probelec) mixture with 24 hr mechanical mixing following a 2000s swell and 2000 s etch treatment at 1160 X magnification

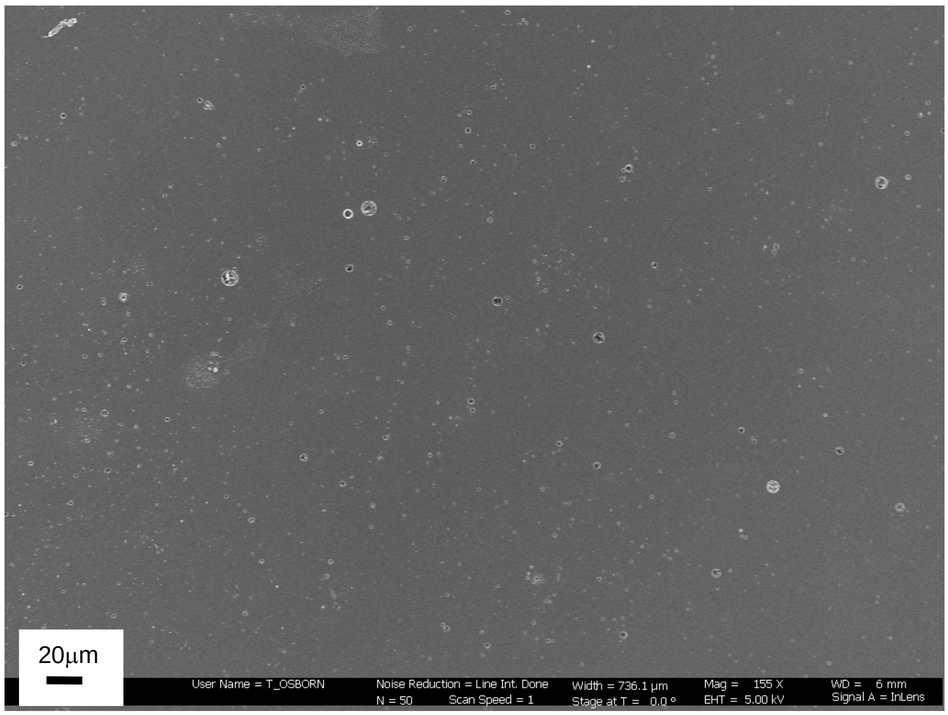

Figure 4.9: SEM image of Avatrel/Probelec (20 % Probelec) mixture with 24 hr mechanical mixing followed by 8 hr ultrasonic agitation and a 2000s swell and 2000 s etch treatment at 155 X magnification

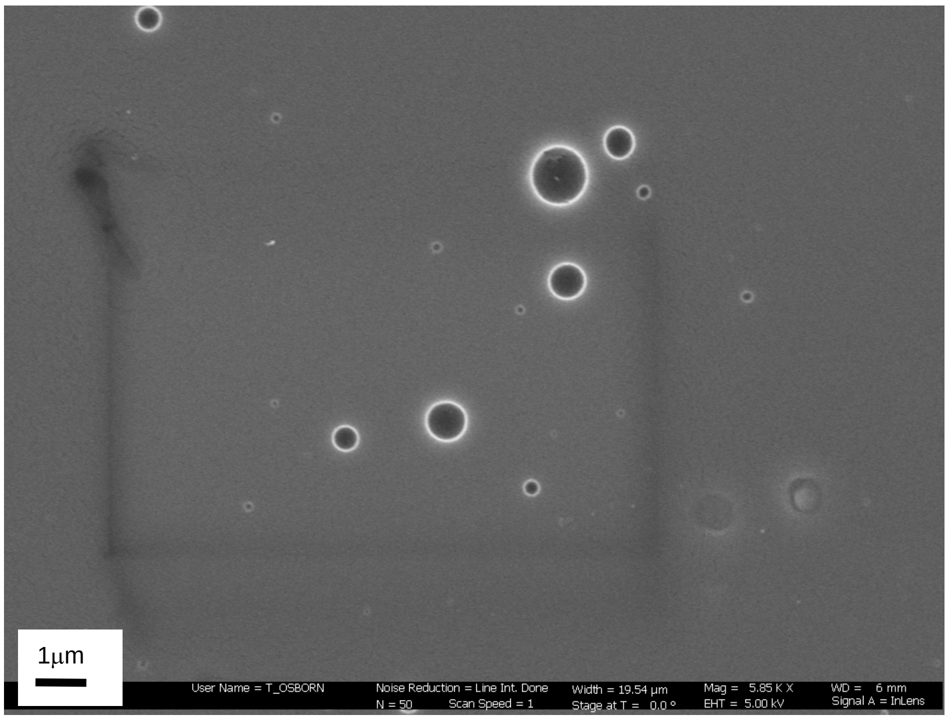

Figure 4.10: SEM image of Avatrel/Probelec (20 % Probelec) mixture with 24 hr mechanical mixing followed by 8 hr ultrasonic agitation and a 2000s swell and 2000 s etch treatment at 5850 X magnification

NH_3 plasma treatments were utilized to enhance catalyst adsorption and chemical bonding on the polymer surfaces. Figure 4.11 presents two XPS survey scans for Probelec, before and after plasma treatment. Before plasma treatment, the Probelec shows the presence of two elements, carbon (73.2%) and oxygen (26.8%). Following plasma treatment, the surface contains three elements, carbon (68.7%), oxygen (23.3%), and nitrogen (8.0%). Figure 4.12 shows XPS survey scans for Avatrel. As with Probelec, there are two elements on the surface before plasma treatment, carbon (91.9%) and oxygen (8.1%), and three present after the plasma, carbon (72.8%) oxygen (22.1%), and nitrogen (5.1%). These plasma treatments also increased adhesion with the electroless copper. The Probelec peel strength increased from 0 to 0.11 N/mm, and the Avatrel peel strength increased from 0 to 0.26 N/mm. In both cases, the RMS roughness of the surface remained below 20 nm following plasma treatments. Increasing plasma power was found to create less chemical modification and more roughness on the Avatrel surface (Table 4.1). These conditions enabled plating but did not create any measurable adhesion, indicating that this level of peak-valley roughness (<20 nm RMS) does not facilitate mechanical anchoring.

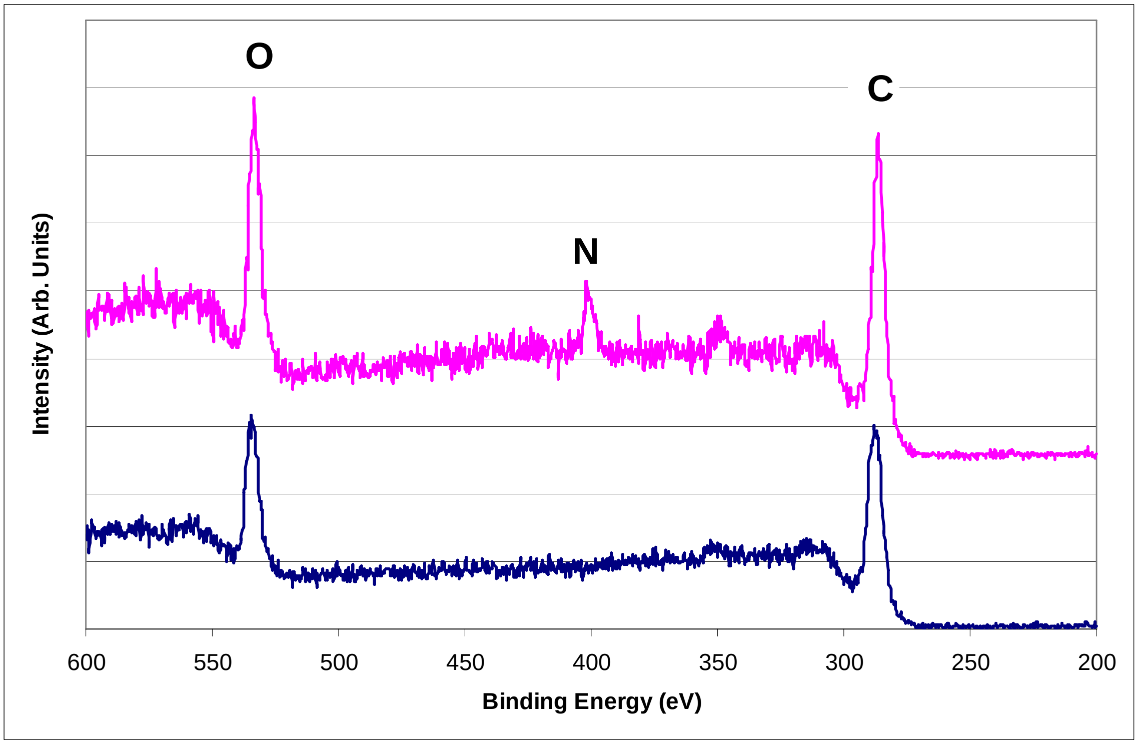

Figure 4.11: XPS survey spectra of Probelec 81/7081 before (blue data set) and after (pink data set) 80 W NH_3 plasma treatment

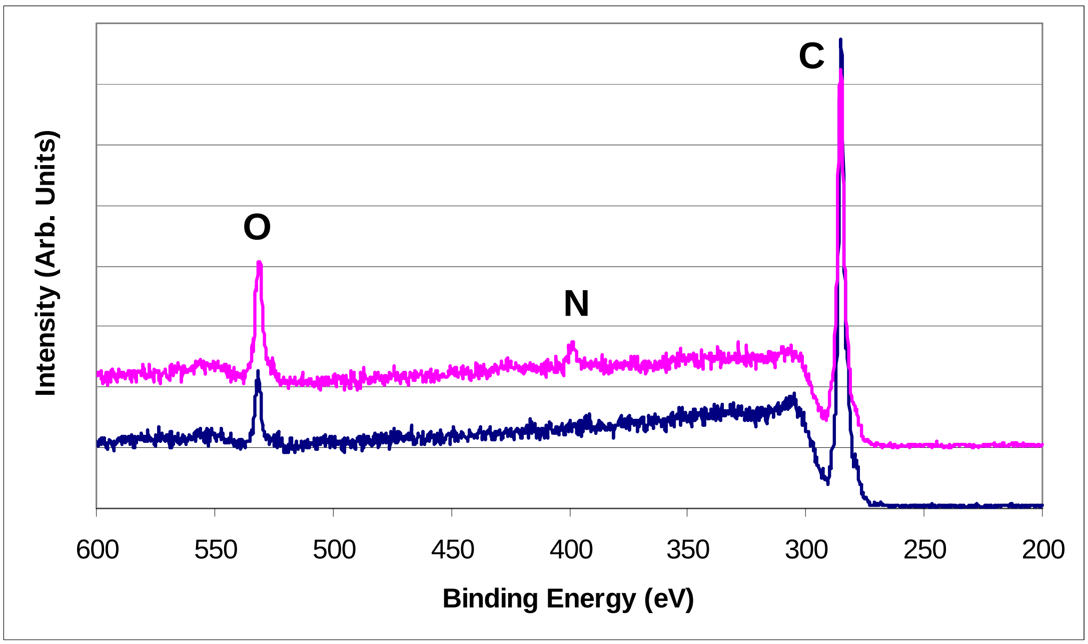

Figure 4.12: XPS survey spectra of Avatrel 2190P before (blue data set) and after (pink data set) 80 W NH_3 plasma treatment

Table 4.1: Peel strength, RMS roughness, and XPS results for Avatrel and AP mixtures

Material	Plasma Treatment	Atomic Concentrations (At %)			RMS Roughness (nm)	Adhesion (N/mm)
		C	O	N		
Avatrel	No Treatment	95.8	4.2	0	1.1	0
AP Mixture	No Treatment	76.1	23.9	0	15.2	0
Avatrel	80 W NH_3	72.5	21.9	5.7	9.3	0.26
AP Mixture	80 W NH_3	75.4	18.2	6.4	13.8	0.51
Avatrel	300 W NH_3	73.5	24.8	1.7	16.3	0

A combined wet-chemical and plasma treatment was investigated with Probelec and the AP mixture in order to create surfaces capable of both mechanical anchoring and chemical bonding. Table 4.2 shows the Probelec adhesion results following swell and etch treatments with and without a 5 min 80W NH_3 plasma treatment. Samples with shorter etch times and lower initial adhesion exhibit reductions in adhesion and roughness following the plasma treatment. For example, the sample with 100 s etch alone exhibited a peel strength of 0.66 N/mm and roughness of 63 nm; however, following plasma treatment the peel strength was reduced to 0.27 N/mm and roughness was reduced to 38nm. Meanwhile, adhesion on samples with high roughness levels was found to be unaffected by the plasma treatment. This effect is evidenced in the samples that had been etched for 300 s, which have the same peel strength with and without the plasma treatment.

Table 4.2: Peel strengths and RMS roughness values for Probelec with and without plasma treatment (all samples received a 30s swell treatment)

Etch Treatment Time (s)	5 min 80 W NH_3 Plasma Treatment	RMS Roughness (nm)	Peel Strength (N/mm)
0	No	3.5	0
0	Yes	17	0.11
50	No	40	0.21
50	Yes	22	0.18
100	No	63	0.66
100	Yes	38	0.27
300	No	350	1.47
300	Yes	310	1.47
600	No	450	1.52
600	Yes	450	1.59

Table 4.3 presents XPS results for combined treatment samples with etch treatment times no greater than 80 s. It can be seen that each sample following plasma treatment has approximately the same nitrogen concentration (7-9%). Also, the oxygen and carbon concentrations are consistent throughout the samples with only small decreases in each following plasma treatment. These decreases are due to the nitrogen added to the surface during plasma treatment. The palladium concentration is also consistent from sample to sample with concentrations ranging from 1.3 to 1.9%. Finally, the last three rows of this table illustrate the effect of varying plasma treatment time on the surface concentrations of nitrogen. It can be seen that reducing the treatment time from 5 minutes to 30 seconds reduces nitrogen concentration from 9.6% to 8.9%.

Table 4.3: Detailed Probelec 81/7081 XPS results (all samples received a 30 s swell treatment)

			Chemical Species Atomic Concentrations				
Etch Treatment Time (s)	80 W NH_3 Plasma Treatment		C	O	N	Pd	Sn
40	No		73.2	26.8	0	--	--
		Sn-Pd	39.7	46.8	3.2	1.4	8.9
60	No		74.9	25.1	0	--	--
		Sn-Pd	37.7	49.2	3.11	1.4	8.6
80	No		72.6	27.4	0	--	--
		Sn-Pd	34.1	51.1	2.5	1.9	10.4
40	30 s		68.7	23.3	8	--	--
		Sn-Pd	33	53	3.1	1.7	9.3
60	30 s		69.9	22.8	7.3	--	--
		Sn-Pd	36.5	49.1	3.1	1.6	9.7
80	30 s		68.9	22.3	8.9	--	--
		Sn-Pd	38.5	48.4	3	1.3	8.9
80	2 min		68	22	10	--	--
80	5 min		67.8	22.7	9.6	--	--

Figure 4.13 shows the peel test results for Probelec with a swell and etch only treatment and with a combined swell, etch, and plasma treatment. In the swell and etch only data set samples received a 30 s swell treatment and a 30-100 s etch treatment. Roughness under these conditions remained below 100 nm in all cases with adhesion ranging from 0.4 N/mm to 0.65 N/mm. The combined treatment data set used the same range of swell and etch conditions, with an additional 30 s 80 W NH_3 plasma treatment. These treatments created improved adhesion when compared to the swell and etch only surface. The offset between the data sets was approximately 0.20 N/mm for a given RMS roughness value. Adhesion between electroless copper and Avatrel materials was also measured. Utilizing the 20% Probelec AP mixture with a 2000 s swell, 2000 s etch, and a 30s 80W NH_3 treatment peel strength increased to 0.51 N/mm with RMS roughness values less than 20 nm (Table 4.1). This peel strength is 0.25 N/mm larger than that obtained with purely chemical bonding from plasma treatments alone.

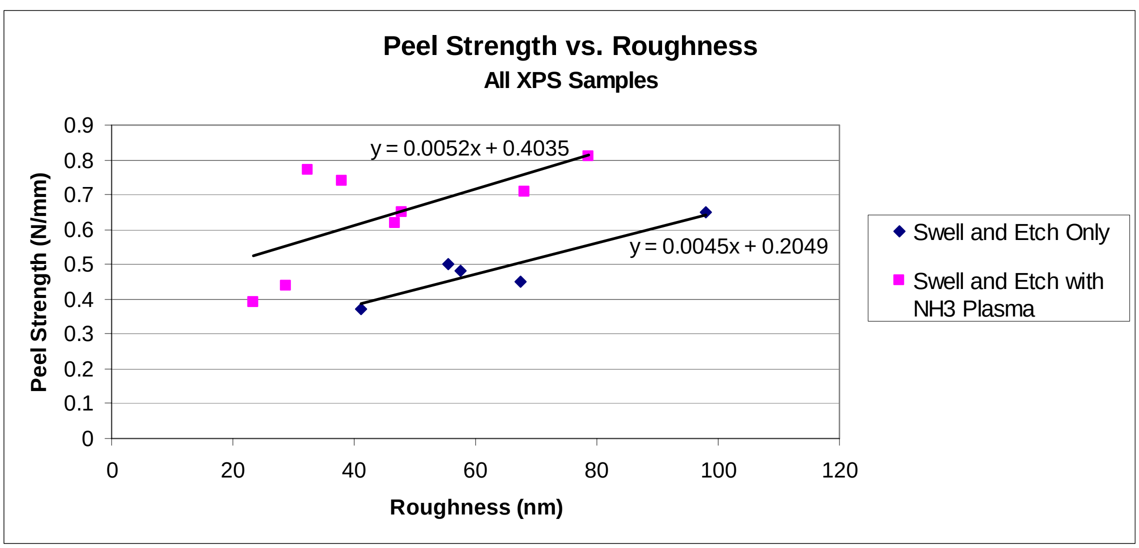

Figure 4.13: Peel strength versus RMS roughness chart for Probelec samples with and without 30 s 80W NH_3 plasma treatments

4.3 Discussion

In order to increase adhesion while maintaining smooth surfaces, processes that combine chemical bonding and mechanical anchoring have been investigated. An attempt was made to quantify the contributions of each mechanism through experimentation, with wet-chemical treatments used for mechanical anchoring improvements and plasma treatments for chemical bonding enhancement. The individual contributions to adhesion have been combined to produce optimum surfaces with the minimum necessary roughness and acceptable adhesion.

When comparing the degree of roughness created in Probelec and Avatrel by wet etching it is apparent that different processes are occurring, producing roughness with different magnitudes and morphologies from one material to the other. The Probelec pore-type roughness formation described in the introduction does not occur in Avatrel because of the location and function of the epoxy groups. In Avatrel, unlike Probelec, the epoxy groups are present as side-groups off of the main polymer chain and are mainly responsible for crosslinking of the polymer. Upon curing, approximately 80% of the epoxide rings are opened and used for crosslinking, producing a series of ether linkages connecting polymer chains.[96] The Avatrel material used in this study, which has a molecular weight of 200,000 a.m.u. contains approximately 200 epoxy-related crosslinks per polymer chain when cured. When the etch process attacks one of the ether linkages on these crosslinks, it enables the attack of subsequent linkages on the same crosslink chain (Figure 4.14). Once all the ether linkages on a given crosslink are etched there is no mechanism for propagation of the etch process into the main polymer chain and it stops. Etching of the maximum length of polymer side group leads to the loss of the equivalent of an eight carbon chain with an approximate length of just 1.2 nm, as opposed to Probelec in which the entire polymer chain can be removed in an etching sequence. Removing repeated small lengths of polymer through extending etching leads to the retention of relatively smooth surfaces with only the peak-valley roughness morphology seen in Figure 4.5B.

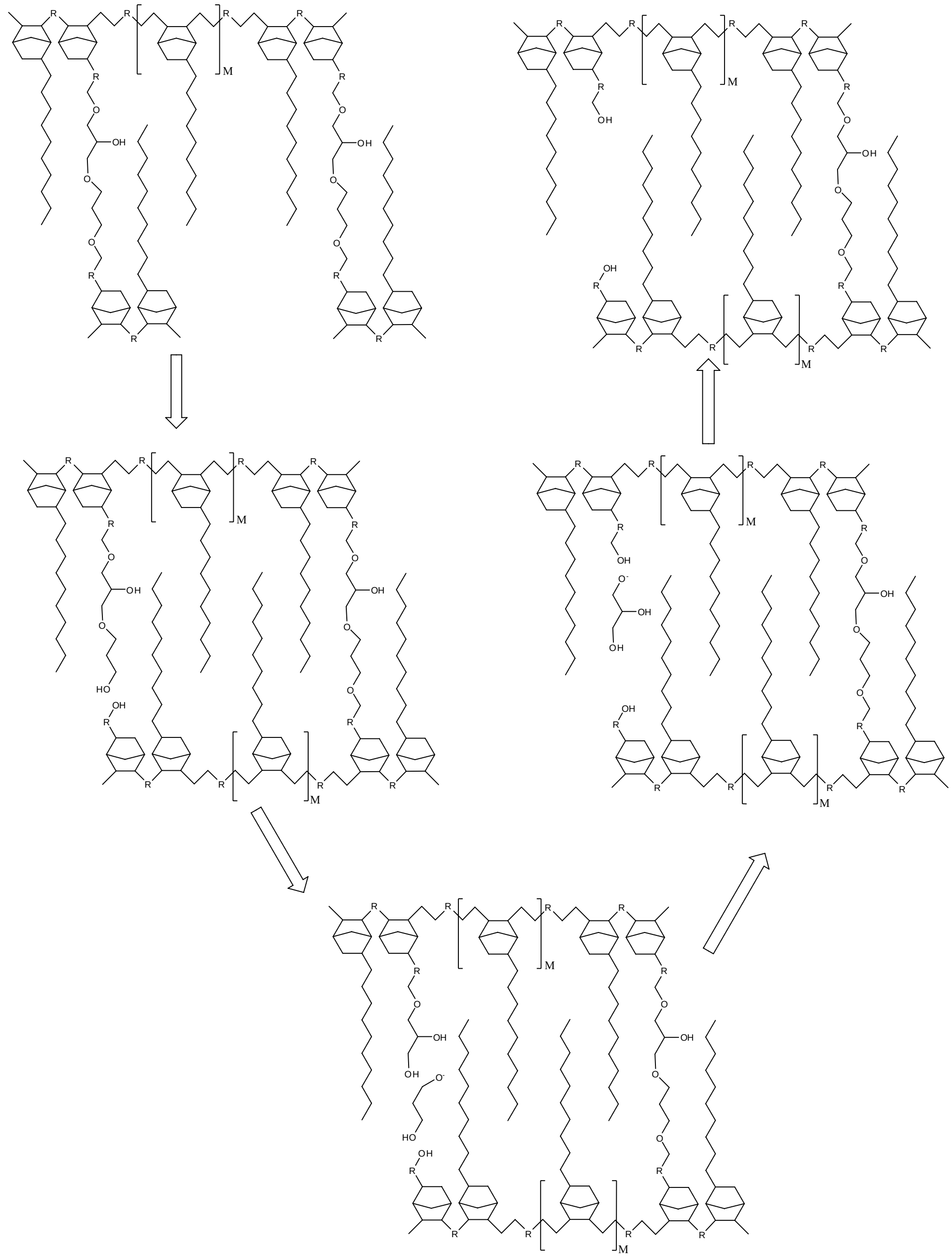

Figure 4.14: Avatrel 2190P proposed etch mechanism schematic

This work illustrates that the epoxy functionality alone is not sufficient for creating high levels of pore-type roughness. If this functionality is present in the polymer backbone it enables pore-formation roughness and enhanced adhesion. Moving this functionality to a side group off of the main polymer chain, however, minimizes the effect of the etch process leaving materials smooth and providing no adhesion enhancement. It is clear that in order to enhance adhesion with advanced materials different techniques are required. A new approach (i.e. using a blend of Avatrel and Probelec) has been taken to form the pore-type roughness needed for mechanical interlocking on the Avatrel surface.

In this approach, a small amount (5-20% by weight) of Probelec in propylene glycol methyl ether acetate (PGMEA) is mixed with Avatrel in mesitylene. The solvents for these polymers are immiscible leading to the formation of two phases in the mixture, with small droplets of Probelec/PGMEA suspended in the Avatrel/mesitylene bulk phase. Ideally these droplets would be small and uniformly dispersed throughout the bulk phase. A process flow diagram for this approach is shown in Figure 4.15. After the mixing, spin-coating, and curing processes described in the experimental procedures section of this report, the AP blend is subjected to a swell and etch treatment that preferentially etches the Probelec areas while leaving the Avatrel areas smooth. The Probelec droplets can be thought of as space-holders which are removed through the etch process to leave pores on the Avatrel surface. The resulting surface contains well-dispersed pores that are 200-500 nm in diameter and 70 nm deep as shown in Figure 4.6. The RMS roughness of these surfaces remains low, less than 20 nm, despite the presence of pores because the

Avatrel surface is largely unaffected by the etch process. The uniformity of these surfaces and the dispersion of pores is strongly affected by the mixing technique used.

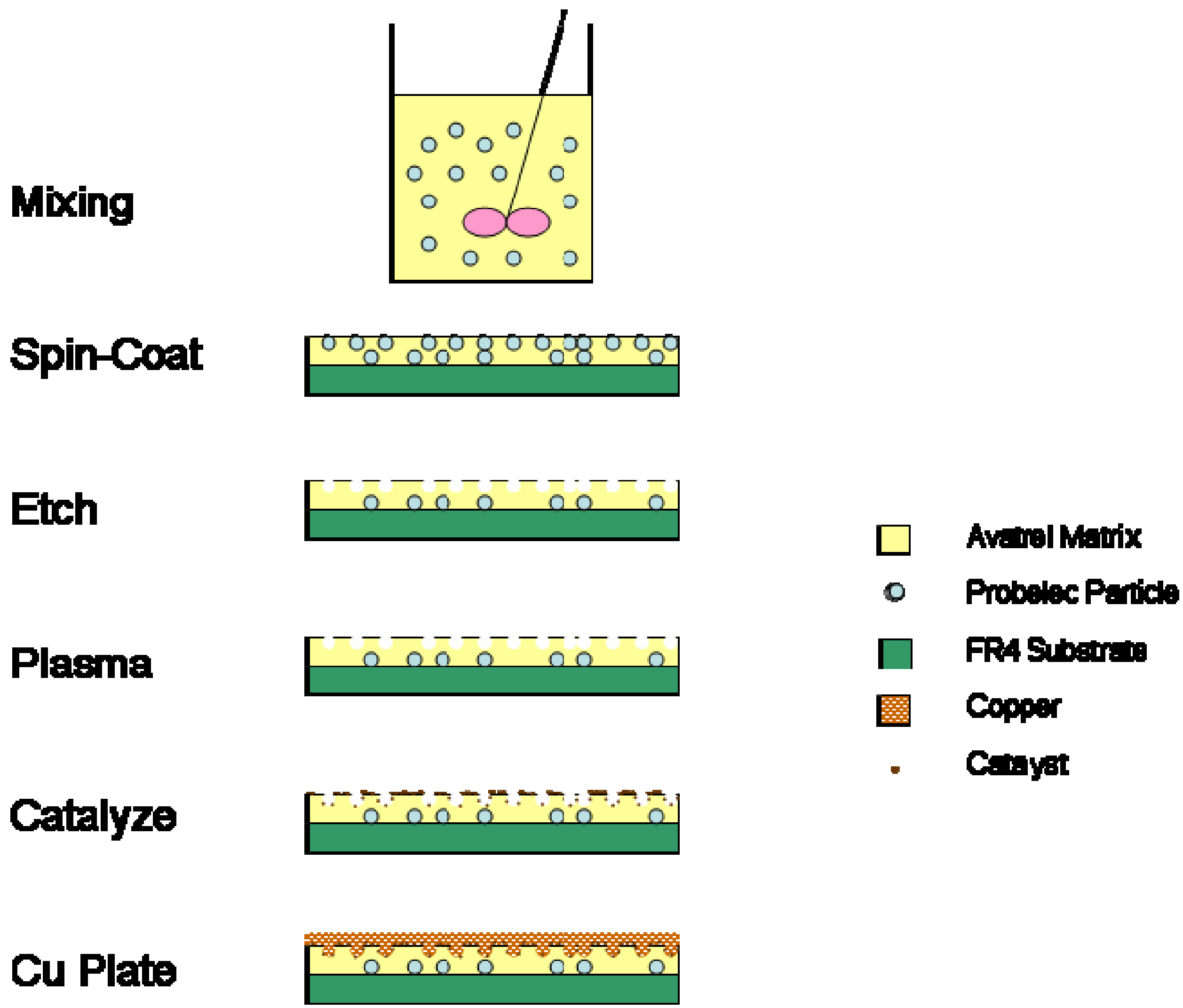

Figure 4.15: Avatrel/Probelec blend process flow diagram

Mechanical mixing alone, as shown in Figure 4.7 and Figure 4.8, does not adequately break-up large Probelec particles, leaving 30-50 μm areas of Probelec on the surface. When these large particles are subjected to the swell and etch process they act like the Probelec bulk material, creating large scale pores and extreme roughness. Probelec particles in the 200-500 nm diameter range are removed completely by the etch process, leaving the same size pore on the surface. The larger particles however, are not completely removed leaving the large pores and high levels of roughness seen in Figure 4.6. This leads to inconsistent adhesion, high adhesion over these Probelec areas and normal adhesion elsewhere, and large variance in roughness across the polymer surface, leading to electrical performance and mechanical reliability issues. Adding ultrasonic mixing to the process enables the break-up of more of these large particles, leaving the surface more uniform (Figures 4.6, 4.9, and 4.10) and minimizing the problems of inconsistent adhesion and roughness across the surface.

Plasma treatments were studied in order to enable catalyst adsorption and improve adhesion through improved chemical bonding. These treatments on Probelec and Avatrel are shown to increase adhesion by 0.15 and 0.26 N/mm respectively while maintaining smooth surfaces. The level of surface roughness created in this process (17 nm for Probelec, 9.4 nm for Avatrel) is quite low. Avatrel materials with similar roughness (16.3 nm) obtained through higher power plasma treatments have shown no adhesion, indicating that this level of peak-valley roughness does not enable mechanical anchoring (Table 4.1). Thus, the adhesion gains realized through these plasma treatments (0.15-0.26 N/mm) can be attributed to chemical bonding improvements on the polymer surface.

Combined treatments, which take advantage of both mechanical anchoring and chemical bonding, were attempted with Probelec and the AP mixture, utilizing the optimum conditions identified in the individual investigations. It was found that the optimum conditions for mechanical anchoring, long swell and etch treatments and rough surfaces, were not suitable for combined treatments. These conditions produced surfaces with more roughness than desired and led to cohesive failure inside the polymer, not adhesive failure at the copper/polymer interface. The effect of plasma treatment which enhances adhesion at the interface is not measured when failure occurs cohesively (Table 4.2, 300 and 600 s etch data). In order to quantify the effect of these treatments, adhesion must occur adhesively at the interface. Limiting the swell to 30 s and the etch 30-100 s produced samples that failed adhesively with and without plasma treatments, while maintaining RMS roughness levels below 100 nm. Utilizing these conditions with a 5 min 80W NH_3 plasma treatment following the swell and etch proved to reduce adhesion compared to the samples with swell and etch alone (Table 4.2, 50 and 100 s etch data). The five minute plasma treatment significantly decreases the roughness of the surface (up to 41 nm RMS roughness reduction) through plasma etching, reducing mechanical anchoring and adhesion. Limiting the plasma time to 30 seconds, thereby reducing the time of plasma etching, minimized the smoothing effect while maintaining the desired chemical modifications of the surface. Table 4.3 confirms the NH_3 plasma treatment creates similar chemical modifications whether treatment time is 30 s, 2 min, or 5 min treatment times as evidenced by consistent nitrogen concentration increases on the surface.

Utilizing a 30 s swell, 30-100 s etch, and 30 s 80 W NH_3 plasma condition, combined treatments were tested. Figure 4.13 compares peel test results with and without the plasma treatment. With a purely swell and etch treatment Probelec exhibits peel strength values between 0.38 and 0.65 N/mm depending on the roughness generated. These peel strength values correspond to the contribution of mechanical anchoring on the surface. Adding the plasma treatment increases adhesion for a given level of RMS roughness. The difference in adhesion before and after plasma treatments for a given RMS value is a measure of the contribution of chemical bonding to adhesion. In these experiments this contribution was consistently 0.20 N/mm. Thus, this technique is capable of combining the effects of chemical bonding and mechanical anchoring and allowing for the quantification of the contributions of each to adhesion. The resulting surfaces are smooth and adherent, with RMS roughness as low as 40 nm and peel strength values over 0.5 N/mm for most samples. The same effect was also realized with the AP mixtures, improving adhesion from 0.26 N/mm with plasma only treatments to 0.51 N/mm with combined treatments (Table 4.1). In this case the 0.26 N/mm corresponds to chemical bonding and the remainder, 0.25 N/mm, is due to enhanced mechanical anchoring contributed by the pores formed on the surface.

4.4 Summary

A study of adhesion between epoxy-containing substrates and electrolessly deposited copper has been presented. In this study the contributions of mechanical anchoring and chemical bonding were measured individually in order to determine their relative magnitudes and suitable conditions for producing optimum surfaces. For the first time, a study of the etch process for materials with epoxy functionalities as side-groups off of the main polymer chain has been presented. A mechanism for this process with Avatrel has been postulated and compared with the process for a traditional dielectric material with epoxy in the polymer backbone. Wet-chemical and plasma treatments which provide optimum mechanical anchoring and chemical bonding respectively have been identified. Following this work, a treatment protocol that allows both mechanical anchoring and chemical bonding to contribute to adhesion on the same sample was identified. These conditions produced adhesion of greater than 0.5 N/mm for samples with RMS roughness less than 50 nm on the surface by combining the benefits of chemical bonding and mechanical anchoring on one surface. These results aid the process of maintaining adequate adhesion on smooth surfaces for use with future microelectronic applications.

CHAPTER 5

CONCLUSIONS AND FUTURE WORK

5.1 Conclusions

The work presented in this dissertation focused on increasing adhesion between electrolessly deposited copper and dielectric materials for use in microelectronic devices. Advances are required because of the ever-evolving technology of the microelectronics industry. Specifically, new dielectric materials with smoother surfaces (to avoid signal scattering and mechanical disconnects) and enhanced electrical properties (to minimize RC delay and loss) are needed. At the same time adhesion must be maintained in order to preserve package reliability and mechanical performance. In order to meet these requirements two approaches were taken: a short-term solution -- smoothing the surface of traditional epoxy dielectric materials while maintaining adhesion, and a long-term solution -- increasing adhesion on advanced dielectric materials through chemical bonding and mechanical anchoring. This work resulted in a number of important conclusion about the roles of chemical bonding and mechanical anchoring in both adhesion and catalyst adsorption.

With a polyimide material, it was found that traditional techniques (i.e., those used for epoxy surface preparation) for enhancing adhesion were ineffective, leaving the surface smooth and not enabling catalyst adsorption. Ar plasma treatments were found to roughen the surface and NH_3 plasma treatments created chemical modifications on that surface. The surface roughening of the Ar treatments did not enable catalyst adsorption or adhesion with electroless copper, while the NH_3 treatment did increase catalyst adsorption, enabling the electroless deposition of copper and increasing adhesion. XPS analysis indicated that the NH_3 treatment chemically modified the surface, creating C=N groups whose concentration corresponded well with increased catalyst adsorption. These functional groups interact with Pd on the surface to form Pd-N complexes that result in the increased catalyst adsorption and adhesion. Combining Ar and NH_3 treatments allowed for further increases in both catalyst adsorption and adhesion with electroless copper. These improvements are likely due to two effects: increased surface area for chemical bonding created by the Ar roughening treatment and some bond rearrangements that occur during the Ar treatment creating a more favorable surface for NH_3 plasma treatments. The maximum adhesion achieved with this material, however, remained below acceptable levels even in the best cases.

Epoxy-based materials were investigated in order to take advantage of the knowledge surrounding adhesion between traditional epoxies and electroless copper. This adhesion is obtained by roughening the polymer surface with a swell and etch process, which attacks the ether linkages located in the polymer backbone removing large areas of polymer. Following this treatment epoxy surfaces have RMS roughness values of 100-500 nm with large pore-type features (>1μm in size) that aid in mechanical anchoring and adhesion but disrupt feature integrity and electrical performance. An investigation with a traditional epoxy was undertaken in order to try to minimize the level of roughness needed to maintain adhesion. It was determined that simply minimizing the swell and etch process, and thereby reducing roughness, produced samples with inadequate adhesion. Combining minimal roughening with NH_3 plasma treatments, however, produced samples with smooth surfaces that maintained adhesion at a higher level. Samples were produced with adhesion of over 0.5 N/mm while maintaining RMS roughness below 50 nm, a large improvement over traditional process conditions that utilize. Analysis of these results allow for the separation of the individual contributions of mechanical anchoring and chemical bonding to adhesion. For the conditions tested, chemical bonding consistently accounted for 0.2 N/mm of adhesion while mechanical anchoring contributed 0.35-0.65 N/mm depending on the roughness developed. This chemical bonding is the result of interactions between surface nitrogen, added through plasma treatments, and palladium and copper deposited on that surface.

Avatrel, a polynorbornene polymer containing epoxy functionalities as side groups off of the polymer backbone was also tested. It was found through swell and etch processing that this material did not enable the same morphology or magnitude of roughness as traditional epoxy materials, despite the presence of similar epoxy groups. The difference is in the placement of these epoxy groups, which are in the polymer backbone for traditional epoxies but are present as side-groups of the main polymer chain and are utilized to form crosslinks in the polynorbornene materials. There are hundreds of these crosslinks on every polymer chain; thus, attacking the same ether linkages as in a traditional epoxy, simply breaks a crosslink and does not allow for the removal of significant lengths of polymer. This leads to a surface without features that aid mechanical anchoring. In order to enhance mechanical anchoring with Avatrel, a novel polymer blend approach was attempted (AP blend). In this approach, a small amount of traditional epoxy (5-20 wt%) was blended with the polynorbornene. The traditional epoxy formed small particles of 200-500 nm diameter in the polynorbornene matrix which were then removed with the swell and etch process. This approach created small pores on the polymer surface, which enabled mechanical anchoring and enhanced adhesion by 0.25 N/mm. Combining the AP blend system with a NH_3 plasma treatment produced samples with smooth surfaces (RMS roughness < 20 nm) and strong adhesion (~0.5 N/mm). As was the case with the traditional epoxy, approximately 0.25 N/mm of the total adhesion was contributed by purely chemical bonding, due to interactions between surface nitrogen and the palladium and copper particles deposited on the surface. Thus, with Avatrel, optimum surfaces were produced by utilizing equivalent levels of chemical bonding and mechanical anchoring to enhance adhesion, resulting in a strongly adherent, smooth metal/polymer interface.

Overall, this project endeavored to increase catalyst adsorption and adhesion on traditional and advanced dielectric materials while maintaining smooth surfaces. This goal was achieved through a combination of wet-chemical and plasma treatment that illustrated the importance of both mechanical and chemical bonding. Specific chemical bonding configurations that aid catalyst adsorption and adhesion were identified as were the individual contributions of mechanical anchoring and chemical bonding to adhesion in certain systems. Optimized surfaces, with very low surface roughness and enhanced adhesion, were achieved by sequential combination of roughness formation and chemical modifications. These improvements will enable the use of both current and advanced materials in future microelectronic devices without fear of severe performance degradation from high surface roughness, low adhesion, or poor electrical properties.

5.2 Recommendations for Future Work

Future work on this project may proceed in a number of directions, including purely chemical and purely physical surface modifications of various polymer materials. Ideally, combined treatments, as illustrated in Chapter 4 of this work would be employed in order to take advantage of both adhesion mechanisms. Three areas appear to provide the most promise: incorporating chemical bonding and catalyst adsorption improvements through wet-chemical processes, continuing the development of controlled surface roughness through various blends, and combining these approaches in order to optimize surfaces in the most practical and controllable manner.

Improvements in chemical bonding through wet-chemical processes should focus on utilizing the identification of certain important bonding groups such as C=N found in the plasma treatment work. Replicating the surface produced through plasma treatments with wet-chemical processes such as the use of coupling agents and wet-chemical synthesis has the promise of significantly lowering processing costs and the likelihood of industrial adoption. An important driver in industry adoption is the cost of a process and wet-chemical approaches that do not require the expensive vacuum equipment of plasma processing have a higher likelihood of being adopted.

The second area of focus should be a continued investigation of blends for creating controlled roughness on a variety of polymer surfaces. Utilizing polymer blends, as explored in this report, is one method of creating controlled roughness on the surface. Another method, which may be more easily controlled, is the use of solid particles instead of a second polymer phase. These particles would act as place-holders in the polymer and would be etch away and removed after the polymer had been cured.

Choosing particles which can be easily removed while also not adversely affecting mechanical or electrical properties of the layer is one key to this approach. The size and shape of the particles could be chosen to maximize adhesion while maintaining roughness and feature sizes below acceptable thresholds. A detailed study of adhesion versus both particle size and shape would be particularly useful for future products.

Finally a combination of these two approaches should be attempted. As in this project, the most likely method of optimizing surfaces for adhesion is to combine the effects of chemical bonding and mechanical anchoring. Completing this approach with a more optimized and reliable surface roughness and a more cost-effective method for enhancing chemical bonding would create a set of solutions that could immediately be implemented in current technology.

REFERENCES

1. Ge, J., R. Tuominen, and J.K. Kivilahti, *Adhesion of electrolessly-deposited copper to photosensitive epoxy.* Journal of Adhesion Science and Technology, 2001. **15**(10): p. 1133-1143.

2. Tummala, R.R., *Fundamentals of microsystems packaging*. 2001, New York: McGraw-Hill. vii, 967 p.

3. *International Technology Roadmap for Semiconductors*. Accessed 10/2006: http://public.itrs.net/

4. Johnson, H.W. and M. Graham, *High-speed signal propagation : advanced black magic*. 2003, Upper Saddle River, NJ: Prentice Hall, Professional Technical Reference. xxx, 766 p.

5. Ge, J., M. Turunen, and J. Kivilahti, *Surface modification and characterization of photodefinable epoxy/copper systems.* Thin Solid Films, 2003. **440**(1-2): p. 198-207.

6. Schroer, D., R.J. Nichols, and H. Meyer, *Pretreatment of Polymer Surfaces - the Crucial Step Prior to Metal-Deposition.* Electrochimica Acta, 1995. **40**(10): p. 1487-1494.

7. Pizzi, A. and K.L. Mittal, *Handbook of adhesive technology*. 2nd ed. 2003, New York: M. Dekker. xii, 1024 p.

8. Ahagon, A. and A.N. Gent, *Effect of Interfacial Bonding on Strength of Adhesion.* Journal of Polymer Science Part B-Polymer Physics, 1975. **13**(7): p. 1285-1300.

9. Charbonnier, M., et al., *Electroless plating of glass and silicon substrates through surface pretreatments involving plasma-polymerization and grafting processes.* Journal of Adhesion, 2004. **80**(12): p. 1103-1130.

10. Fowkes, F.M., *Attractive Forces at Interfaces.* Industrial and Engineering Chemistry, 1964. **56**(12): p. 40-&.

11. Chen, M., et al., *Patterned metallization of diamond and alumina substrates.* JOURNAL OF THE ELECTROCHEMICAL SOCIETY, 2000. **147**(7): p. 2607-2610.

12. Chen, M., et al., *Channel-constrained electroless metal deposition on ligating self-assembled film surfaces.* JOURNAL OF THE ELECTROCHEMICAL SOCIETY, 1999. **146**(4): p. 1421-1430.

13. Siau, S., et al., *Influence of chemical pretreatment of epoxy polymers on the adhesion strength of electrochemically deposited Cu for use in electronic interconnections.* Journal of the Electrochemical Society, 2004. **151**(2): p. C133-C141.

14. Siau, S., et al., *Epoxy polymer surface roughness modeling based on kinetic studies of wet chemical treatments.* Journal of the Electrochemical Society, 2004. **151**(8): p. J54-J61.

15. Siau, S., et al., *Kinetic study of wet chemical treatments on the surface roughness of epoxy polymer layers for buildup layers - II. Oxidative treatment of the surface.* Journal of the Electrochemical Society, 2004. **151**(12): p. C831-C849.

16. Wang, Z., et al., *Adhesion improvement of electroless copper to a polyimide film substrate by combining surface microroughening and imide ring cleavage.* Journal of Adhesion Science and Technology, 2002. **16**(8): p. 1027-1040.

17. Bhusari, D., et al., *Plasma treatment and surface analysis of polyimide films for electroless copper buildup process.* Journal of the Electrochemical Society, 2005. **152**(10): p. F162-F170.

18. Friedrich, J.F., et al., *Chemical reactions at polymer surfaces interacting with a gas plasma or with metal atoms - their relevance to adhesion.* Surface & Coatings Technology, 1999. **119**: p. 772-782.

19. Ge, J., M. Turunen, and J. Kivilahti, *Surface modification of a liquid-crystalline polymer for copper metallization.* Journal of Polymer Science Part B-Polymer Physics, 2003. **41**(6): p. 623-636.

20. Li, Y.M. and D.W. Hess, *Plasma etching of thick polynorbornene layers for electronic packaging applications.* Journal of Vacuum Science & Technology B, 2002. **20**(5): p. 2007-2012.

21. Yang, C.Y., J.S. Chen, and S.L.C. Hsu, *Effects of O-2 and N-2 plasma treatment on 6FDA-BisAAF fluorine-contained polyimide.* Journal of the Electrochemical Society, 2006. **153**(6): p. F120-F125.

22. Egitto, F. and L. Matienzo, *Plasma Modification of Polymer Surfaces for Adhesion Improvement.* IBM Journal of Research and Development, 1994. **38**(4): p. 423-439.

23. Ektessabi, A.M. and S. Hakamata, *XPS study of ion beam modified polyimide films.* Thin Solid Films, 2000. **377**: p. 621-625.

24. Flitsch, R. and D.Y. Shih, *An XPS study of argon ion beam and oxygen RIE modified BPDA-PDA polyimide as related to adhesion.* Journal of Adhesion Science and Technology, 1996. **10**(12): p. 1241-1253.

25. Girardeaux, C., et al., *The Polyimide (Pmda-Oda) Titanium Interface .2. Xps Study of Polyimide Treatments and Aging.* Journal of Electron Spectroscopy and Related Phenomena, 1995. **74**(1): p. 57-66.

26. Nakamura, Y., Y. Suzuki, and Y. Watanabe, *Effect of oxygen plasma etching on adhesion between polyimide films and metal.* Thin Solid Films, 1996. **291**: p. 367-369.

27. Zhang, L.L., et al., *Changes in chemical structure and optical properties of polyimide films induced by ion bombardment.* Journal of Applied Physics, 1999. **86**(2): p. 779-781.

28. Bhowmik, S., et al., *Physicochemical and adhesion characteristics of high-density polyethylene when treated in a low-pressure plasma under different electrodes.* Journal of Adhesion, 2006. **82**(1): p. 1-18.

29. Bodo, P. and J.E. Sundgren, *Adhesion of Evaporated Titanium to Polyethylene - Effects of Ion-Bombardment Pretreatment.* Journal of Vacuum Science & Technology a-Vacuum Surfaces and Films, 1984. **2**(4): p. 1498-1502.

30. Bodo, P. and J.E. Sundgren, *Adhesion of Evaporated Titanium Films to Ion-Bombarded Polyethylene.* Journal of Applied Physics, 1986. **60**(3): p. 1161-1168.

31. Collaud, M., et al., *Plasma Treatment of Polymers - the Effect of the Plasma Parameters on the Chemical, Physical, and Morphological States of the Polymer Surface and on the Metal-Polymer Interface.* Journal of Adhesion Science and Technology, 1994. **8**(10): p. 1115-1127.

32. Collaud, M., et al., *Surface Modifications of Polypropylene after in-Situ Ar and N-2 Plasma Treatments - an Xps Study.* Applied Surface Science, 1993. **72**(1): p. 19-29.

33. Foerch, R. and D.H. Hunter, *Remote Nitrogen Plasma Treatment of Polymers - Polyethylene, Nylon 6,6, Poly(Ethylene Vinyl Alcohol), and Poly(Ethylene-Terephthalate).* Journal of Polymer Science Part a-Polymer Chemistry, 1992. **30**(2): p. 279-286.

34. Gerenser, L.J., *An X-Ray Photoemission Spectroscopy Study of Chemical Interactions at Silver Plasma Modified Polyethylene Interfaces - Correlations with Adhesion.* Journal of Vacuum Science & Technology a-Vacuum Surfaces and Films, 1988. **6**(5): p. 2897-2903.

35. Harth, K. and H. Hibst, *Surface Modification of Polypropylene in Oxygen and Nitrogen Plasmas.* Surface & Coatings Technology, 1993. **59**(1-3): p. 350-355.

36. Howlader, M., et al., *Surface activated bonding of LCP/Cu for electronic packaging.* Journal of Materials Science, 2005. **40**(12): p. 3177-3184.

37. Normand, F., et al., *Surface-Treatment of Polypropylene by Oxygen Microwave-Discharge.* Materials Science and Engineering a-Structural Materials Properties Microstructure and Processing, 1991. **139**: p. 103-109.

38. Nowak, S., et al., *X-Ray Photoelectron-Spectroscopy Study of the Polypropylene Magnesium Interface after Insitu Plasma and Ion Treatment - Sticking, Bonding, and Film Growth.* Journal of Vacuum Science & Technology a-Vacuum Surfaces and Films, 1993. **11**(3): p. 481-489.

39. Friedrich, J.F., R. Mix, and G. Kuhn, *Adhesion of metals to plasma-induced functional groups at polymer surfaces.* Surface & Coatings Technology, 2005. **200**(1-4): p. 565-568.

40. Gerenser, L.J., *Photoemission Investigation of Silver Poly(Ethylene-Terephthalate) Interfacial Chemistry - the Effect of Oxygen-Plasma Treatment.*

Journal of Vacuum Science & Technology a-Vacuum Surfaces and Films, 1990. **8**(5): p. 3682-3691.

41. Pascu, M., et al., *Study of electroless copper plating onto PVDF modified by radio frequency plasma treatment.* Journal of Physics D-Applied Physics, 2006. **39**(10): p. 2224-2230.

42. Zhu, Q.Y., et al., *Influence of plasma treatment on the electroless deposition of copper on carbon fibers.* Journal of Macromolecular Science Part a-Pure and Applied Chemistry, 2006. **43**(11): p. 1853-1865.

43. Chen, M.S., S.L. Brandow, and W.J. Dressick, *Additive channel-constrained metallization of high-resolution features.* Thin Solid Films, 2000. **379**(1-2): p. 203-212.

44. Chen, M.S., et al., *Channel-constrained electroless metal deposition on ligating self-assembled film surfaces.* Journal of the Electrochemical Society, 1999. **146**(4): p. 1421-1430.

45. Chen, M.S., et al., *Patterned metallization of diamond and alumina substrates.* Journal of the Electrochemical Society, 2000. **147**(7): p. 2607-2610.

46. Chen, Y.J., et al., *Electroless metallization of glass surfaces functionalized by silanization and graft polymerization of aniline.* Langmuir, 2001. **17**(23): p. 7425-7432.

47. Siau, S., et al., *Chemical modification of buildup epoxy surfaces for altering the adhesion of electrochemically deposited copper.* Journal of the Electrochemical Society, 2005. **152**(9): p. D136-D150.

48. Siau, S., et al., *Epoxy polymer surface modification through wet-chemical organic surface synthesis for adhesion improvement in microelectronics.* Thin Solid Films, 2006. **495**(1-2): p. 348-356.

49. Chan-Park, M.B. and S.S. Tan, *Thermal graft copolymerization of 4-vinyl pyridine on polyimide to improve adhesion to copper.* International Journal of Adhesion and Adhesives, 2002. **22**(6): p. 471-475.

50. Friedrich, J.F., R. Mix, and G. Kuhn, *Functional groups bearing plasma homo and copolymer layers as adhesion promoters in metal-polymer composites.* Surface & Coatings Technology, 2003. **174**: p. 811-815.

51. Shojaei, A., R. Fathi, and N. Sheikh, *Adhesion modification of polyethylenes for metallization using radiation-induced grafting of vinyl monomers.* Surface & Coatings Technology, 2007. **201**(16-17): p. 7519-7529.

52. Yu, W.H., E.T. Kang, and K.G. Neoh, *Electroless plating of copper on (100)-oriented single crystal silicon substrates modified by plasma graft polymerization of 4-vinylpyridine.* Journal of the Electrochemical Society, 2002. **149**(11): p. C592-C599.

53. Yu, W.H., et al., *Electroless plating of copper via a Sn-free process on dielectric SiLK surface modified by UV-induced graft copolymerization with 4-vinylpyridine and 1-vinylimidazole.* Journal of the Electrochemical Society, 2002. **149**(10): p. C521-C528.

54. Yu, Z., E. Kang, and K. Neoh, *Electroless plating of copper on polyimide films modified by surface grafting of tertiary and quaternary amines polymers.* Polymer, 2002. **43**(15): p. 4137-4146.

55. Yu, Z.J., E.T. Kang, and K.G. Neoh, *Amidoximation of the acrylonitrile polymer grafted on poly(tetrafluoroethylene-co-hexafluoropropylene) films and its relevance to the electroless plating of copper.* Langmuir, 2002. **18**(26): p. 10221-10230.

56. Wu, J.Z., et al., *Surface modification of poly(Tetrafluoroethylene) films by graft copolymerization for adhesion improvement with sputtered In-Sn oxides.* Journal of Adhesion, 1999. **71**(4): p. 357-376.

57. Wu, S.Y., E.T. Kang, and K.G. Neoh, *Surface modification of poly(tetrafluoroethylene) films by graft copolymerization for adhesion enhancement with electrolessly deposited copper.* Journal of Adhesion Science and Technology, 2000. **14**(11): p. 1451-1468.

58. Wu, S.Y., et al., *Surface modification of poly(tetrafluoroethylene) films by graft copolymerization for adhesion improvement with evaporated copper.* Macromolecules, 1999. **32**(1): p. 186-193.

59. Wu, S.Y., et al., *Surface modification of poly(tetrafluoroethylene) films by double graft copolymerization for adhesion improvement with evaporated copper.* Polymer, 1999. **40**(25): p. 6955-6964.

60. Aithal, R.K., et al., *Electroless copper deposition on silicon with titanium seed layer.* Materials Chemistry and Physics, 2006. **98**(1): p. 95-102.

61. Atanasoska, L., et al., *Xps Study of Chemical Bonding at Polyimide Interfaces with Metal and Semiconductor Overlayers.* Vacuum, 1990. **40**(1-2): p. 85-90.

62. Kim, J.J. and S.H. Cha, *Optimized surface treatment of indium tin oxide (ITO) for copper electroless plating.* Japanese Journal of Applied Physics Part 2-Letters, 2002. **41**(11A): p. L1269-L1271.

63. Sun, R.D., et al., *Adhesion of electroless deposited Cu on ZnO-coated glass substrates: The effect of the ZnO surface morphology.* Journal of the Electrochemical Society, 1999. **146**(6): p. 2117-2122.

64. H. D. Merchant, J.T.W., L. A. Giannuzzi, Y. L. Liu, *Metallurgy and performance of electrodeposited copper for flexible circuits.* Circuit World, 2000. **26**(4): p. 7-14.

65. Iwamori, S., et al., *Effect of an interfacial layer on adhesion strength deterioration between a copper thin film and polyimide substrate.* Vacuum, 1998. **51**(4): p. 615-618.

66. Tseng, W.T., C.H. Lo, and S.C. Lee, *Electroless deposition of Cu thin films with CuCl2-HNO3 based chemistry - I. Chemical formulation and reaction mechanisms.* Journal of the Electrochemical Society, 2001. **148**(5): p. C327-C332.

67. Tseng, W.-T., C.-H. Lo, and S.-C. Lee, *Electroless deposition of Cu thin films with CuCl2-HNO3 based chemistry I. Chemical formulation and reaction mechanisms.* Journal of the Electrochemical Society, 2001. **148**(5): p. C327-C332.

68. Krulik, G.A., *Tin-Palladium Catalysts for Electroless Plating.* Platinum Metals Review, 1982. **26**(2): p. 58-64.

69. Schlesinger, M. and M. Paunovic, *Modern electroplating*. 4th edition ed. 2000, New York: John Wiley. xiv, 868 p.

70. Li, J., H. Hayden, and P.A. Kohl, *The influence of 2,2 '-dipyridyl on non-formaldehyde electroless copper plating.* Electrochimica Acta, 2004. **49**(11): p. 1789-1795.

71. Paunovic, M. and R. Arndt, *The Effect of Some Additives on Electroless Copper Deposition.* Journal of the Electrochemical Society, 1983. **130**(4): p. 794-799.

72. Schoenbe.Ln, *Use of Organic Additives to Stabilize and Enhance Deposition Rate of Electroless Copper Plating.* Journal of the Electrochemical Society, 1972. **119**(11): p. 1491-&.

73. Vitkavage, D. and M. Paunovic, *Maximum Rate of the Cathodic Reaction in Electroless Copper Deposition.* Plating and Surface Finishing, 1983. **70**(4): p. 48-50.

74. HDMicrosystems, *Product Information Bulletin: Pyralin 2555*. 2001.

75. Huntsman, *Probelec 81 7081 Technical Data Sheet*. 2003.

76. Promerus, *Avatrel 2190P Properties.*

77. Gwyddion. *Gwyddion User Guide*. http://gwyddion.net/documentation/user-guide/, Accessed 8/2007.

78. ASTM International., *Annual book of ASTM standards*. 2002, ASTM International: West Conshohocken, PA. p. v.

79. Okumura, H., et al., *Depth profile analysis of polyimide film treated by potassium hydroxide.* Journal of Polymer Science Part B-Polymer Physics, 2003. **41**(17): p. 2071-2078.

80. Inagaki, N., S. Tasaka, and A. Onodera, *Improved adhesion between Kapton film and copper metal by silane-coupling reactions.* Journal of Applied Polymer Science, 1999. **73**(9): p. 1645-1654.

81. Jang, J., I. Jang, and H. Kim, *Adhesion promotion of the polyimide-copper interface using silane-modified polyvinylimidazoles.* Journal of Applied Polymer Science, 1998. **68**(8): p. 1343-1351.

82. Seo, J., et al., *Synthesis of polyimides containing triazole to improve their adhesion to copper substrate.* Journal of Adhesion Science and Technology, 2002. **16**(13): p. 1839-1851.

83. Saraf, R., J. Roldan, and T. Derderian, *Tailoring the Surface Morphology of Polyimide for Improved Adhesion.* IBM Journal of Research and Development, 1994. **38**(4): p. 441-456.

84. Burrell, M.C., et al., *Interfacial Reactions at Copper Surfaces Coated with Polyimide Films Prepared from Poly(Amide-Acid) Precursors.* Journal of Vacuum Science & Technology a-Vacuum Surfaces and Films, 1989. **7**(1): p. 55-58.

85. Charlier, J., et al., *Study of ultrathin polyamide-6,6 films on clean copper and platinum.* Journal of Vacuum Science & Technology a-Vacuum Surfaces and Films, 1997. **15**(2): p. 353-364.

86. Chou, N.J., et al., *An Xps and Tem Study of Intrinsic Adhesion between Polyimide and Cr Films.* Journal of the Electrochemical Society, 1984. **131**(10): p. 2335-2340.

87. Charbonnier, M., M. Alami, and M. Romand, *Plasma treatment process for palladium chemisorption onto polymers before electroless deposition.* Journal of the Electrochemical Society, 1996. **143**(2): p. 472-480.

88. Beamson, G. and D. Briggs, *High resolution XPS of organic polymers : the Scienta ESCA300 database*. 1992, Chichester [England] ; New York: Wiley. 295 p.

89. Lee, W.J., et al., *Adhesion and interface chemical reactions of Cu/polyimide and Cu/TiN by XPS.* Applied Surface Science, 2003. **205**(1-4): p. 128-136.

90. Vorobyova, T.N., *Adhesion interaction between electrolessly deposited copper film and polyimide.* Journal of Adhesion Science and Technology, 1997. **11**(2): p. 167-182.

91. Siau, S., et al., *Adhesion strength of the epoxy polymer/copper interface for use in microelectronics.* Journal of the Electrochemical Society, 2005. **152**(6): p. C442-C455.

92. Siau, S., et al., *Kinetic study of wet chemical treatments on the surface roughness of epoxy polymer layers for buildup layers - I. Sweller influence.* Journal of the Electrochemical Society, 2004. **151**(12): p. C816-C830.

93. Dressick, W., et al., *Covalent Binding of Pd Catalysts to Ligating Self-Assembled Monolayer Films for Selective Electroless Metal-Deposition.* Journal of the Electrochemical Society, 1994. **141**(1): p. 210-220.

94. Gent, A.N. and S.M. Lai, *Interfacial Bonding, Energy-Dissipation, and Adhesion.* Journal of Polymer Science Part B-Polymer Physics, 1994. **32**(8): p. 1543-1555.

95. Koh, S.K., et al., *Surface modification of polytetrafluoroethylene by Ar+ irradiation for improved adhesion to other materials.* Journal of Applied Polymer Science, 1997. **64**(10): p. 1913-1921.

96. Chiniwalla, P., et al., *Crosslinking and decomposition reactions of epoxide functionalized polynorbornene. Part I. FTIR and thermogravimetric analysis.* Journal of Applied Polymer Science, 2003. **89**(2): p. 568-577.